2019

A Process, Structure, and Property Study of Gallium-based Room Temperature Metallic Alloys

Courtney Lyn Titus
University of North Florida, n01386056@unf.edu

A Process, Structure, and Property Study of Gallium-based Room Temperature Metallic Alloys

By
Courtney Titus

A thesis submitted to the School of Engineering

in partial fulfillment of the requirements for the degree of

Master's of Science in Mechanical Engineering

University of North Florida

College of Computing, Engineering, and Construction

April 2019

This Thesis titled A Process, Structure, and Property Study of Gallium-based Room Temperature Metallic Alloys is approved:

Approved by the thesis committee: **Date**

_____ _____

Dr. Stephen Stagon

Thesis Advisor and Committee Chairperson

_____ _____

Dr. Paul Eason

_____ _____

Dr. Grant Bevill

Accepted for the School of Engineering:

_____ _____

Dr. Osama Jadaan

Director of the School of Engineering

Accepted for the College of Computing, Engineering, and Construction:

_____ _____

Dr. William Klostermeyer

Dean of the College

Accepted for the University:

_____ _____

Dr. John Kantner

Dean of the Graduate School

ACKNOWLEDGMENTS

I would like to thank my advisor and committee chair, Dr. Stephen Stagon, for his mentorship through graduate research and school. I would also like to thank Dr. Paul Eason for his knowledge and expertise in material science and providing the equipment at the Materials Science and Engineering Research Facility (MSERF) at the University of North Florida (UNF). I would like to thank Albina Mikhaylova for also providing me with knowledge along with assistance to use the equipment at MSERF. Also, I would like the thank Dr. Grant Bevill for his knowledge and expertise in mechanical properties of metals. I would also like to thank my family and friends for their unconditional love and support through my two years at UNF. All my mentors have provided me with great advice and guidance to continue my engineering career professionally in Washington D.C. as a developmental engineer with the U.S. Navy Strategic Systems Program (SSP).

TABLE OF CONTENTS

LIST OF FIGURES

LIST OF TABLES

ABSTRACT

Amalgamations are a promising replacement for electronic solders, thermal interface materials, and other conductive joining materials. Amalgams are mechanically alloyed materials of a liquid constituent with a solid powder. Unlike traditional solders, these materials are processed at room temperature or slightly above, and can often operate at temperatures near, or beyond, their processing temperatures. Existing bonding processes require an excessive amount of heat, which may cause thermal stress to the electronic components and delaminate the attachment. Amalgams have promising characteristics for thermal interface materials (TIMs) due to being fully metallic, relatively easy of handling, and possessing metallic strength similar to solder or braze. Non-toxic gallium (Ga) based room temperature liquid metal alloys are a favorable material for structural amalgamations over conventional mercury (Hg). Unlike Hg amalgamations, Ga-based amalgamations have not been widely studied in the literature.

In this work, the authors investigate a novel Ga-based amalgamation, further detailing the fabrication process and characterize the physical structure, chemistry, and mechanical strength. Different packing ratios are examined, by weight, 2:1, 1:1, 4:3, and 4:1 of Galinstan, which is composed of 68wt% Ga, 22wt% indium (In), 10wt% tin (Sn), to copper (Cu) powder. These ratios are molded into three-dimensional (3D) printed tensile bars of the American Society of Testing and Materials (ASTM) standard dimensions of a model that is per D638 TypeIV. The tensile bars are cured for 24-hours at three different temperatures (room temperature, 100°C, 200°C).

The 4:1 ratio was the only specimen that failed to solidify. After allowing 24-hours of undisturbed curing, the samples that solidified were tested for their ultimate tensile strength. The optimal strength was achieved with the 2:1 ratio cured at 100°C, reaching an average tensile strength of 32.0 MPa. A scanning electron microscope (SEM), equipped with energy dispersive

spectroscopy (EDS), was then utilized to perform microstructural characterization and local chemical composition mapping of fractured and polished sample surfaces. It is concluded that, of the packing ratios that set, there is no statistically significant correlation between packing ratio and tensile strength. Further, the phases formed during curing at room temperature are the same for all packing ratios but are present at different dispersions. However, it is found that the tensile strength decreases with statistical significance as the cure temperature is increased to 200°C. This change can be attributed to the presence of new phases that occur when the sample is heated to 200°C vs. when cured at room temperature. In the room temperature sample, x-ray diffraction (XRD) revealed the existence of pure Cu, $CuGa_2$, and In_3Sn. At 200°C, XRD shows a decrease in pure Cu, the presence of $CuGa_2$ and In_3Sn, and the emergence of a new Cu_2Ga phase. These different phases form different interfaces with different bond energies, resulting in a change in tensile strength.

INTRODUCTION

TIMs are essential to the operation of modern integrated circuit (IC) devices, as they allow the dissipation of waste heat from critical processing components to heat mitigation devices, like heat sinks and spreaders. For example, this bonding material is used to join a CPU die in an electronic device with the heat sink. The performance and dependability of devices deteriorate with increasing temperature and any additional thermal impedance between the heat source and the heat sink will cause the functioning temperature to rise [1]. The TIM is applied to conform to any surface roughness and displace air voids, thereby providing a path of heat conduction [1]. Using a low temperature hermetic seal to join two components together in an electronic device is desired to increase the lifetime. This joining method is required with the function of still supplying adequate electrical and thermal conductivity. Thermal conductivity of air is four orders of magnitude lower than metals, therefore, metals are ideal for making these bonds. Unfortunately, soldering, brazing, and welding damage the components during processing, due to the elevated temperatures, require a highly specific set of operator skills, and involve expensive equipment. Alternatively, existing low temperature bonding solutions, such as thermal pastes have leakage when used as a TIM and low thermal conductance – roughly two orders of magnitude less than the components they are bonding [1]. A metallic glue is proposed for use as a joining method in the microelectronic packaging industry and may replace existing bonding methods as it transfers heat more efficiently while being processed at room, or near room, temperatures [2].

The overarching goal of this study is to create a joining method that combines the simplicity of polymeric handling and processing with the performance of the metallic joints. This material is needed for future progress and cost reduction in the IC industry, particularly for scenarios where organic based thermal paste are not applicable. A Ga-based room temperature metallic alloy is a

potential material to meet the specific properties needed for this application. As this material is entirely metal, with no organic constituent, thermal and electrical conductivity are superior to organic based paste analogs, with the advantage of significantly higher operating temperature while maintaining ease of handling. The advantages of low melting temperature of Ga also introduce the idea that Ga layers can act as a reversible and switchable adhesive [2].

Ga-alloy metallic pastes, known as amalgamations, can be formed by mechanically alloying liquid Ga-alloy and solid metallic powder constituents at room temperature. Amalgamations are alloys formed by combining a liquid base mixture with a metallic powder to create a paste, which begins to solidify within minutes after processing at room temperature. They have classically been used for dental fillings, because of the strength and cost-effective implementation. The resulting material is mechanically strong, electrically and thermally conductive, and capable of forming a hermetic seal at room temperature.

For this thesis, the process, structure, and property of a Ga-based alloy is characterized. The impact of the mixing ratio and cure temperature on mechanical strength and microstructure of the Ga-based amalgamations is investigated. Mixing ratios, by weight, of 2:1, 1:1 4:3, and 4:1 of Galinstan (68wt% Ga, 22wt% In, 10wt% Sn) to Cu powder are investigated. The mixtures are be molded into three-dimensional (3D) printed tensile bars complying to ASTM standard tensile bar that is per D638 TypeIV. Samples are cured, undisturbed, for 24-hours at three different temperatures (room temperature, 100°C, 200°C). The interplay of different ratios and cure temperatures were investigated for statistically significant effects on the mechanical properties, handling properties, and the phases that form in the resulting alloy.

After performing the synthesis and characterization experiments, it was found that the packing ratio did not have a statistically significant effect on the mechanical properties of the

samples. Of the ratios that set, mechanical strength was similar when cure temperature was held constant. Alternatively, the other experimental variable, cure temperature, demonstrates a statistically significant effect on the sample's mechanical strength. A microstructural origin, owing to the development of a new Cu_2Ga phase, is proposed after analysis of microstructure and local chemical composition using SEM, EDS, and XRD. It was found that increasing cure temperature resulted in a decrease in tensile strength in the range from room temperature to 200°C. The authors hypothesize that the reduction in tensile strength stems from the formation of different phases than the specimen cured at room temperature. At room temperature, the resulting phases in the microstructure were identified by XRD as $CuGa_2$, pure Cu, and In_3Sn. The presence of these phases in XRD validates and strengthens the chemical composition maps generated from EDS. At 200°C, there was a decrease in the $CuGa_2$ and pure Cu and it was found that a new phase of Cu_2Ga forms, while In_3Sn still remained.

Structurally, this thesis outlines the background of the application and motivation for this study, the background of the methods chosen for this research, a descriptive step-by-step procedure of the first-hand design of experiment (DoE), and the conclusions drawn. Chapter one provides information about the background of TIMs. Next, chapter two delivers details of what an amalgamation is, and previous literature done with other alloys that helped design the hypothesis for this new investigation. There is also background on the characterization methods along with the equipment used in this experiment. Chapter three is the fabrication process of preparing the specimen to be characterized. Then, the final chapter entails the conclusions drawn from the testing of this metallic alloy. This section includes the development process of the complex microstructure with the four elements, the mechanical properties tested with supporting data, and the material characterization, including SEM images, EDS chemical maps, and XRD spectrums.

CHAPTER 1: THERMAL INTERFACE MATERIALS

1.1 BACKGROUND OF THERMAL INTERFACE MATERIALS

The increasing power and decreasing die size used in modern processors creates a need for significantly enhanced TIMs [1]. A TIM can be defined as a material applied between the interfaces of two components to encapsulate a device for functionality and effectively move heat from one surface to the other [3]. A TIM is placed between two mating surfaces to increase the electrical and thermal conductance across the interface [4]. The effective transfer of heat is crucial to ensure reliable operation and enhance the lifetime of the semiconductor core of the processor [3].

It is common knowledge that when you place two hard solid materials together they experience contact only at the top surface of the face, caused by artifact roughness from the fabrication process and lack of compliance of the surface under loading. For example, if a heat sink and CPU core die are placed into contact without a TIM, heat transfer is prohibitively low. There is little contact between the two surfaces, a high thermal contact resistance results due to the air that is trapped in the micron scale roughness, that is characteristic of their respective manufacturing processes [4, 5]. Thermal interface resistance is measured on how difficult it is for the heat to dissipate across the interface [3]. A TIM is used in the gap between the CPU die and the heat sink, which conforms to the surfaces and minimized trapped air [6]. In the absence of a filler, there is low electrical and thermal conductivity, which does not benefit devices ability to work as efficiently as possible.

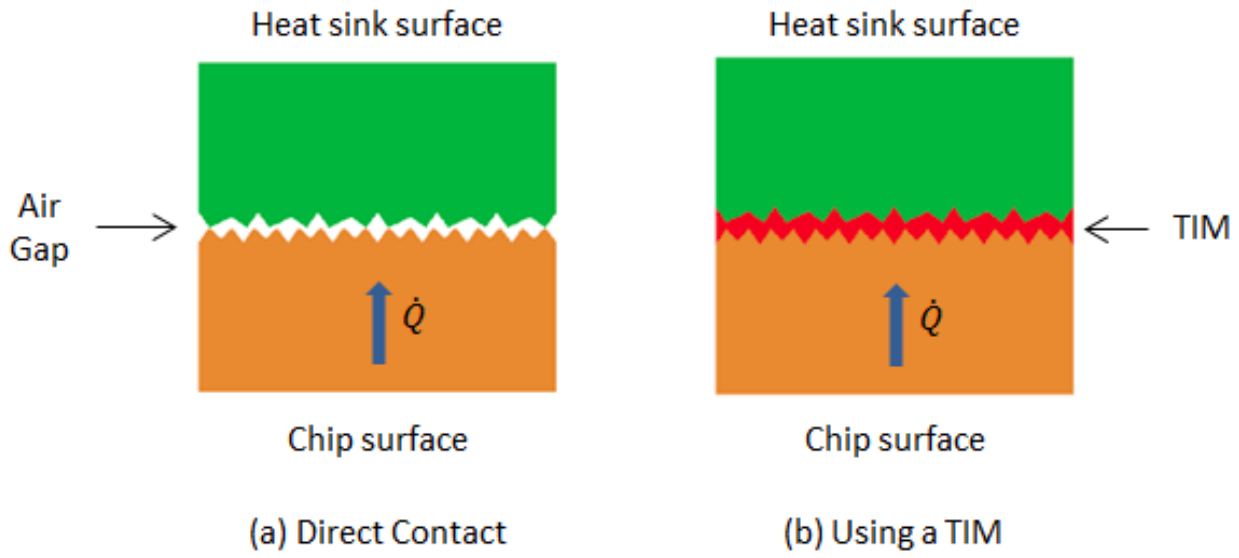

Figure 1: a) Diagram of a chip surface and a heat sink surface without a TIM placed within the interface. There is a clear airgap resulting in thermal interface resistance. b) Diagram of a chip surface and a heat sink surface with a TIM placed within the two interfaces. This eliminates the air gap resulting in lower resistance and better heat transfer *[7]*.

The application of a TIM benefits in obtaining a lower value of thermal contact resistance but is limited by the bulk thermal conductivity of the TIM material itself. When compared to the materials and metals that the CPU die and heat sink are made from, conventional TIMs have roughly 10 times lower thermal conductivity (10 W $m^{-1}k^{-1}$ for TIM vs 100+ W $m^{-1}k^{-1}$ for metals). The thermal gradient in the bond line thickness (BLT) of the TIM transfers heat from the die to the heat sink through the bulk. A sharp thermal gradient appears at the two mating surface interfaces, where the heat transfer has trouble dissipating from one surface to the other because of their different properties, shown by R_{c1} and R_{c2}, in Figure 2 [8].

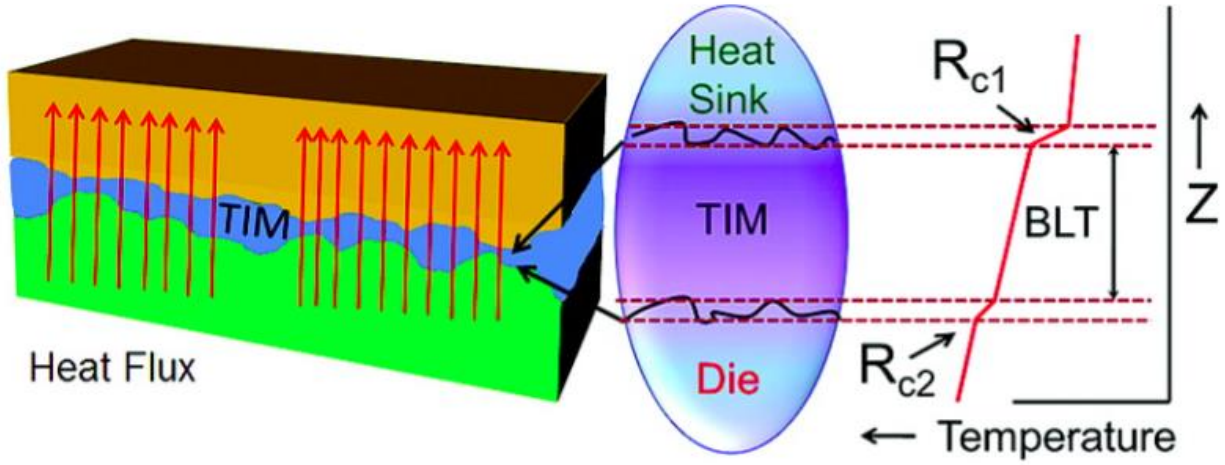

Figure 2: Diagram illustrating thermal contact resistance (R_{c1}, R_{c2}) areas that classify as regions where the die and heatsink meet the TIM due to the high temperature difference of the different materials contacting and heat not being transferred as efficiently *[8]*.

This interface resistance is generally the result of micron-scale gaps of air remaining trapped. The governing phenomena to eliminate this air gap would be to apply a material with a higher thermal conductivity than the air [3]. Figures 2 shows the total thermal resistance with the application of a TIM between the two substrates in a processor. The total thermal resistance with a TIM can be calculated by the equation:

$$R_{TIM} = \frac{BLT}{k_{TIM}} + R_{c1} + R_{c2} \qquad (1)$$

where k_{TIM} is the thermal conductivity of the TIM (all other variables have been previously defined) [3]. The main objective of thermal management in electronic packaging is eliminating the heat from the semiconducting device to the atmosphere [3]. The conformability of the TIM is important in reducing R_{TIM} as it will be able to create an attachment to the rough surfaces in a tough geometry. Therefore, a soft material is desired as an interface material between to two mating surfaces [1, 3]. Limitations stem from the bulk thermal conductivity depending on the BLT and the intrinsic thermal conductivity (k_{TIM}) which defines the overall effectiveness of the material

[3]. The overall, device level, thermal resistance are highly depending on BLT and thermal conductivity. As the BLT is the length of the TIM after set between the two substrates, minimizing this thickness will result in the overall optimization of the resistance. Intrinsic thermal conductivity of the TIM is the property to conduct heat and can be defined in terms of Fourier's law for one dimensional heat conduction under steady state conditions:

$$k = \frac{Q}{A}\frac{\Delta x}{\Delta T} \qquad (2)$$

where, Q is the heat flow in watts (W), A is the surface area in meters (m^2), ΔT is the temperature difference between the two surfaces in kelvin (K), Δx= BLT= thickness of the TIM (m), and the *k* is the thermal conductivity ($Wm^{-1}K^{-1}$) [9].

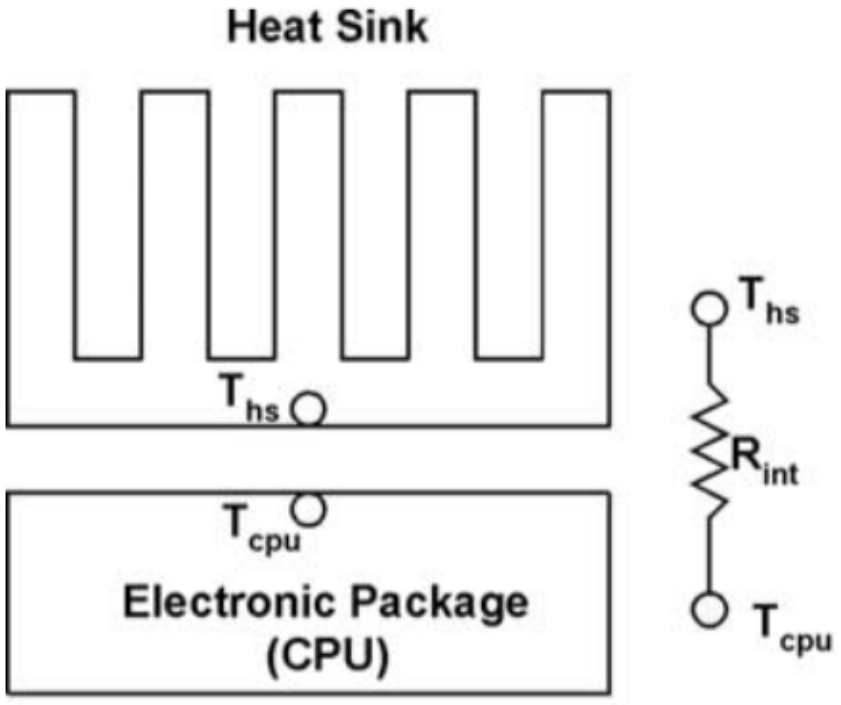

Figure 3: Simple thermal circuit of the CPU and the heatsink. *[1]*

The goal is the decrease the thermal resistance throughout the packaging in a semiconductor. The figure above illustrates the different temperatures with the interface resistance

from the TIM. There is no perfect TIM, but there are required aspects of the materials that would benefit in dissipating the heat efficiently to increase the lifespan of the device. The desirable properties of the ideal TIM would be: 1) the ability to form thin bond line with uniform thickness across the interfaces; 2) low thermal impedance; 3) low thermal stress during application; 4) no leakage off the sides of the interface; 5) appreciable formability; 6) non-toxic material; and 7) maintenance of performance indefinitely [1].

1.2 EXISTING BONDING PROCESSES

Thermal conductance gap filling materials exist with processes known as brazing, soldering, welding, and thermal pastes [10]. As described before, the ideal TIM needs low thermal stress during application, which forms during joining high temperature processing of brazing, soldering, and welding. If the device is heated excessively during processing, the lifetime of the device can be decreased through the presence of thermal set stress and modified doping profiles [3].

Brazing and soldering join two similar or dissimilar metals together by heating a metallic filler alloy that bonds to the two pieces [10]. Alloyed metals can be joined by a molten material to close the gap of two substrates and then solidify without causing melting in the base materials [11]. Brazing and soldering are comparable to adhesive bonding by the similar process of using fillers in liquid form to be distributed over as a coating for the surfaces to be bonded [11]. A substantial difference between the brazing, soldering, and adhesive bonding is brazed fillers melt and join at temperatures above 450°C and require flux [11]. Additionally, the operation temperature of brazed joints is much less than the process temperature. The extensive heat required to reach the melting temperature of the metallic filler alloys creates the problem of intrinsic stress formed in components, due to the different coefficients of thermal expansion and non-equivalent contraction

during cooling. The thermal stress can fail bonded joints and components prematurely. The significant difference in temperatures will cause damage to the components being joined together by this process. Soldering is a bonding done at lower temperatures then brazing, which has the advantage of not exceeding the thermal budget but brings other disadvantages. Because of the decrease in temperature the solder dissolves, but does not melt, resulting in the formation of an intermetallic compound (IMC) with the base material through the chemical reaction [11]. An IMC is usually a brittle phase diminishing the mechanical interlocking of the bond [11]. The method of welding is the joining of two similar metals togethers with higher homologous temperatures, causing the base material to melt along with the filler material [10]. Flux has a dual role of reducing oxidation and wetting the surfaces at high temperatures but is nearly inert at room temperature [11].

Established adhesive bonding uses organic materials with inorganic filler. Thermal pastes are a type of organic adhesive bonding and suffer from poor thermal conductivity compared to fully metallic solders, brazes, and welds [4] . The thermal conductivity, typically around 1-10 $Wm^{-1}k^{-1}$, is the result of the small content of a metallic or carbon filler compared to the organic matrix, which is generally silicone based [1]. Further, over time, thermal pastes suffer breakdown due to the decomposition of the organic component at elevated temperatures. As the thermal conductivity is low, operational temperatures may increase with time and cause further degradation to the material [1]. Additionally, handling of thermal pastes are difficult, due to its intrinsic viscosity and non-Newtonian behavior which results in leakage when the heat generator and heat sink are joined together during manufacturing [4]. This leakage can cause contamination to other components and cause electrical shorts [1]. Fundamentally, the formability of thermal pastes is insufficient for the demand of TIMs.

A joining method that combines the simplicity of polymeric handling and processing with the performance of metallic joints is needed by the IC industry to continue to increase power densities and for expand to next generation semiconductor devices which operate at temperature beyond the limit of organic materials. An amalgamation, or amalgam, could be a potential solution for an improved bonding method in semiconductors. It is a mixture of a solid and liquid metal constituents, resulting in a glue-like consistency. Unlike thermal pastes, amalgams viscosity can be controlled by the addition of more or less of both constituents, eliminating leakages when pressure is applied for connection. Fortunately, like polymeric adhesives, amalgamations are mechanically applied to the bonding surface after being mixed, which results in no excessive amounts of heats during processing, but only minimal pressure applied to push air from the gap. Along with their manageable handling properties, the two constituents are both metals, principally having a desirable thermal conductivity for the heat to transfer from the CPU to the heat sink effectively.

CHAPTER 2: LITERATURE REVIEW

2.1 BACKGROUND OF AMALGAMATIONS

The development of highly integrated electronics and size limitations require specific needs for proper functionality [12]. Solders have been the material of choice until limitations occurred and became an issue with temperature excursion cure processing [13]. The temperature excursions lead to high thermal stress and distortion in the electronic pieces creating problems when the device is operated [13]. Recent research into non-toxic Ga-based room temperature liquid metal alloys have spurred a new generation of investigation into structural amalgamations for microelectronic bonding [13]. A diagram of the typical assembly of an amalgamator machine is pictured in Figure 4. It shows the two separate constituents, powder and a liquid metal, after being placed into a small capsule to be combined, like a mortar and pestle process, within the wishbone.

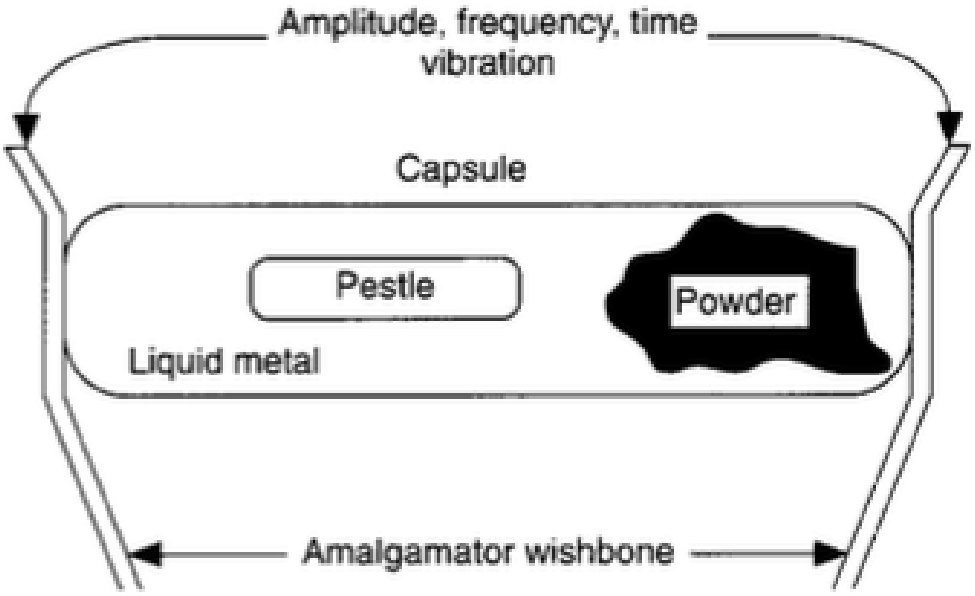

Figure 4: Diagram of dental amalgamator before mixing occurs. The two constituents are separate in the capsule and positioned in the wishbones of the amalgamator to be alloyed together *[13]*.

Amalgamations are mechanically alloyed and formed by combining a liquid base mixture with a metallic powder to create a paste, which sets within hours at room temperature, or slightly above. The combining of the liquid metal and the powder are set to shake in a linear motion. Basically, the goal is for the oscillation and vibration of the machine to create an even mixture of the powder and liquid metal. The consistency desired for the amalgam is dependent on the amount of each constituent. Having more of the base, being liquid metal, will create a more fluid like material and, alternatively, more solid particles will create a thicker paste. When considering the amounts of each ingredient, mixing time is a significant factor that needs to be considered. When a mixture is over amalgamated, it will turn into a hot rock-like structure, which defeats the purpose of creating a metallic glue. Under mixing is seen when you can still see solid particles after the machine was ran to the desired amalgamation time. The metal must wet the powder and the two must be evenly mixed. After the two constituents become one, the amalgam usually will start to set within one hour.

Amalgams have classically been used for dental fillings, because of the strength and cost-effective implementation [14]. Dental fillings are typically Hg-based alloys but have been discovered to be toxic and a hazard to the environment [15]. Despite the findings of toxicity issues, a study has shown that compressive strength of a Hg-based amalgam alloyed with silver (Ag) powder, Sn, and Cu value to 176.2 MPa [14]. Since Hg-based alloys are hazardous, the same study compares Ga-based amalgamations as a replacement for Hg-based. Ga has the second lowest melting point of all metals, after Hg, and when alloyed with In and Sn produces a liquid at room temperature [16]. In the state of being liquid at room temperature, Ga-based amalgams offer the reduction in equipment complexity and cost and more efficient processing [13]. The gluing can be performed at room temperature, requiring some pressure (<100psi) [2]. With the goal to substitute

Hg with Ga-based alloys, the average compressive strength for Ga is 324 MPa when alloyed with Sn. Another unique characteristic of amalgamations is the fact that they are conformable, which enables difficult geometries to be able to be attached to one another because of the mechanical strength they hold [13]. Due to its metallic properties, it has an appreciable conductivity, which could potentially allow IC devices to operate at higher power densities. Like with Hg, Ga amalgamations have a range of properties that are strongly dependent on mixing and curing times, temperature, and chemical composition [17].

2.2 PREVIOUS LITERATURE

The baseline for this literature began with the investigation from studies with amalgamations as dental fillings. Most of the research in the literature includes only Hg-based alloys as the base material. Studying papers on Hg-based alloys has guided the process, property, and structure for Ga-based amalgamations. Expanding knowledge on known amalgamations has motivated the investigation for specifically focusing on Ga and the properties offered over Hg. In the literature, mechanical data and material characterization of these alloys was of most importance. Each article will be analyzed that was beneficial in the unique DoE for the amalgamations studied in this thesis.

A recent study by Dr. Jamal Al-Deen and Sura Shahee focused on the replacement of Hg with different Ga alloys. Three different types of Ga-based alloys were investigated, including Ga-In, Ga-Sn, and Ga-In-Sn amalgamated with a powder constituent of several different elements [14]. The other amalgamation investigated was a Hg-based alloy to compare the results and support that need Ga to replace it.

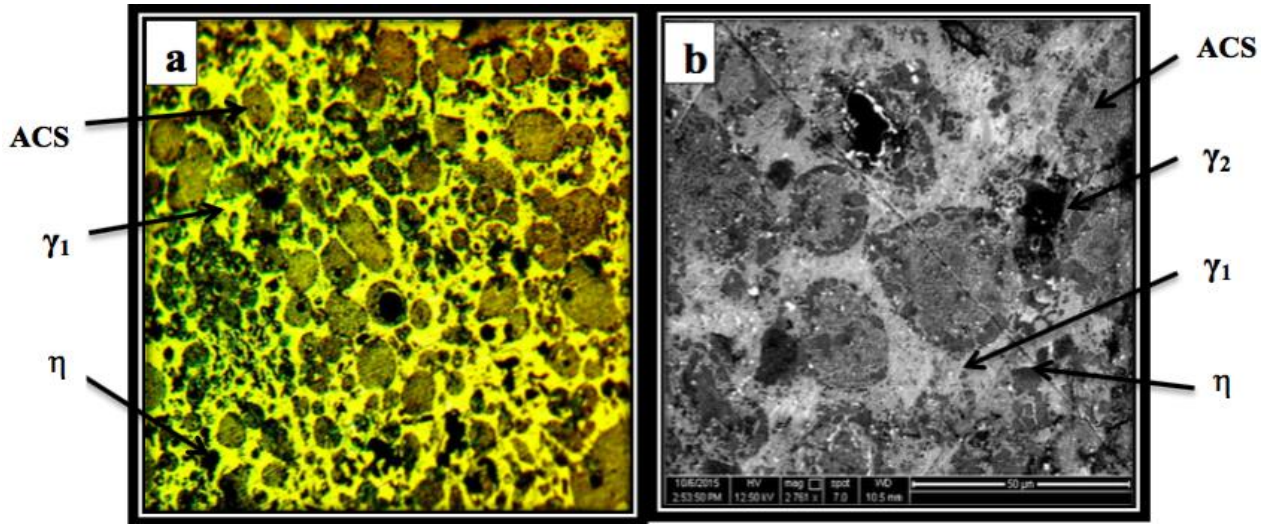

Figure 5: a) Optical microscope image of a Hg-based alloy: liquid constituent (100wt% Hg), solid constituent (44.5wt% Ag, 30wt% Sn, 25.5wt% Cu). The phases seen can be classified with abbreviations meaning Silver-copper-tin (ACS), γ_1- Ag_2Hg_3, γ_2- uncharacterized, and η- Cu_6Sn_5. b) SEM image of the same Hg-based alloy in figure a *[14]*.

The microstructure reveals different phases throughout the cross section, which were verified and identified using XRD. The predominate phase, Ag_2Hg_3, was the matrix of the microstructure [14]. While a legitimate characterization process was done throughout the scope of this paper, there is no connection established between the microstructure, phases, and mechanical performance. The average compressive strength was measured in this work as 176.2 MPa for Hg based material [14]. Given the results for the Hg-based structure, it was found that the mechanical strength of the Ga alloys was stronger, the strongest having a value of 324 MPa when alloyed with Sn [14]. The strength has direct correlation to the phases that form through the solidification of the mixture of these alloys, but the strengthening mechanisms are not discussed thoroughly.

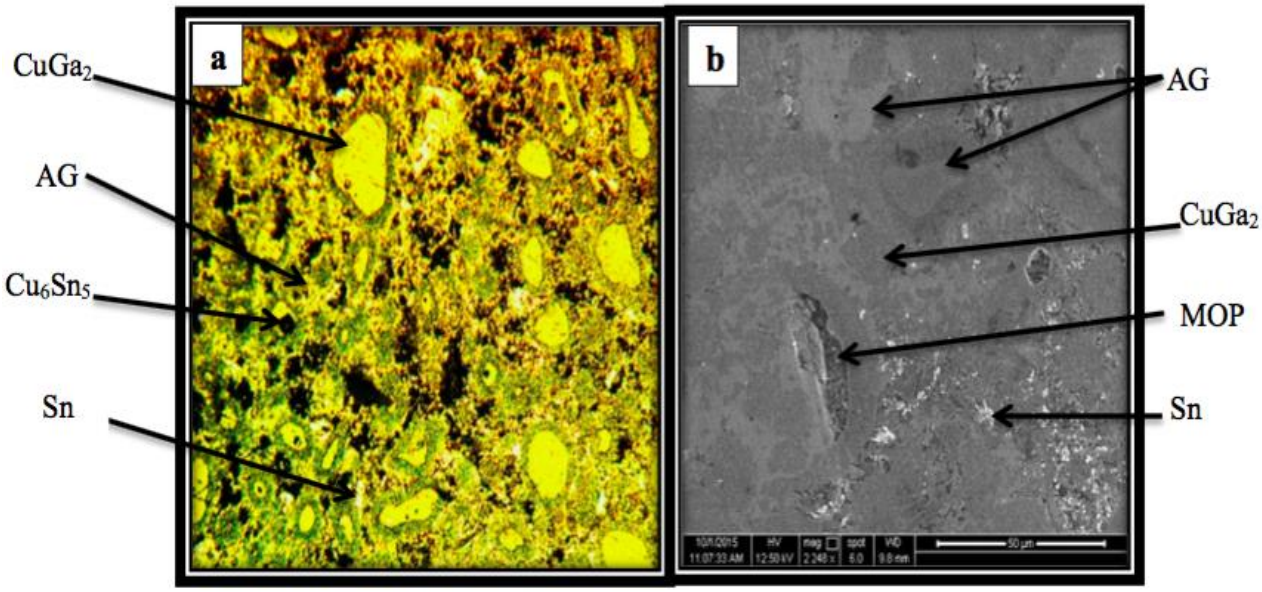

Figure 6: a) Optical microscope image of Ga-Sn alloy consisting of solid constituent (86.5 wt% Ga, 13.5 wt% Sn), solid constituent (44.5wt% Ag, 30wt% Sn, 25.5wt% Cu). b) SEM image of GaSn alloy with mixture of phases (MOP) and silver-gallium (AG) phase representing these abbreviations *[14]*.

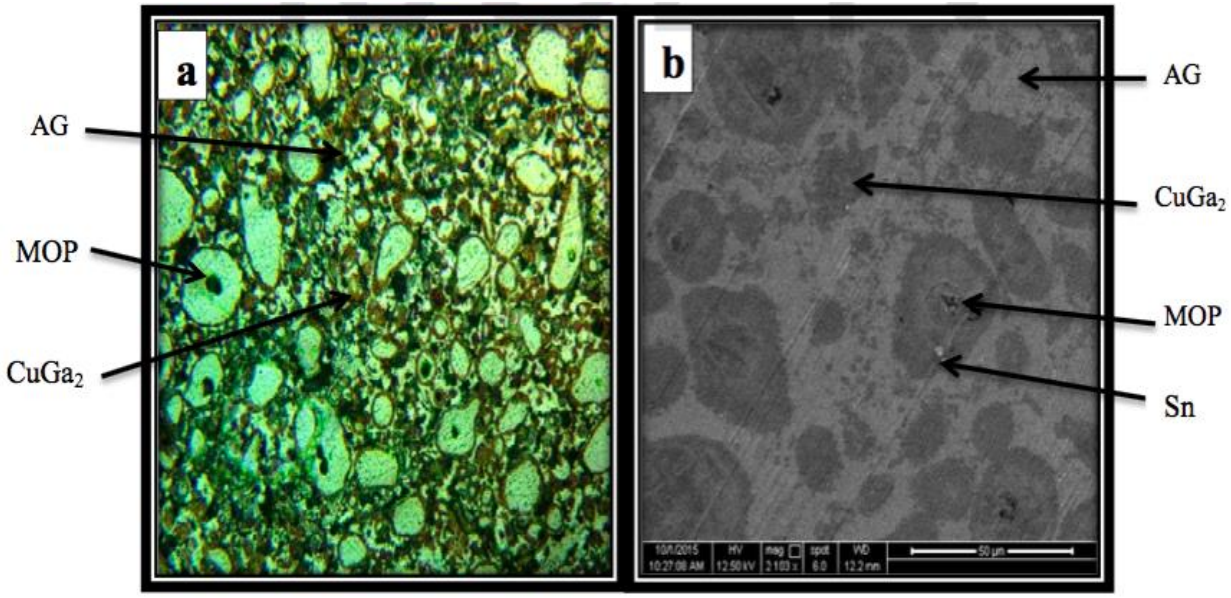

Figure 7: a) Optical microscope image of (Ga-In-Sn) alloy consisting of liquid constituent (68 wt% Ga, 22 wt% In, 10 wt% Sn), solid constituent (44.5wt% Ag, 30wt% Sn, 25.5wt% Cu). b) SEM image of Ga-In-Sn alloy *[14]*.

The microstructure of the all the Ga alloys revealed light gray regions, the matrix of $CuGa_2$ and white color regions, representing a rich Sn area [14]. In evaluation of mechanical strength, the

optimal result for the average compressive strength was 324MPa for the Ga-Sn alloy, while the other alloys fell below that value, at about 100-200MPa less [14]. The conclusion to draw from the average strength is the significantly higher value tested with all the Ga alloys compared to the Hg amalgamation [14]. Not only does Ga mix and cure to form a stronger alloy, it is also a non-toxic material, unlike Hg. Since Ga-based alloys are environmentally benign and increase in strength, they are promising substitutes [2]. Ga is therefore being used for further investigation [17].

In MacKay's article published in 1993, amalgamations were briefly investigated. The machine utilized for the amalgamation process was a commercial dental amalgamator [13]. He found that the time of the amalgamation after the powder particles are immersed is the most important variable. The powder particle size affects the consistency of the mixture, as finer powders reacted more quickly than coarser ones [13]. In this research paper, several different amalgamations were processed including the metals of Cu powder, Ga, nickel (Ni), and Ag. The phases that the alloy has formed with only two constituents is focused on. Ga and Cu form amalgams cured between a range of 35°C-100°C in the composition range of 25% Cu and 40% Cu to Ga were analyzed under a SEM [13]. The micrograph revealed results with the matrix compound being $CuGa_2$ [13]. Thermal cycle experiments with this alloy showed no phase change problems [13].

Cu and Ga amalgams were also investigated over two decades ago in a study at Rutgers University. They were investigated for bonding ceramics and metals containing a composition of 66wt% Cu to 34wt% Ga [18]. The shear strength was tested to evaluate high temperature heat treatment for these alloys. The highest result they found was when bonding Si_3N_4-to-Si_3N_4 with a value of 19MPa [18]. Testing these specimens at such high temperature, they found that above

800°C started to form an oxygen rich shell causing a decreasing value in the yield strength [18]. From the experiments conducted, it can be concluded that the temperature has an extreme effect on the strength of the alloy. Therefore, curing Ga-based alloys near room temperature could have a great impact on the results for the joining material.

The literature mentioned has similar DoE process with major differences to the factors studied in this thesis. When drawing conclusions from the different studies, the papers have different elements in the alloys or a different temperature range studied for the phase developments throughout the structure compared to what is desired in this work. Classifying the phases with the elements used in previous experiments will make major contributions to the knowledge for the material chosen for the DoE this thesis follows.

Aside from the testing the mechanical properties of these alloys, the compound formation when the two materials are alloyed together can be shown on a binary phase diagram, which analyzes their phases developed due to their weight percent composition as a function of temperature. Phase diagrams have been experimentally generated for certain alloys that are concentrated on in the capacity of this thesis. Cu and Ga have been analyzed in the literature, and phases formed are shown at different temperatures and compositions with the base element being Ga in Figure 8 [19]. The γ-phase is formed in the range of 600°C -800°C with 30 wt% Ga is represented as Cu_2Ga [19]. Information is not available in the literature for the range from 0°C-200°C, the area of importance for this study. The θ-phase classifying as $CuGa_2$ is hypotheically correlated as a dashed line, but not proven to be a phase of formation via experimental results [19].

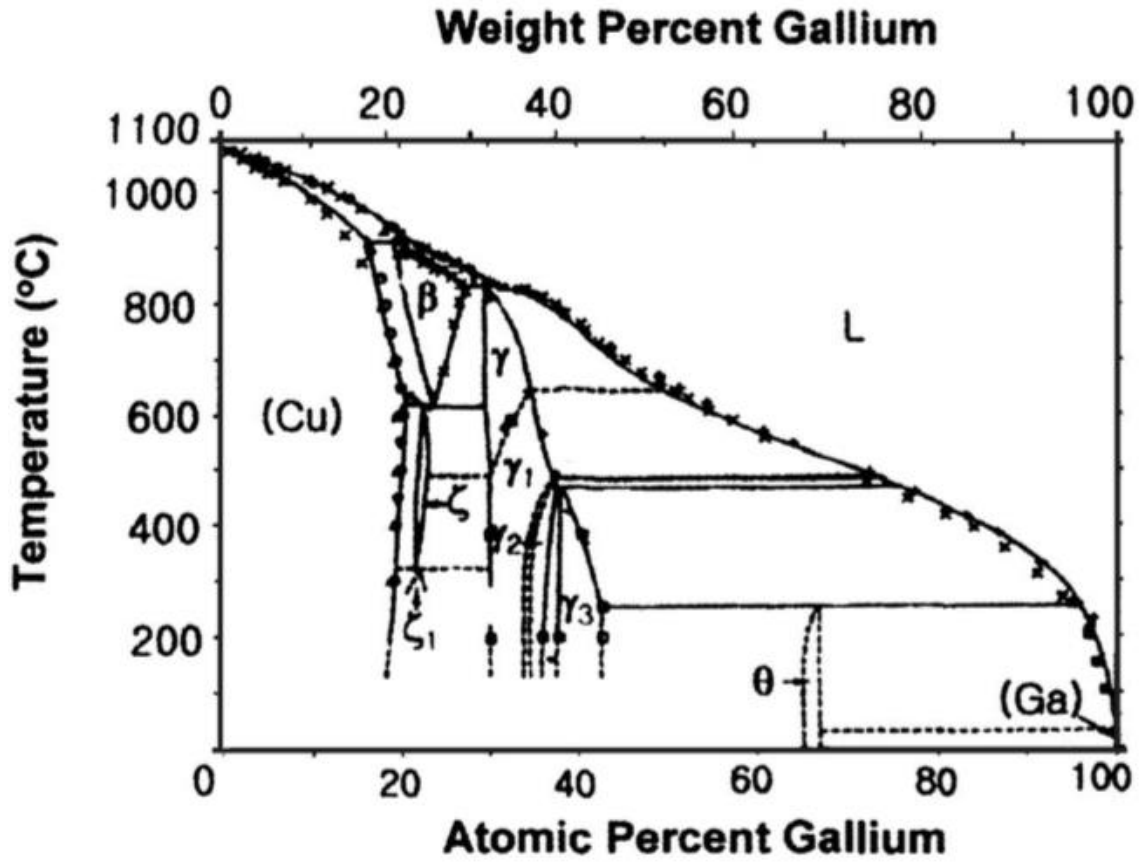

Figure 8: Binary phase diagram for Cu and Ga *[19]*.

Experiments in this thesis offer experimental results below 200°C. For a better understanding of alloying Cu and Ga, these two elements are not in equilibrium so phases in between need to be present to become stable. To visualize the process of stabilization, a diagram in Figure 9 shows the compounds formed when combining Cu and Ga. First, through amalgamation, the Cu powder is dispersed into the Ga, which is a liquid. Due to chemical affinity, Ga can diffuse into the Cu particle. As the diffusion progresses, different phases are formed distributed radially. The diffusion and formation of intermediate phases between pure Cu and pure Ga progress until the kinetic driving force across the intermediate phases becomes too small for diffusion to progress. It is shown that the Cu_2Ga phase has a smaller length scale than the $CuGa_2$

phase as the chemical potential provided by the local chemical gradient is smaller at the $CuGa_2$ - Cu_2Ga interphase than at the $CuGa_2$-Ga interface.

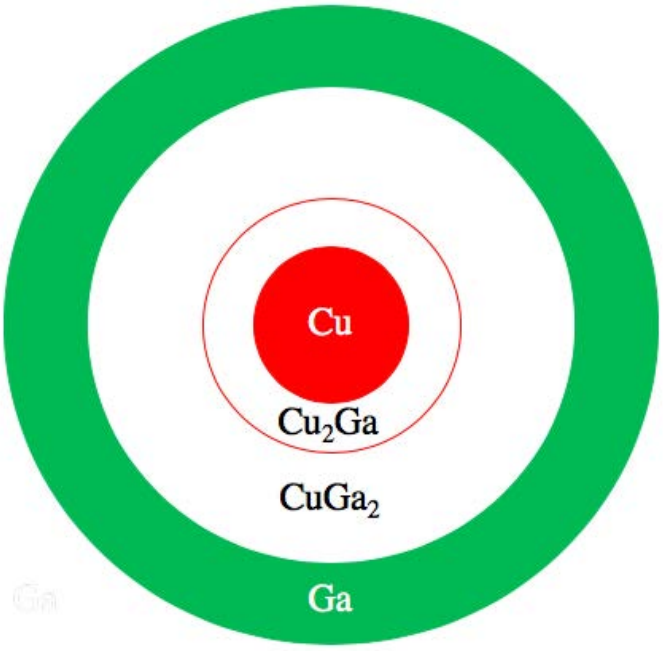

Figure 9: Ga and Cu as separate constituents forming the IMCs in between each other as alloying together to be in equilibrium.

As Cu and Ga have significantly higher chemical affinity than Cu-In, Cu-Sn, Ga-In, and Ga-Sn at room temperature, Cu and Ga form preferred alloys, precipitating out In and Sn, which form a mixed solid phase at room temperature. We next examine the In-Sn phase diagram to have a theoretical estimation of phases that are expected to form during the curing process at room temperature. The In-Sn phase diagram does accumulate development of phases in the temperature range from room temperature, 25°C, to 200°C [20]. Phases present in the phase diagram are the $InSn_4$, γ-phase, and the In_3Sn, β-phase, which are stable at room temperature [20]. XRD is performed in this literature at different temperature increments at the composition of In located in the middle region, 35-75 wt% In, resulting in phases being identified as multiple peaks of γ, β, and pure In [20].

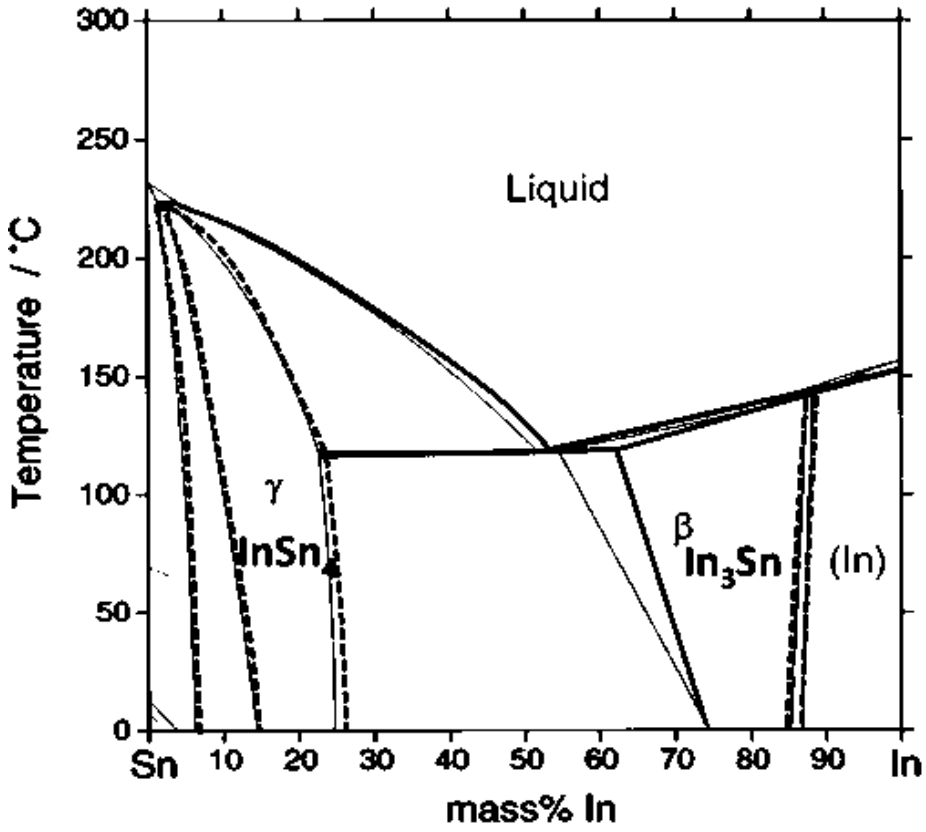

Figure 10: Binary phase diagram for In and Sn *[20]*.

Cu-Ga phase diagram is elaborated on above, and the same case is displayed in the Cu-In and Ga-In diagrams, where there is no discovery in developing a compound at the temperatures studied in this thesis.

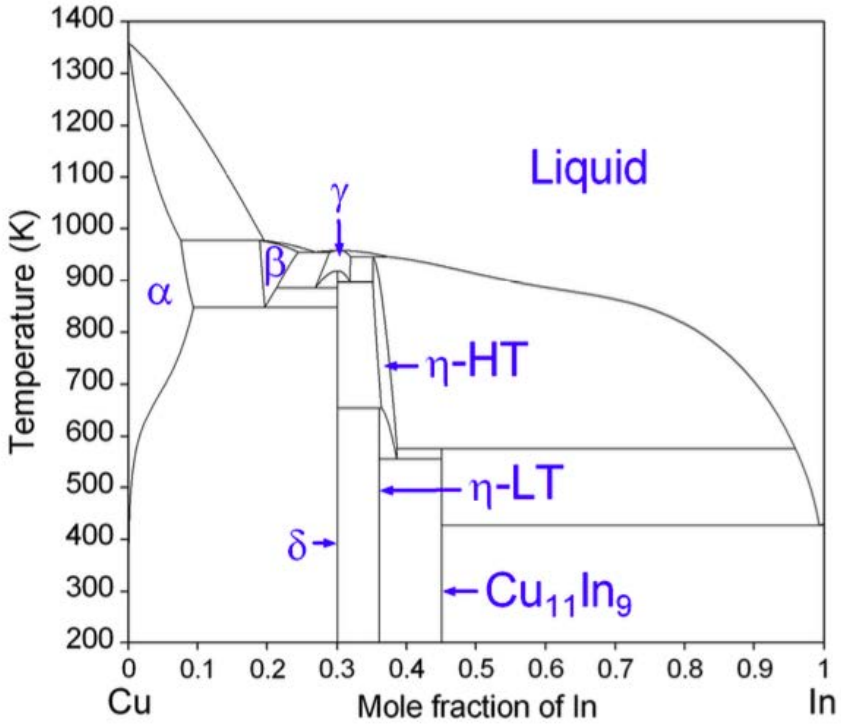

Figure 11: Binary phase diagram for Cu-In *[21]*.

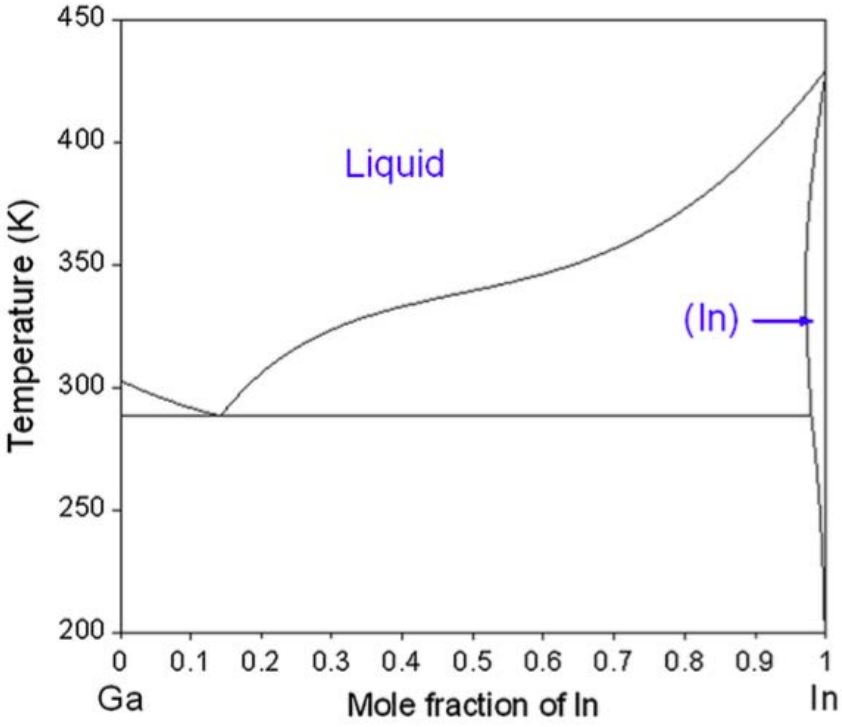

Figure 12: Binary phase diagram for Ga-In *[21]*.

The previous literature evaluated with Ga-based alloys releases information about specific liquid to solid relationships with different elements than those studied in this paper [13, 14, 18]. There is no correlation of the mechanical properties of this alloy with the microstructure found in the literature. The phases formed at the different cure temperatures and liquid to solid ratios will be an important aspect to understanding the mechanical behavior of the material. The packing ratios, the mixing duration, and the cure temperature are expected to have an effect on the phases of the material that forms, and this work aims to be the first to investigate the formation of a solid that has been experimentally observed at room temperature to 200°C. It is highly likely that above 200°C, there will be additional phases formed between Cu-Ga-In-Sn that were not thermodynamically preferable below 200°C. The investigation above becomes very complex due to the four elements being present, and future experiments via x-ray crystallography to help guide the discovery of the phases formed are proposed. The scope of this thesis is to obtain a first level of understanding of the process, property, and structure of Ga-Cu-In-Sn solids formed from amalgamation at room temperature.

2.3 TENSILE TESTING

Tensile testing is a type of mechanical testing to see if materials can withstand a force in tension without elongation or rupture. When the load is applied, and the specimen will elastically and plastically deform until rupture [22]. Materials are usually tested for their ultimate tensile stress to see if their strength can be applied in real world engineering applications [22]. Usually new materials, like these Ga-based amalgamations, are tested for tensile properties so there can be comparison to other materials and processes [22]. The framework of a tensile bar consists of the two shoulders and gauge length. The two shoulders are placed between the grips in the machine and constrained to move relative to one another. The most critical part of the tensile bar in this

process is the gauge length, as the cross-sectional area is reduced for higher local stresses, so that deformation and failure will be localized in this region [22].

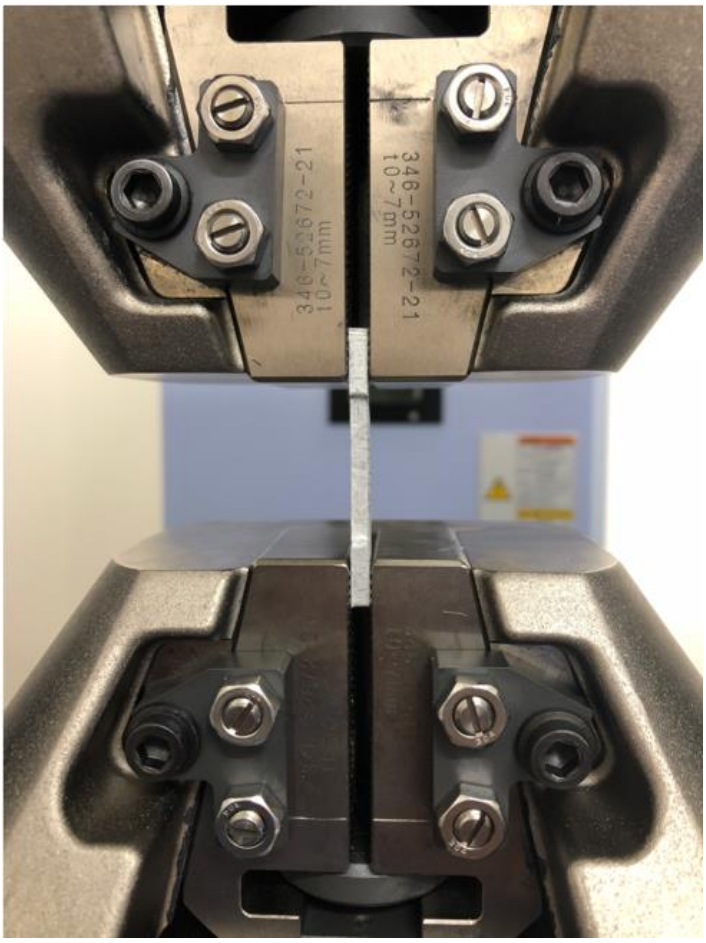

Figure 13: The shoulders are placed between the grip section in the tensile machine and the tensile bar is properly positioned for testing.

The tensile bar is mounted in the machine as shown above in Figure 13. Next, the machine is either controlled to an applied load while the elongation is measured, or to a controlled elongation while the load is measured [22]. In this work, displacement control is used, to conform to ASTM standards. The most useful data obtained from the tensile test in the stress versus strain curve, which will give values of ultimate stress and strain, and can describe the behavior of the specimen in correlation to what type of material it acts as. A brittle material will have a linear slope

with minimal plastic deformation before fracturing [22]. A more ductile material will sustain significant plastic deformation prior to fracturing [22]. Engineers and metallurgists perform tensile tests because of the interest in mechanical properties data [22].

2.4 SCANNING ELECTRON MICROSCOPE

SEM is an instrument for material characterization that scans, or rasters, a focused electron beam over a surface of a sample for interaction to create an image [23]. The signals obtained contain information about the material's surface topography and local chemical composition [23]. The SEM has various sample interactions, as seen below in Figure 14 [24].

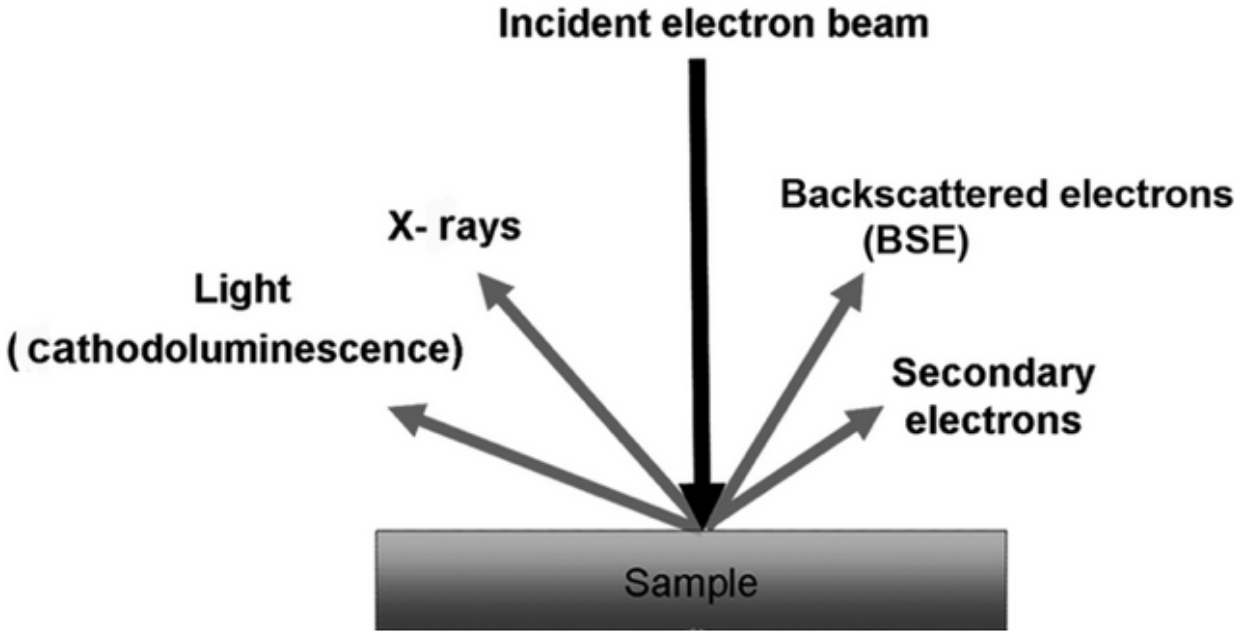

Figure 14: Potential signals generated during the interaction of an electron beam with a sample. The directions shown for each signal do not always represent the physical direction of the signal, it is indication of how strong the signal is *[24]*.

Secondary electron (SE) imaging allows for the collection of near-surface topographic data, while back-scattered electron (BSE) imaging allows for the collection of phase contract data due to different electron penetration depths between phases. These images are created to obtain an understanding of the microstructural distribution of the phases within a specimen, leading to the

morphological differences of the phases relative to each other. This method is used for amalgamations because of the phase development in the structure. In this work, the authors aim to garner phase distribution and microstructural data to understand the results of mechanical testing.

The metals mixed together in an amalgam react in a matter due to their metallic properties to form different compounds with an inhomogeneous distribution. For the compounds to be characterized, samples need to be prepared for the SEM. The SEM can image the fractured surface of the tested tensile bars to obtain information on the break experienced during tension testing. Another feature as previously mentioned is the investigation of polished sample cross-sections to characterize the phase development within the solidified amalgam by differentiating the shades in the colors, interconnected to another material characterization technique specifically used for chemical mapping of the image.

2.5 ENERGY DISPERSIVE SPECTROCOPY

EDS is equipped to the SEM as a technique to determine the chemical composition of the sample [23]. EDS detects the characteristic x-rays generated all throughout the interaction volume and is used for both qualitative and quantitative analysis of the chemical concentration [23]. The morphological information in a SE image only reveals the surface and near surface structure, whereas x-ray data is largely sub-surface, and may contain data from phase regions that are not visible in the SE image [23]. Qualitatively, EDS reveals a chemical mapping correlating a color to each element detected. With this data, the percentages of each composition in the image will be quantified locally. EDS is able to measure a spatial distribution of x-ray emission to obtain a transformed or correlated mass ratio in the excitation volume. Spot analysis is also used in areas of particular interest, to identify approximate local chemical composition. Distinguishing a

specific area with spot identification will give valid results in characterizing the element to link it to failure.

2.6 X-RAY DIFFRACTION

XRD is a powerful technique performed to determine the structure in a crystalline material [23]. XRD uses x-rays elastically scattered by the atoms in the periodic crystal lattice [23]. The incident x-rays are detected when constructively interfering in the phase to be reflected, following Bragg's law, which is the principal formula in obtaining the resulting planar spacings detected [23]. Bragg's law is:

$$n\lambda = 2d\ sin\ \theta \qquad (3)$$

where n is an integer called the order of reflection, λ is the wavelength of x-rays, d is the characteristic spacing between the crystal planes of a given specimen, and θ is the angle between the incident beam and the normal to the reflecting lattice plane [23]. Constructive interference allows the measurement of the angle, θ, alloy for the spacing of every single crystallographic phase present, as long as the reflection is not forbidden, to be determined. To better visualize the concept of Bragg's law, the diagram of the movement of the x-rays path is in the schematic figured below.

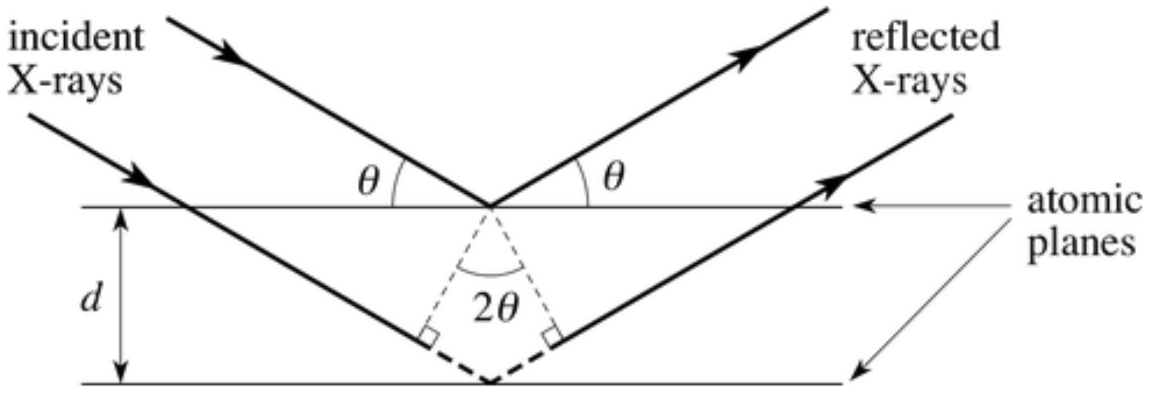

Figure 15: Basic principle of Bragg's Law *[25]*.

Each material characterization method used here is necessary for validation of the hypotheses drawn in this work. XRD is a method used for the identification of the unknown phases, which is important in progress to structurally inherit data on a newly synthesized material.

CHAPTER 3: EXPERIMENTAL PROCEDURE

3.1 FABRICATION

A first-hand DoE was executed to investigate specific parameters of Ga-based metallic alloys as an adhesive. An adhesive must obtain certain viscid properties to be manageable to create a hermetic seal. When producing the desired material, it is identified as an amalgamation because of the combination of a liquid and solid constituent. The liquid constituent in this study is called Galinstan, which is compositionally made up of Ga, In, and Sn. The solid ingredients are Cu particles, with a reported average diameter of eight microns.

Figure 16: Galinstan is a Ga-based alloy composed of 68.5wt% Ga, 21.5wt% In, 10wt% Sn. This container held the Galinstan and removed with a syringe when needed to be measured in the correct ratio.

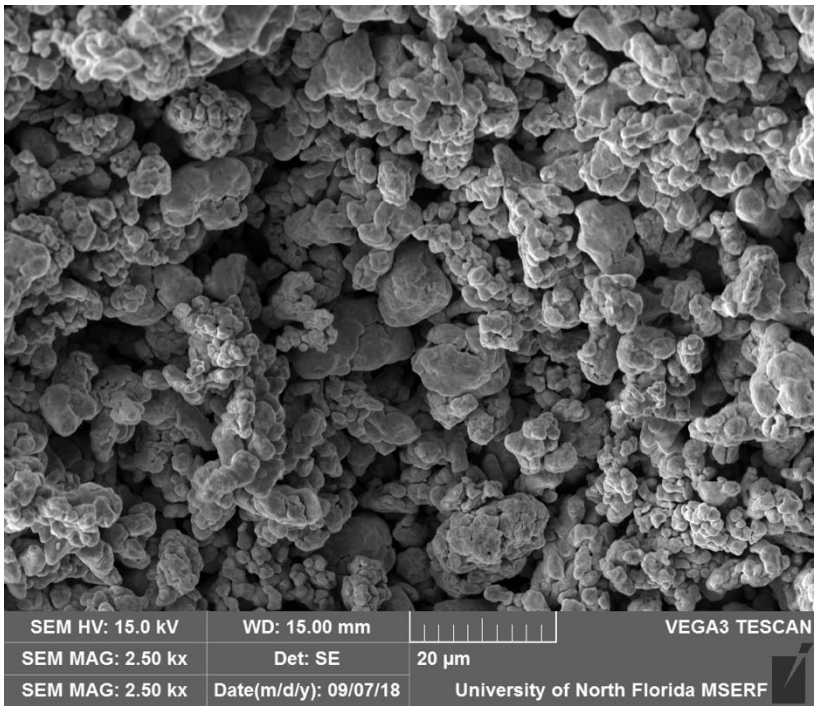

Figure 17: SEM image of Cu powder (8 µm) used as the packing factor in the amalgamation. Note the variable particle size and surface roughness of each particle.

Ga-based alloys are investigated at specific ratios of liquid to solid material. The ratios are spread at logical variable intervals to fabricate samples starting at one known condition that works. The governing ratio studied was 2:1 liquid to solid. The three other ratios were determined by considering half and double of the beginning ratio and a simple ratio amongst the others, resulting in 1:1, 4:3, and 4:1 relationship.

Preparation of the materials is an extremely important process because accuracy is essential as composition is a variable being studied for the effects of characterizing of this alloy. Galinstan is a Ga-based alloy composed of 68.5wt% Ga, 21.5wt% In, 10wt% Sn. This alloy is fabricated by measuring the three metals in a proportional ratio in the amount of 62.5 grams (g) of Ga, 21.5g of In, and 16.0g of Sn. The specifics of the proportion mentioned fills the entire glass container, pictured in Figure 16, which is used to store the Galinstan in the laboratory. The other constituent is distributed as a powder of consistent size, eight micron reported diameter, from a single batch.

The particle size and batch were held constant to remove additional confounding variables. When the two constituents are produced, the next step was weighing the materials to meet the relationship of the ratio being evaluated. For example, the 2:1 ratio was weighed with two grams of Galinstan and one gram of Cu particles in a microcentrifuge that is assembled in the amalgamator for mixing.

Figure 18: Dental Amalgamator used for the mechanical process of mixing these alloys.

The amalgamator used was a Daryou High Speed Digital Dental Amalgamator Amalgam Lab Electrical Mixer G6 USA (model/product code: HL-AH/1161082067). It has a mixing speed of 4200 revolutions per minute. A factor highly considered during the process of the two-metals amalgamated was the time the machine operates. Amalgamation time is crucial is creating an amalgam that can be handled properly. All the ratios had different lengths of amalgamating time, 2:1, 1:1, 4:3, and 4:1 had times of 12, 6, 8, and 5 seconds, respectively. The period of mixing was experimentally executed when creating the different ratios individually by setting the length of

time on the digital portion of the appliance. When the amalgams were over mixed, they turned into an extremely hot rock-like structure. This was not beneficial in forming an adhesive. If the Cu particles were still visible in the microcentrifuge due to under mixing, the amalgam is not completely developed and ready. To get a homogenous mixture, the amalgamation time was a key factor to be able to obtain a mixture which could be handled and applied to a device.

After developing the proper consistency from mixing, the material is placed in a tensile bar mold to be solidified. The tensile bar mold was 3D printed to ASTM standards using the computer-aided design (CAD) design file of ASTM D638 TypeIV, seen below [26].

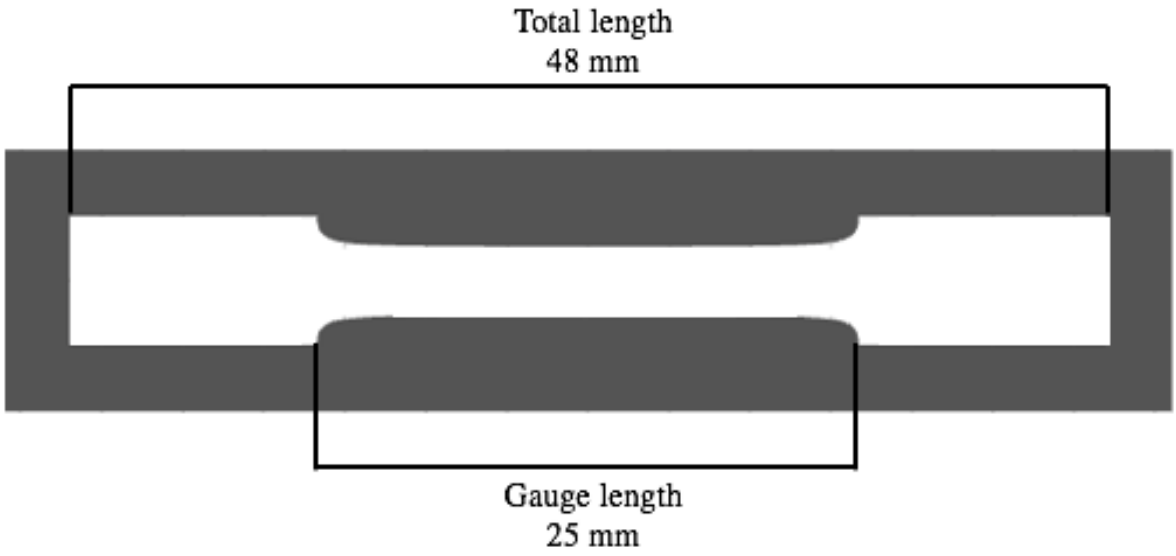

Figure 19: Tensile bar mold design used for the fabrication of metallic tensile bars. Width (W)= 3.12 mm, Thickness (t)= 3.15 mm

The use of a stereolithography (SLA) 3D printer was an ideal method for creating the molds because of the small size requirements needed for testing. The printer used was a Formlabs Form 2 (SN: ExcitedPeafowl, Somerville, MA), it is a class one laser product having an ultraviolet (UV) laser to cure liquid resin into hardened plastic. The wide selection of resins provided by Formlabs have different purposes and properties. For the tensile bar mold, the Grey Pro resin (RS-F2-PRGR-

1, Somerville, MA) was selected because its primary function is for assessing form, fit, and functionality as a mold.

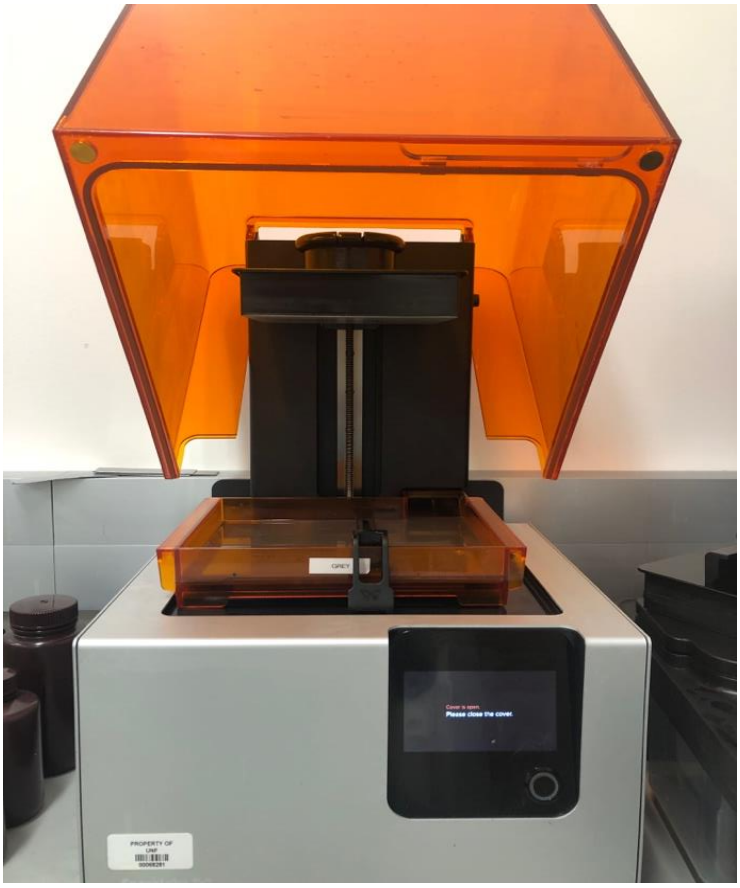

Figure 20: Formlabs Form 2 SLA 3D Printer

Amalgamating time was extremely important not only for the consistency but because the tensile bar molds are small, needing them to be completely packed with no air bubbles. Each specimen took about three Costar microcentrifuge tubes (1.7 mL) (CN: 3207, Salt Lake City, UT) to fill them completely.

The cure temperature is the other major experimental variable being investigated. Each ratio was cured at room temperature, 100°C, and 200°C for 24-hours until completely solidified. The minor temperature change from room temperature is considered because organic semiconductors operate at 100°C, and IC industry engineers through private conversations have requested the operating temperature of 200°C. Mixing time was discovered to be a factor in the

adhesion process. It was also discovered that the adhesion status of Ga-based alloys can be controlled by a slight temperature change [2]. At each ratio, 2:1, 1:1, 4:3, and 4:1, seven samples were fabricated and cured at each different temperature resulting in almost 90 samples made throughout this study.

Figure 21: Metallic tensile specimen (2:1 @ 100°C) after being cured and 3D printed mold was removed. Samples were ready for mechanical and material characterization.

When the specimens cured, the 3D printed material was carefully released to get the final product of the sample. The final dimensions of the bar have a gauge length of 25 mm, gauge width of 3.12 mm, and a gauge thickness equal to 3.15 mm. The overall length of these tensile bars was 47.75 mm. A first screening – solidification or no solidification – process is implemented in the beginning stage of the characterizing the amalgamation.

CHAPTER 4: RESULTS

4.1 DEVELOPMENT OF THE MICROSTRUCTURE

Room temperature Ga-based alloys have not been investigated to the extent where there is a significant amount of literature on the development of a solid after being amalgamated. Hg-based amalgamations in previous research and applications have a similar process but are considerably different due to the use of Ga and other alloyed metals. From the literature, a hypothesis can be drawn on the development of the microstructure in Galinstan and Cu powder amalgamation. Dissolution of the materials, diffusion, IMCs composition, and epitaxial growth of the IMC grains are potential mechanisms used in the formation [2]. Also, factors such as cure time and environmental influences should be taken into consideration.

The two constituents, Galinstan and Cu powder, are amalgamated together to begin the process of dissolution. The solute in this case would be the Cu particles and Galinstan is classified as the solvent. When the mixture is mechanically alloyed, the solute is dispersed into the solvent. Liquid Ga-based alloys interact with solid Cu substrates [2]. The full dispersion of the Cu particles into the liquid substance will depend on the ability of the Ga to wet the substrate material [2]. Wetting of the substrate material is heavily influenced by the liquid-solid alloying [2]. Before the process of amalgamation occurs, the separated constituents are drawn to diffuse. The concentration will equalize from a non-homogenous to homogenous mixture. The particles will be transferred from a high concentration to a low concentration given the concentration gradient.

The solidification process is based off the metals interacting with each other chemically. The interaction of the Ga and In in the Ga-In-Sn alloy form a liquid strongly influencing the property result of the melting point being -19°C [2, 27]. The Cu powder (8μm) is mixed as a

material for the Galinstan to interact with as a diffusion solidifying agent [28]. After being mechanically alloyed, the next figure shows the beginning of the diffusion process.

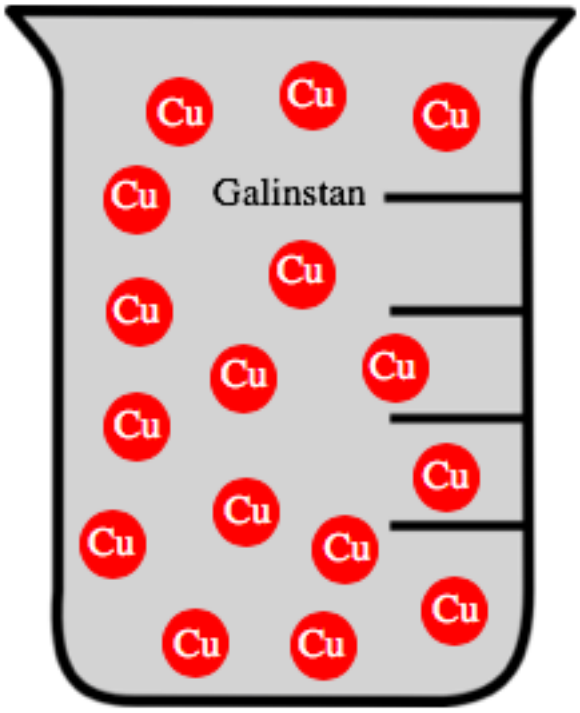

Figure 22: Cu particles being dispersed into Galinstan after being mixed. The two constituents started as two separate constituents, but kinetic energy used in mixes the liquid and solid to evenly disperse Cu particles throughout.

With the addition of the Cu component, there are studies to believe that the Cu and Ga interact to form an IMC [2, 28]. Ga has high solubility in the face centered cubic (FCC) Cu-rich phase [2]. Since Ga and Cu are assumed to form a bond, Sn and In interact to result in a metal bond, as seen in Figure 23.

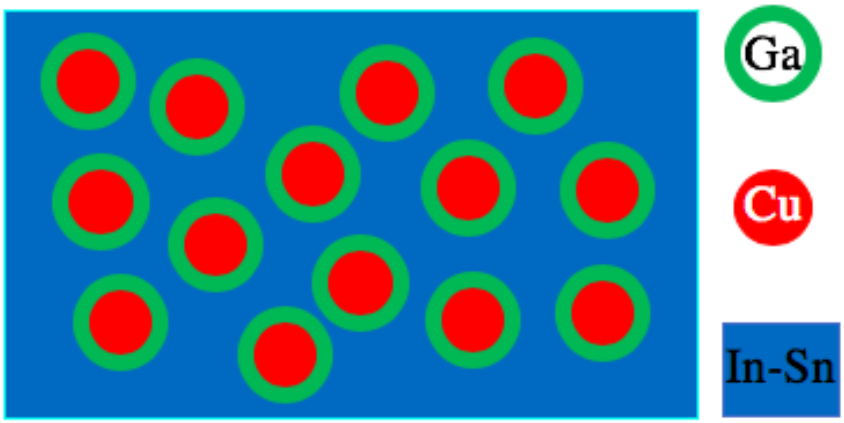

Figure 23: The solidified formation of the alloy, theoretically, Cu and Ga begin to create some phase in a metallic bond and In and Sn nucleate out of the liquid phase and precipitate a crystal.

With the different liquid and solid metals interacting, the compounds can create distinct properties in the resulting alloy. Features influenced by developed phases are the mechanical performance, microstructure, thermal conductivity, and electrical conductivity. For example, if the Cu and Ga bond creates a brittle region, this could negatively influence the mechanical properties of the specimen. In previous literature with a similar metallic alloy, cracks and voids were exposed in the CuGa formation due to the $CuGa_2$ phase forming at the interface [2]. In the same study, the effective packaging of eutectic Ga and In (EGaIn) and $CuGa_2$ remarkably enhanced the electrical conductivity ($6x10^6$ S m^{-1}) and thermal conductivity (50 W $m^{-1}K^{-1}$) compared to just EGaIn, $3.4x10^6$ S m^{-1} and 40 W $m^{-1}K^{-1}$, the electrical and thermal conductance of EGaIn respectively [2]. As this topic has not been heavily investigated, the results are being further investigated because the increase in thermal and electrical conductivity indicates that the composite behaves differently from the matrix [29]. These studies have helped design the hypothesis of the phases that form in the solidification of the Ga-based metallic alloy studied in this thesis. Factors like cure temperature are believed to impact the phases as thermal energy input will allow for higher diffusion. Cure

temperature will be investigated in this study to see the effect it has on the mechanical and material characterization.

4.2 INTRODUCTION TO MATERIAL ANALYSIS

Material characterization is a process of investigating a materials structural and chemical composition. This thesis follows the fundamental development of the process, structure, and property of the room temperature Ga-based metallic alloy. Properties of the alloy are determined mechanically and chemically using tension testing, SEM imaging, EDS, and XRD. The analysis is performed on machines in MSERF located on the University of North Florida campus. Without the proper equipment, the development of characteristics with supporting data for a material are unobtainable.

The sample prepared in the packing ratio of 4:1 was not mechanically tested or prepared for SEM analysis. The liquid constituent in this case was four times the amount of powder to be amalgamated. Not only was the 4:1 relationship unappreciable to handle, it failed to solidify after 24-hours at the three temperatures investigated. This ratio would be unreasonable for the properties TIMs desire. This investigation entailed a first screening of examining the different packing ratios ability to solidify. The 4:1 mixing ratio did not solidify; therefore, it was not characterized in this thesis.

4.2.1 MECHANICAL CHARACTERIZATION

Tensile testing was performed to generate data on the mechanical properties of this Ga-based metallic alloy. At each liquid to solid ratio and cure temperature, there were approximately six samples tested to calculate a range of values for their average tensile strength. The strain rate used in all experiments was 2 mm/min, consistent with ASTM D638. For example, six samples were pulled of the ratio 2:1 cured at room temperature, six samples at 2:1 cured at 100°C, and so

on. Tensile testing was performed because microelectronic companies desire this value for the engineering application of a TIM. The specimen prepared were pulled on a Shimadzu tensile testing machine (Model#: AGS-50kNX, Kyoto, Japan). With careful consideration to the size of these specimen and in accordance with ASTM standards, the load rate applied for testing was 2 mm/min.

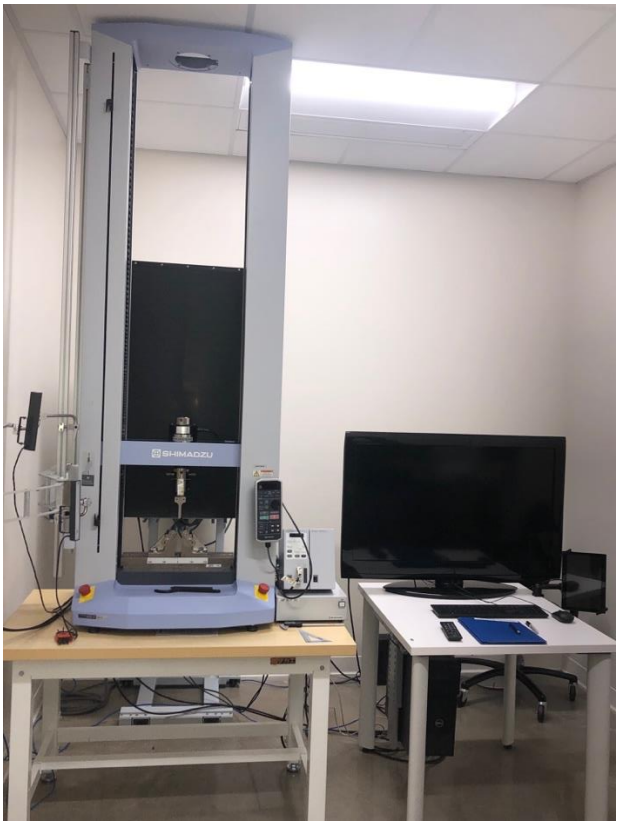

Figure 24: Shimadzu tensile machine operated for testing of the samples.

Table 1 below shows the average maximum stress of each sample condition used, with calculated standard deviations. The optimal result for average stress corresponds to the specimen with a 2:1 ratio cured at 100°C, with a calculated value of 32.0 MPa. All the average stresses are displayed for each ratio and temperature tested.

Table 1: Average stresses and standard deviations calculated for each ratio and temperature.

Mixing Ratio	Temperature	Average Stress (MPa)	Standard Deviation
2:1	Room Temperature	20.8	8.2
2:1	100°C	32.0	5.7
2:1	200°C	14.8	7.6
1:1	Room Temperature	23.2	11.0
1:1	100°C	15.3	5.9
1:1	200°C	17.7	7.0
4:3	Room Temperature	24.5	2.7
4:3	100°C	16.1	11.4
4:3	200°C	11.8	3.3

In Figure 25 below, the stress-strain curve for the 2:1 cured at 100°C is illustrated. This individual specimen held the greatest amount of load before fracturing, having the ultimate tensile strength of around 36 MPa. For supporting data of the stress and strain and how this relationship reacts, a computational code using the software MATLAB was utilized to manipulate the raw data of force versus displacement to create a stress versus strain curve. This code can be found in Appendix A.

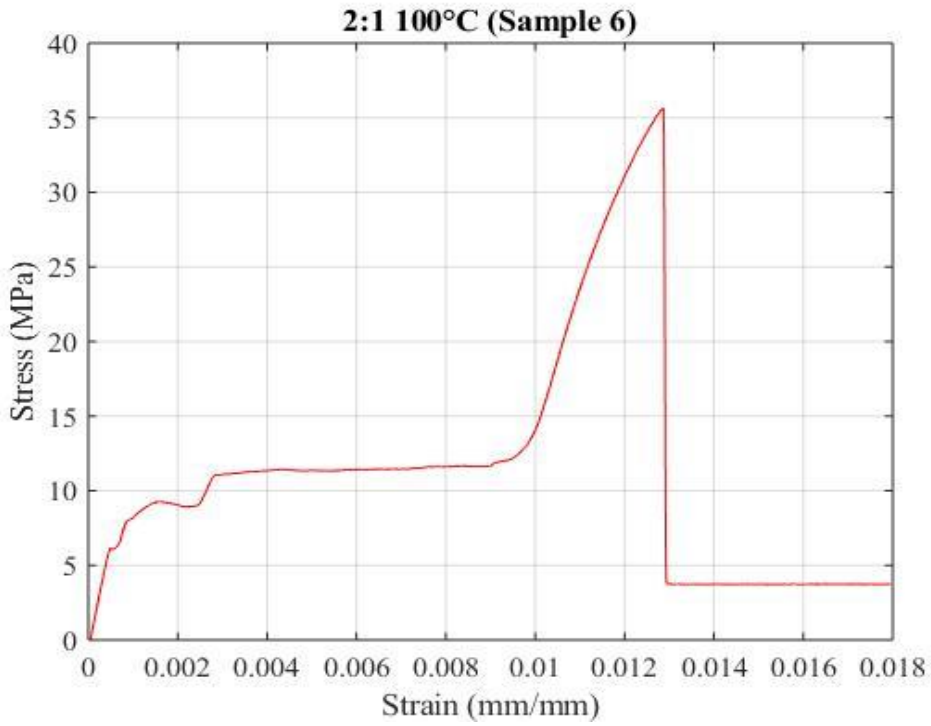

Figure 25: Stress vs. Strain curve for 2:1 @ 100°C

All the ratios prepared that are cured at room temperature resulted in similar maximum tensile strength values, on the order of 22 MPa. These values support the conclusion that mixing ratio does not have a huge factor in the strength of the alloy. The mixing ratio itself does not seem to impact the strength but an evenly dispersed mixture is important for achieving the strongest amalgamations. The intermetallic alloy dictates the mechanical properties of the resulting alloy since it forms its weakest link in the inhomogeneous mixture, due to its brittle nature [17]. Although Ga-Cu-In-Sn materials are referred to as alloys, they may be closer metallurgically to ceramic materials in which the powder particles are held together by limited alloying action with the liquid component [30]. In respect to having an evenly mixed alloy, if there was a void in the specimen after curing, the sample would fracture in that region due to that empty space. Due to the brittleness of the material, gripping the specimen in the clamps of the tensile machine could cause local plastic deformation of the surface, to create an undesired behavior in the stress-strain

curve. Another complication experienced would be the idea to eliminate deformation from the grips by overcompensating and not tightening the shoulder to a set point, which would lead to the sample slipping in the machine.

The average stresses of these specimen cured at room temperature are all calculated to have a value in the lower twenties, which is the next highest average set of data with standard deviations that do not show a specific pattern. In Figure 26, the 1:1 sample #3 cured at room temperature shows behavior that can be analyzed in sections. The specimen failed properly fracturing in the middle of the gauge length. In the first region from 0.0%-0.5% strain, the specimen experiences an increase in load from the initial force. From 0.5%-1.5%, there is a constant region which could represent slip in the grip region. Usually, this type of behavior on the graph would be seen in a polymer due to elastic properties, but because ceramic-like materials and metals do not experience this strain behavior, this region should be classified as slip. The region between 1.5%-2.0% then experiences a significant spike in stress, identical to a brittle material which leads to the point of failure.

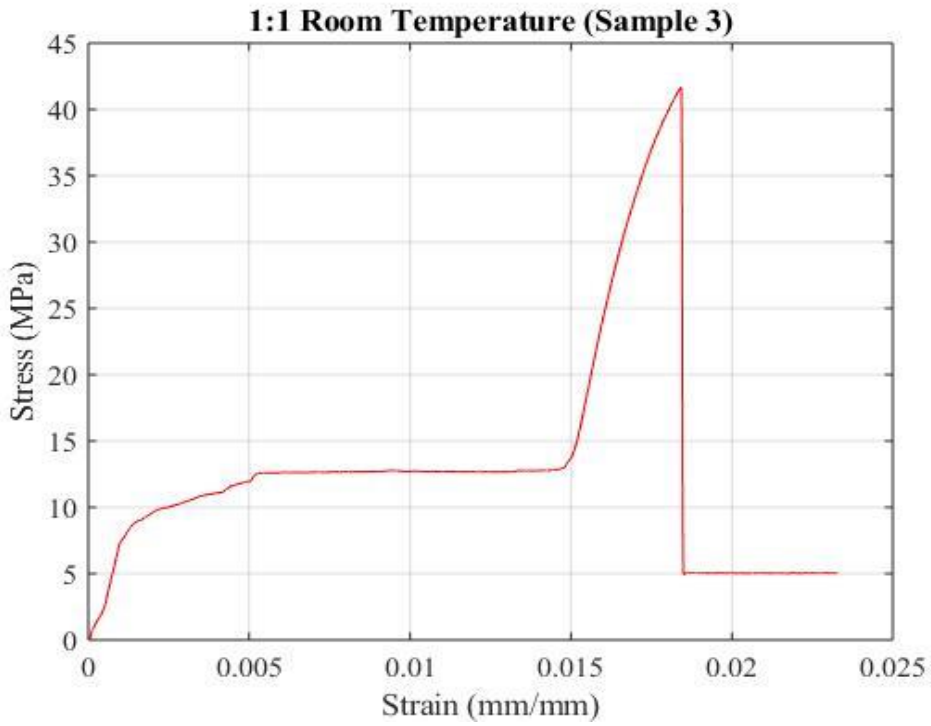

Figure 26: Stress vs. Strain curve for 1:1 @ Room Temperature

The 4:3 liquid to solid relationship cured at room temperature average to about the same value of stress experienced before failure as the 1:1 at room temperature, but the stress-strain behavior does not visually look the same. The individual sample #5 tested with the greatest result is seen in Figure 27, was around 28 MPa. The qualitative nature of the curve has an escalating elastic modulus from the window of strain ranging from 0.0%-0.2% representing an extreme stiffness. The entirety of the remaining portion of the graph shows a lower modulus until point of failure; this region on the graph represents the outside of the surface in the cross-sectional area surrounding a void initiating fracture. The void in the cross-sectional area of break is an amalgamation issue. It does directly influence the strength of the material as it will be weakest at this point where the material developed an empty space.

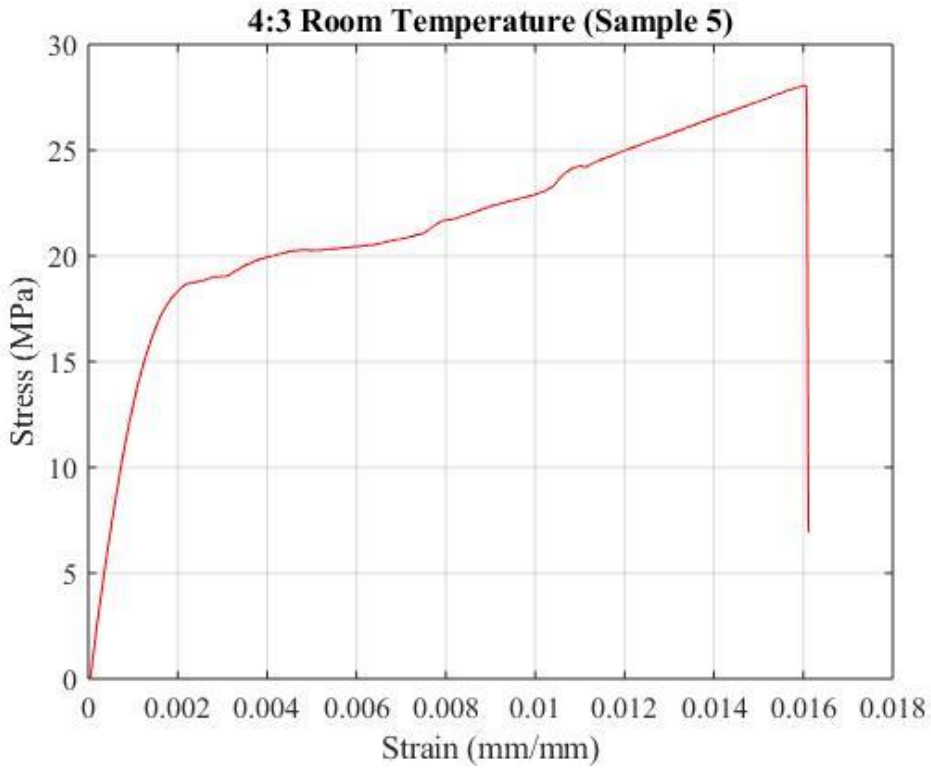

Figure 27: Stress vs. Strain curve for 4:3 @ room temperature

Figure 28: Image of fractured specimen cured at room temperature with a mixing ratio of 4:3 displaying the region of fracture in the gauge length of the tensile bar. The point of fracture was the area where there is a void located in the cross section.

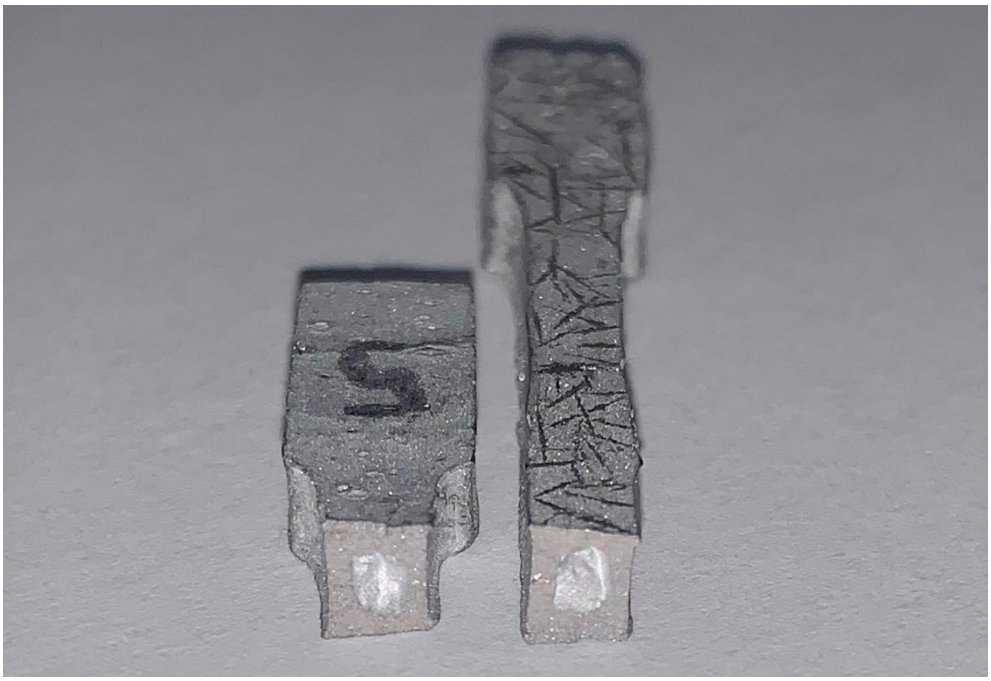

Figure 29: Image of the broken specimen mixed at 4:3 and cured at room temperature cross-section displayed the void.

Since there is no significant difference in the tensile strengths when comparing the different mixing ratio of liquid to solid, the other variable investigated was the change in cure temperature. As the temperature increases for curing, the strength decreases significantly. The ultimate tensile strength obtained for sample #14, having a mixing ratio of 2:1 cured at 200°C, can be seen in Figure 30. Due to this decrease in strength, the material becomes noticeably more brittle. When placing the specimen in the clamps for testing, the grip tightening induces stress to the shoulders of the sample creating the fracture in that region of the tensile bar. The nature of this break is not reflective of the material's true properties. The data gained for the tensile strengths of the 2:1 cured at 200°C are invalid due to the deformation of the surface from the grips causing the fracture region in the shoulder. This occurrence defeats the importance of reducing the cross-sectional area to measure the deformation and failure concentrated in the region of the gauge length. The failure event in the shoulder experimentally proved that the material is weaker when cured at a higher temperature.

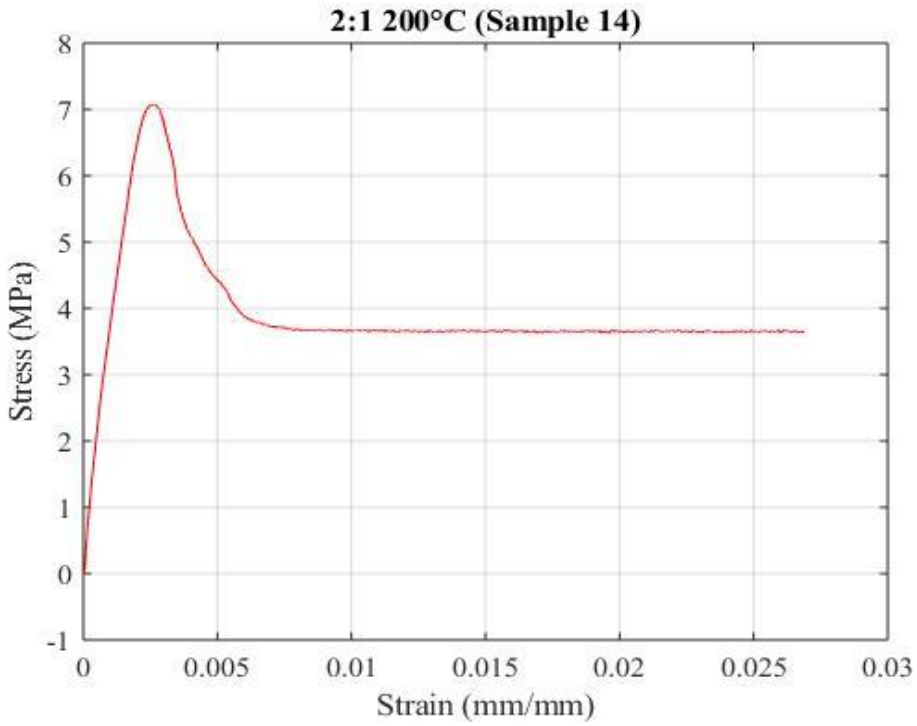

Figure 30: Stress vs. Strain curve for 2:1 @ 200°C

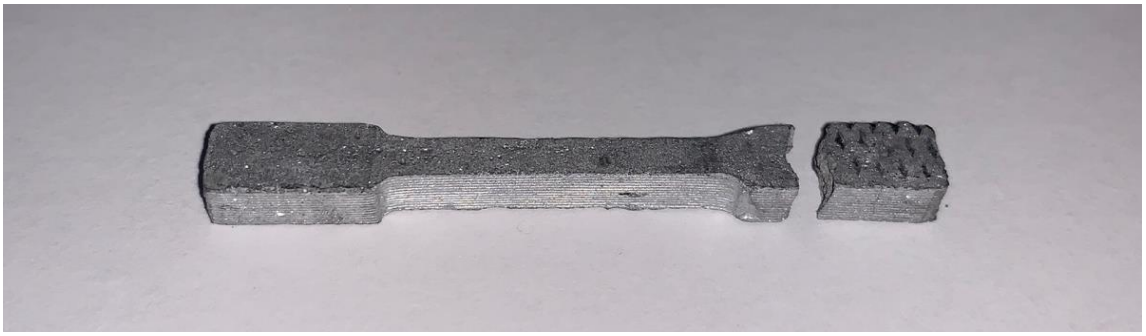

Figure 31: Image of the broken specimen mixed at 2:1 and cured at 200°C fracturing on the shoulder region of the tensile bar due to deformation from the grips.

Figure 32: Image of the shoulder displaying the indentation from the grips of the 2:1 @ 200°C.

The remainder of the stress versus strain curves for all the specimen can be found in Appendix B. The method of tensile testing was successful in the material synthesis of Ga-based metallic alloys to obtain the result of getting the ultimate tensile strengths. The performances of the Ga-based alloys showed complications during the process of tensile testing, which made it hard to interpret what exactly happens during testing due to various factors. When placing the specimen in the tensile machine, the samples could experience stress induced deformation of the surface material because of the clamps grip. This constricted impact to the shoulders created hesitance in clamping the samples in the grips too tight. With the hesitance in securing your sample properly, the created potential slipping when the force is loaded. For future research, three-point bend testing would be a more beneficial way to characterize mechanical properties because of the brittle nature of the amalgam. The advantage for this test method would lie in the ease of the preparation and testing of the sample while experiencing load to characterize the mechanical behavior. It would result in the stress required to fracture a material in the motion of bending, the stress-deflection curve. Another method to test the mechanical properties of this material would be hardness testing. It results in evaluating a materials ability to resist deformation, bending, and scratching. Microhardness testing measurements can be correlated to yield strength. The brittle-like nature of

this Ga-based alloy may be more accurate as less force would be applied to the material in a less strenuous manner.

4.2.2 MATERIAL CHARACTERIZATION

Each specimen was analyzed under the SEM, which was equipped with EDS. The compounds formed were then confirmed under XRD for the identifying phase formation in the alloy. Under the SEM, the cross-sectional areas were imaged at their fractured surface followed by being polished down three times, to perform quasi-serial sectioning. The concentration for imaging the different sections was to characterize the break of the samples and to see the developed formation of the phases given the different variables changed during fabrication. The fractured samples were readily prepared for the SEM analysis because of their conductive properties of being a metallic alloy. For polishing the samples down, the process used for a uniformly flat and smooth cross-section is shown below in Table 2. The products used for the metallographic surface preparation and analysis were provided by the Allied High-Tech Products, Inc. (Rancho Dominuez, CA).

Table 2: Polishing steps for the samples imaged under the SEM.

Abrasive surface	Lubricant	Force (LbF)	Time (minutes)
120 Grit Silicon Carbide Paper Adhesive Back 8” Disc	Water	2	1
320 Grit Silicon Carbide Paper Adhesive Back 8” Disc	Water	2	1
600 Grit Silicon Carbide Paper Adhesive Back 8” Disc	Water	2	1
800 Grit Silicon Carbide Paper Adhesive Back 8” Disc	Water	2	1
1200 (P-4000) Grit Silicon Carbide Paper Adhesive Back 8” Disc	Water	2	2
Gold Label Adhesive Back Disc 8”/200 mm	6 µm Polycrystalline Diamond Suspension Glycol Based	2	2
White Label Adhesive Back Disc 8”/200 mm	1 µm Polycrystalline Diamond Suspension Glycol Based	2	2
Final A Adhesive Back Disc 8”/200 mm	0.04 µm Collodial Silica Suspension Non-stick/Rinsable	2	1

The mixing ratio and temperature were the two experimental variables in characterizing this material. In Figure 33, 34, and 35 below, the same cure temperature is used for all the specimens at the three different ratios. Considering the different liquid to solid relationships, all three images show a uniformly surfaced area with no pores throughout. There is also no significant correlation to a difference in strength for the different ratios.

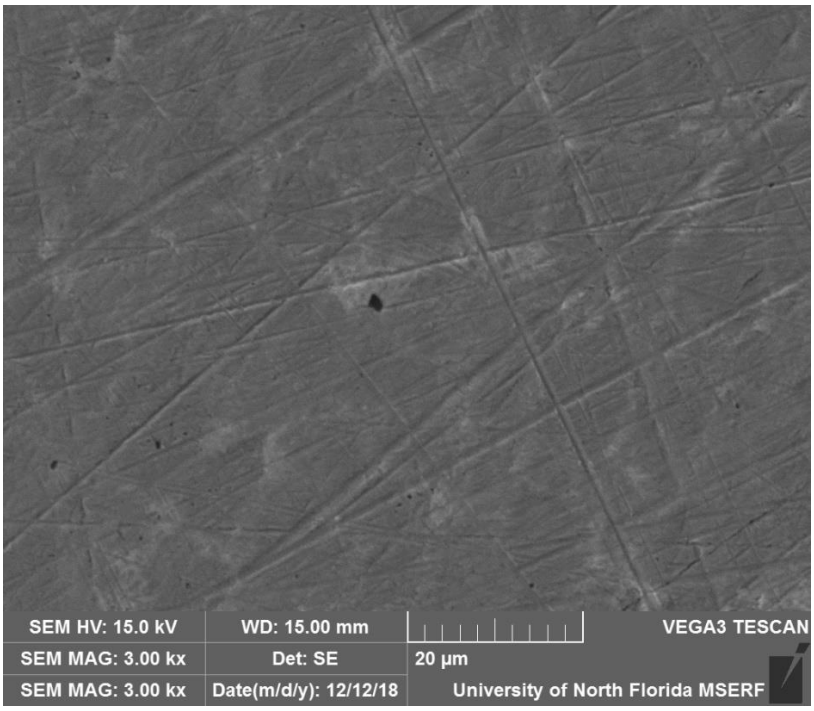

Figure 33: SEM image of 1:1 cured at room temperature of polished area on cross section. Average strength for this specimen was 20.8 MPa.

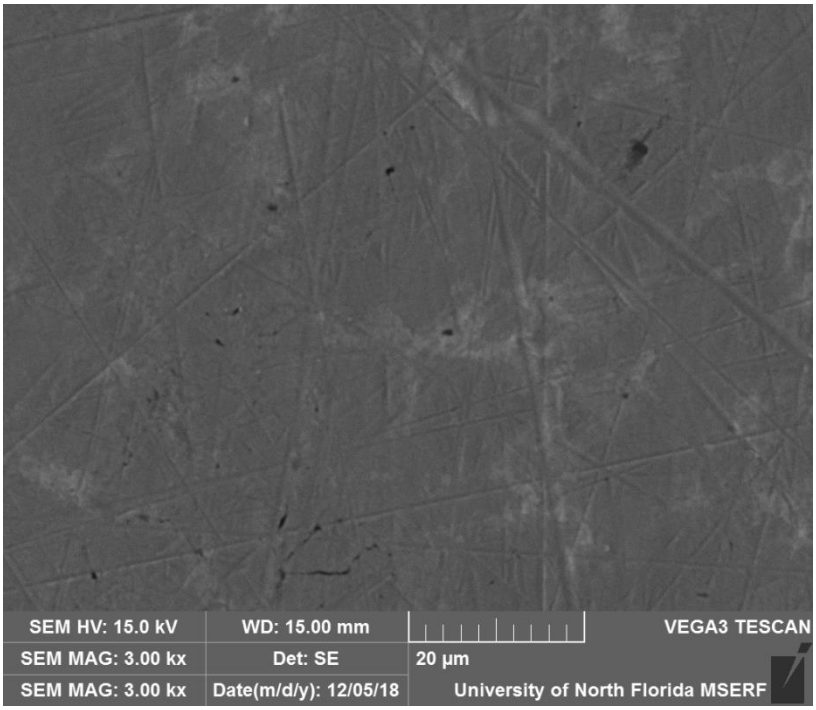

Figure 34: SEM image of 2:1 cured at room temperature of polished area on cross section. Average strength for this specimen was 23.2 MPa.

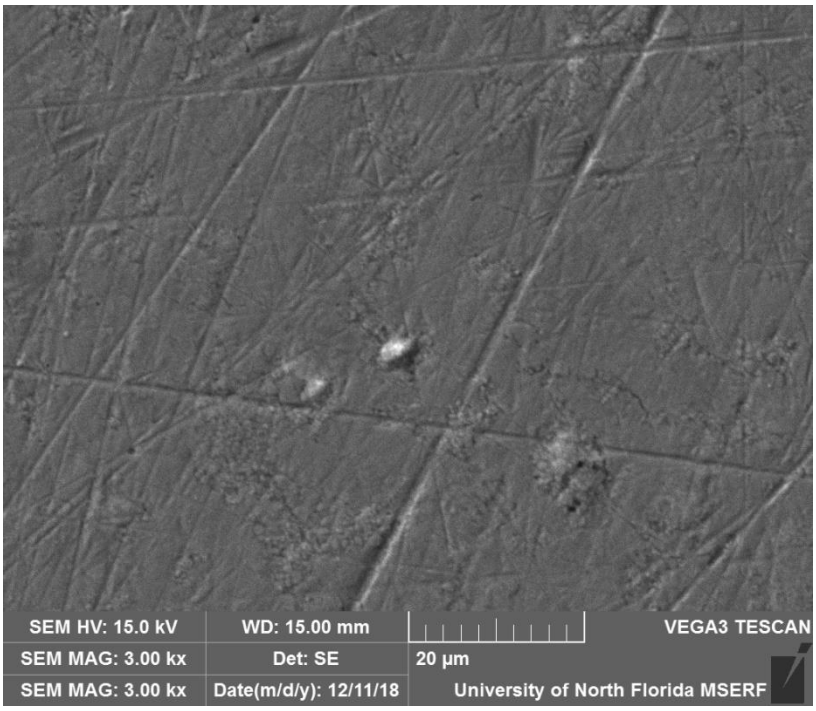

Figure 35: SEM image of 4:3 cured at room temperature of polished area on cross section. Average strength for this specimen was 24.5 MPa.

The next set of images is comparing the fractured surface of each sample with the same ratio cured at a different temperature. The 2:1 specimen cured at room temperature showed a surface with more dimples consuming the imaged area, indicating a more ductile break. This allows the material cured at room temperature to withstand more tensile stress than the sample cured at 200°C. The material cured at a higher temperature has plate-like pieces throughout the SEM image, and less dimples, which correlates to a material behaving more brittle. The only difference between these specimens is a change in temperature, therefore, temperature creates a change in the material being ductile to brittle. From room temperature to 200°C, the strength decreases significantly. The change in strength correlates to microstructure and the new phases forming when heating. The differences in the fractured surfaces at the three temperatures can be seen in the figures below.

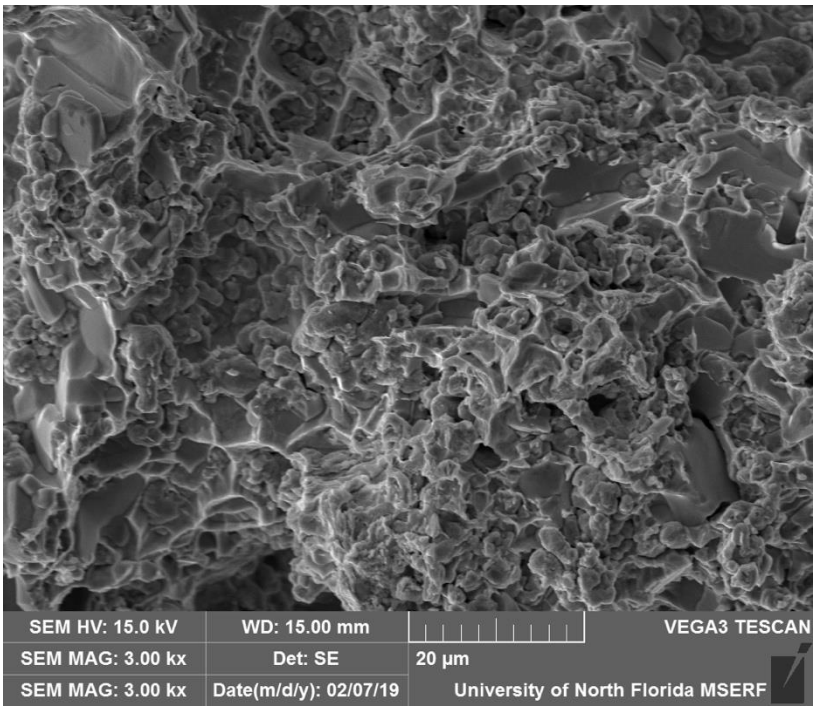

Figure 36: SEM image of fractured surface of specimen 2:1 at room temperature.

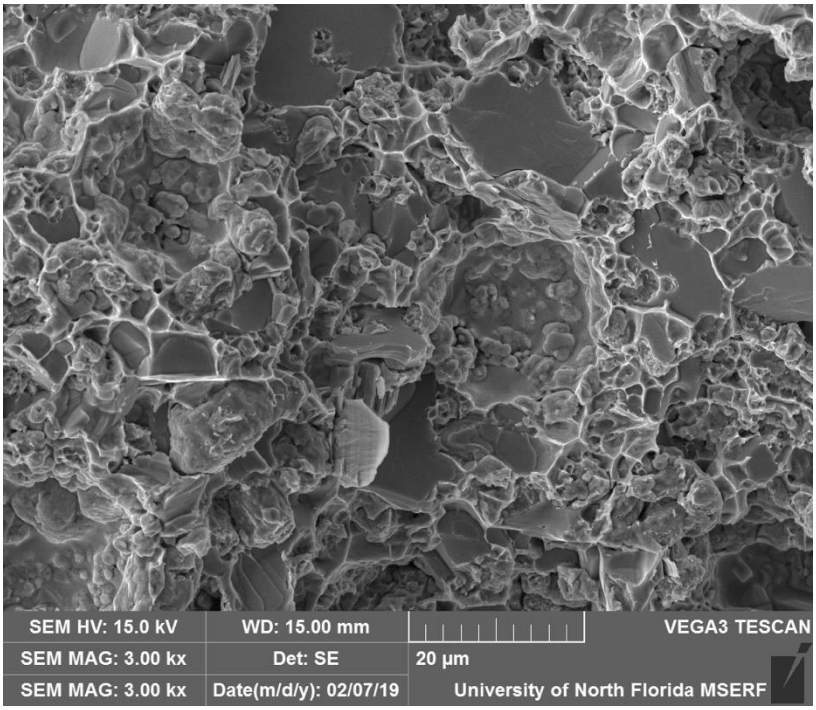

Figure 37: SEM image of fractured surface of specimen 2:1 at 100°C.

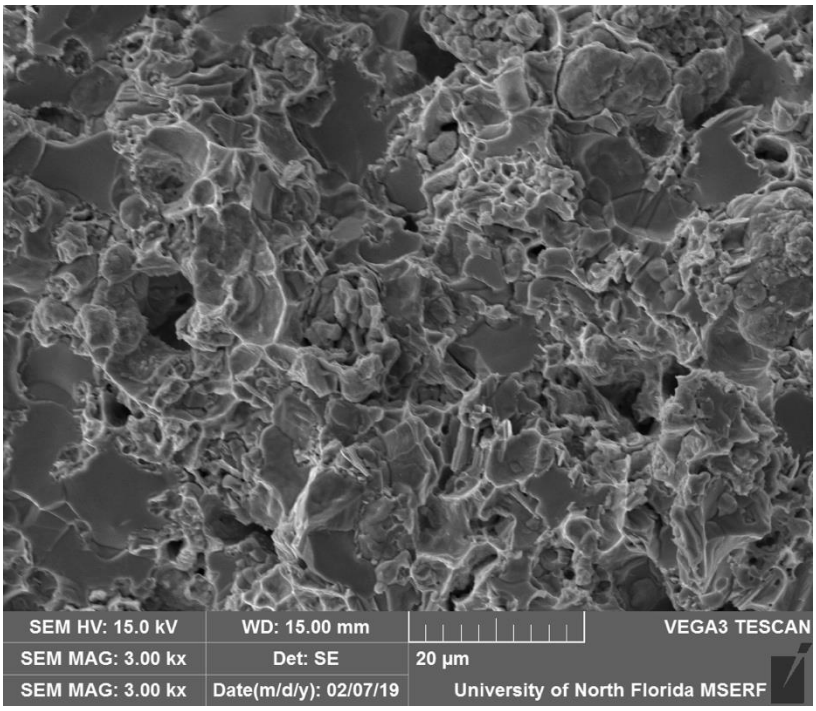

Figure 38: SEM image of fractured surface of specimen 2:1 at 200°C.

Another comparison that can be concluded from the change in temperature is the growth of the pores in the material, seen in Figure 39, 40, and 41. Pores are highly dependent on temperature. Annealing the samples forms pores which can correlate to the weaker average tensile strength of the specimen cured in the different heated environments.

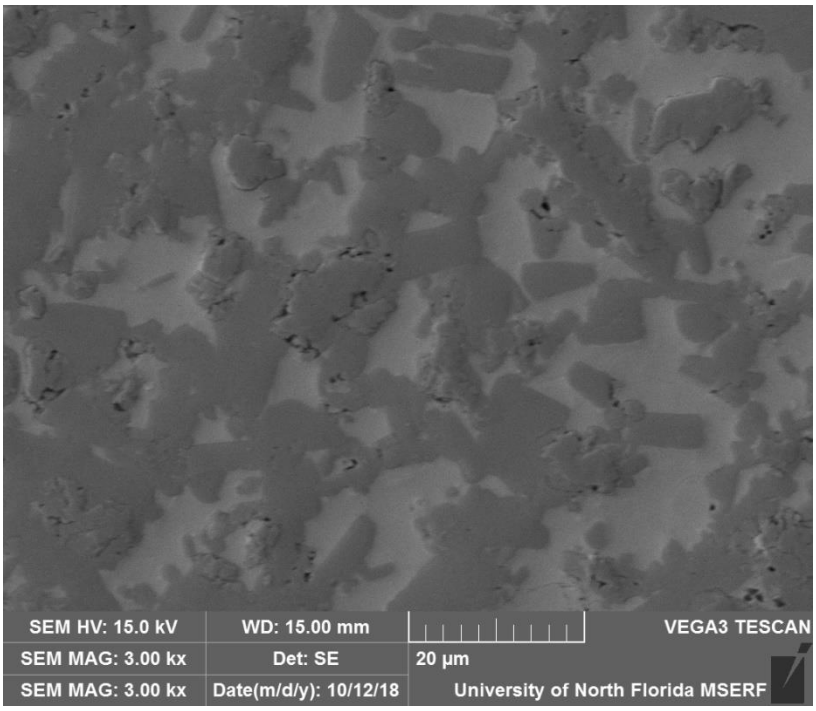

Figure 39: SEM image of polished surface of 2:1 sample at room temperature.

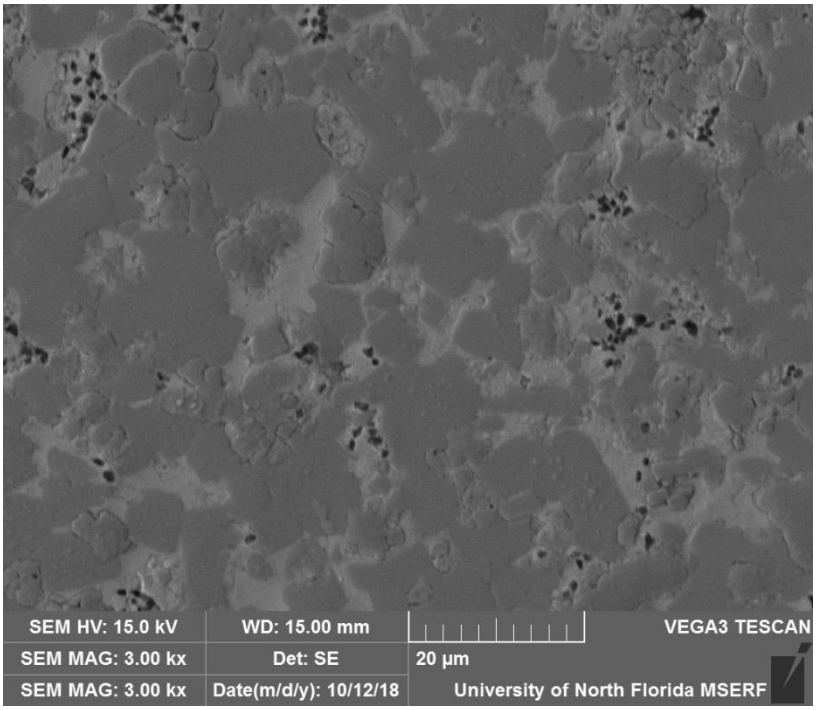

Figure 40: SEM image of polished surface of 2:1 sample at 100°C.

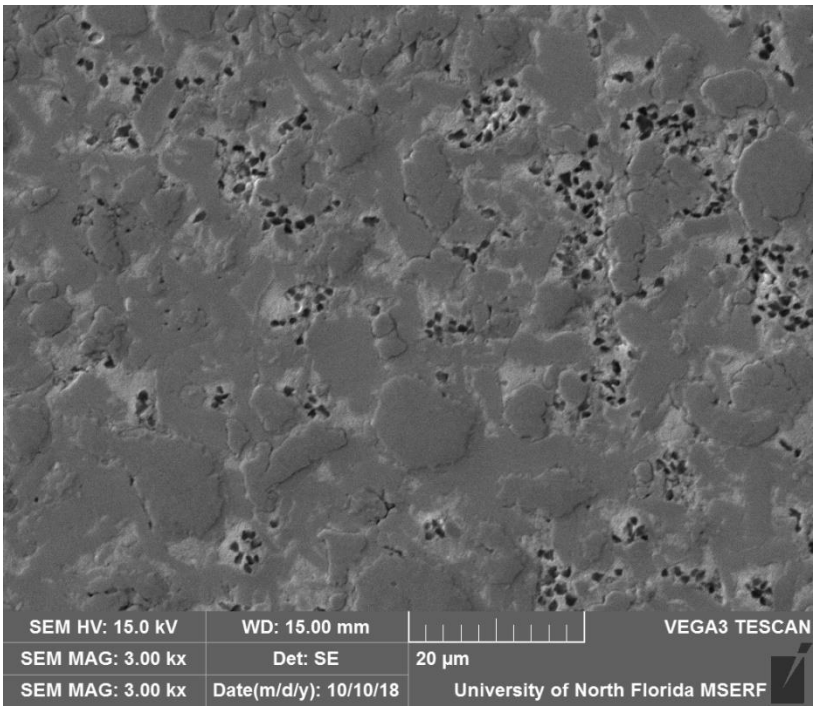

Figure 41: SEM image of polished surface of 1:1 sample at 200°C.

The next four consecutive images are an SEM image, the summation chemical mapping, and the individual chemical maps of the 1:1 at room temperature and 200°C. Figure 42, 43, 44, and 45 show the conclusive result from this EDS analysis that Cu is left in some areas and there are brighter areas showing of In and Sn that do not appear to have Cu and Ga in them. In the individual mappings, Figure 43 and Figure 45 for both cure temperatures, there is a clear Cu phase that has no other elements mixed in. There is a Ga phase located outside the regions of just pure Cu. The Ga phase at all locations has Cu mixed into it, also. There are also In and Sn regions that are all overlapping. Based on the spatial distribution, there must be at least three compounds present: Cu, Cu and Ga, and In and Sn. Based on the ratio present in the mixture, the In and Sn are likely to form In_2Sn, the Cu and Ga may be one or more phases, which will be examined in the XRD as the local quantitative data is inconclusive here based on the contrast.

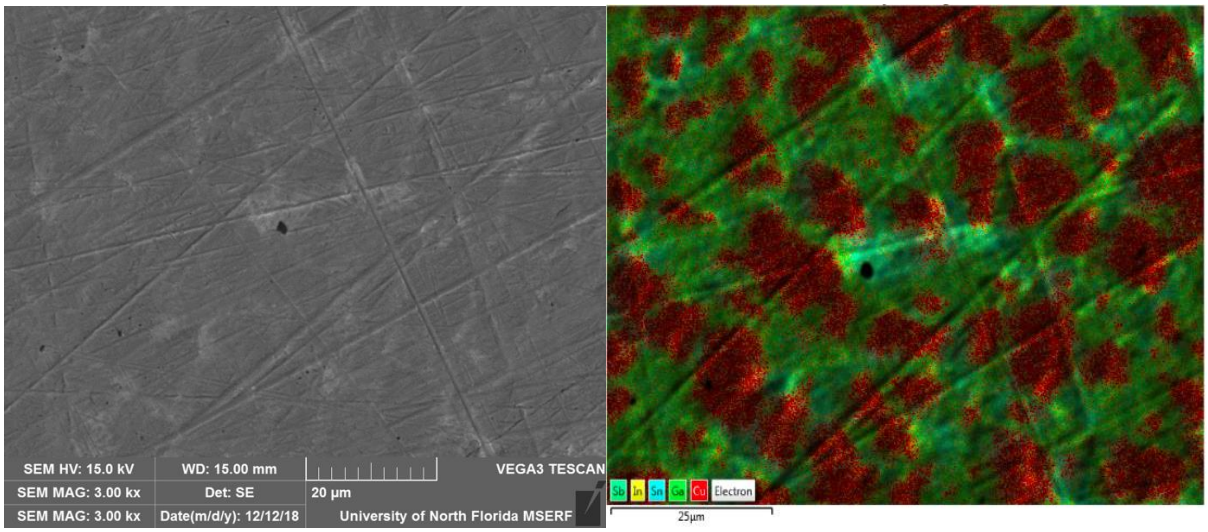

Figure 42: SEM image and EDS of 1:1 cured at room temperature.

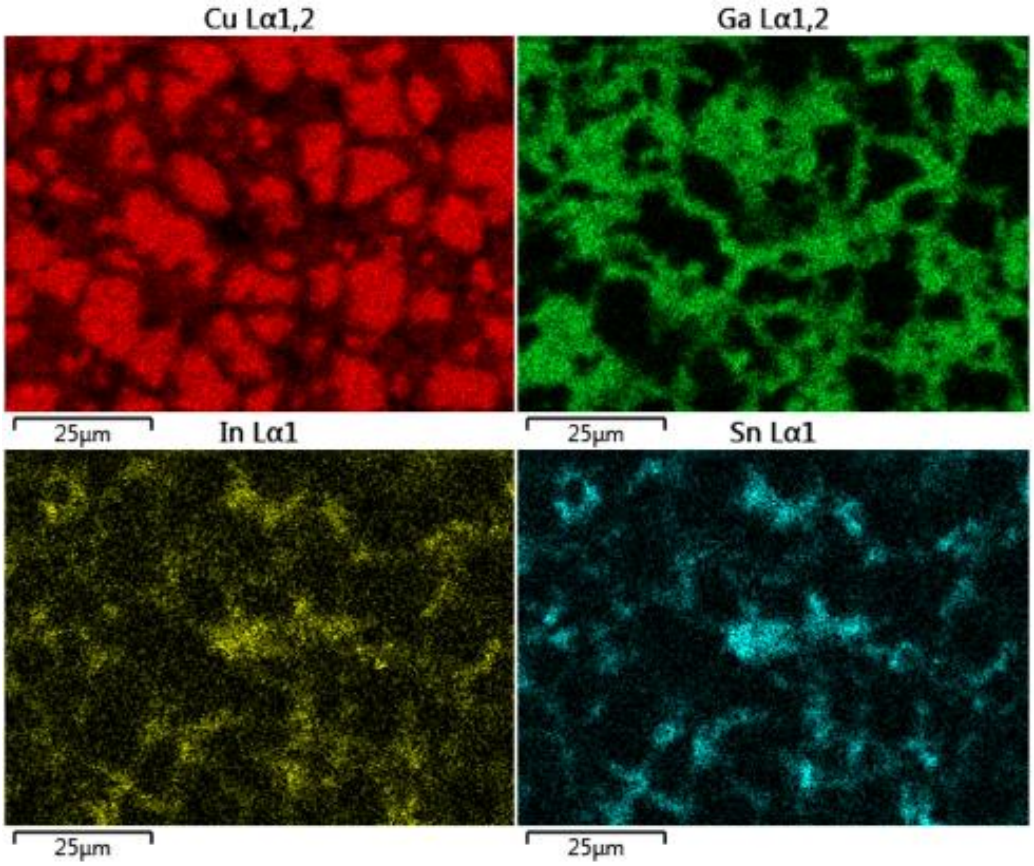

Figure 43: Individual chemical mapping images of elements displayed throughout 1:1 cured at room temperature.

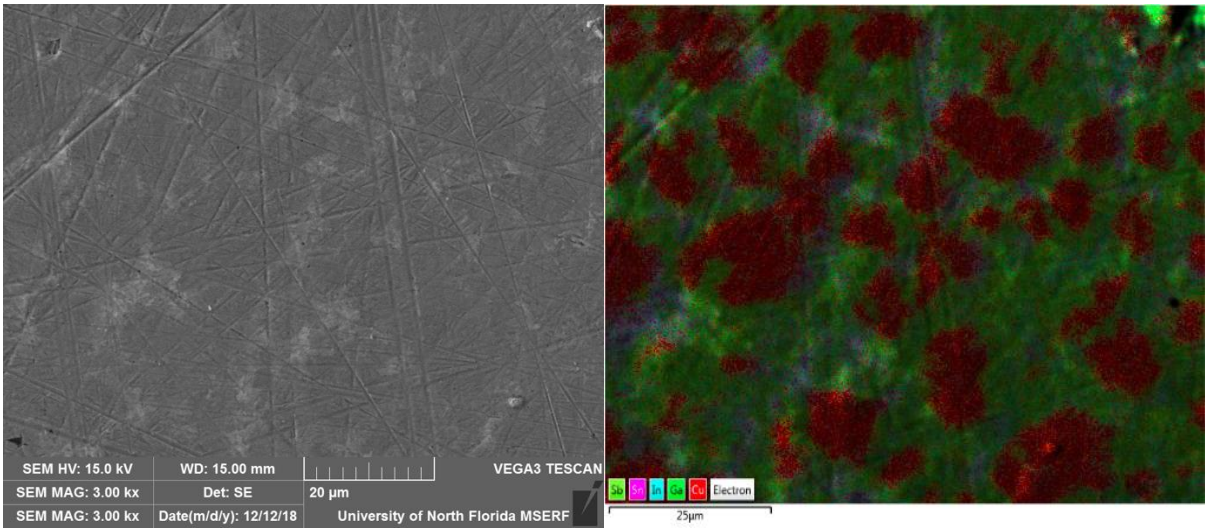

Figure 44: SEM image and EDS of 1:1 cured at 200°C.

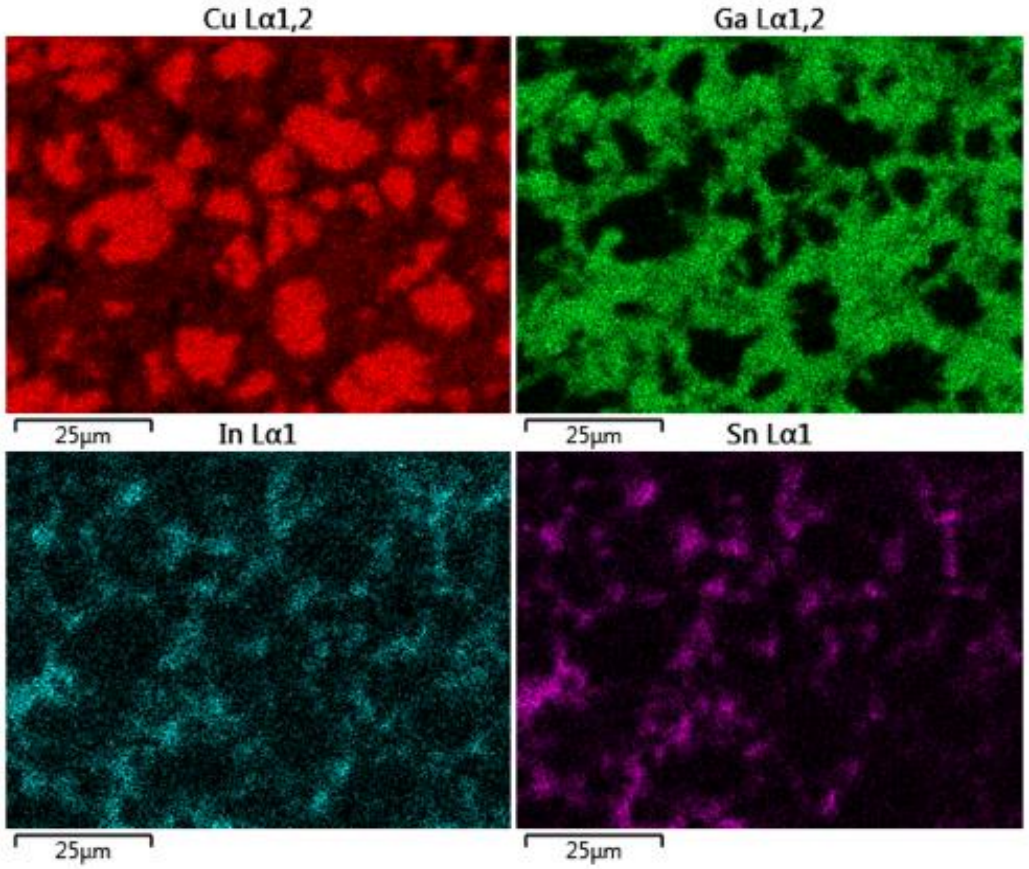

Figure 45: Individual chemical mapping images of elements displayed throughout 1:1 cured at 200°C.

When analyzing the morphology of a fractured surface, there will be differences on the surfaces structure depending on what type of break is experienced during mechanical testing. The significant difference in strength from lower to higher temperatures correlates to the dimple formation in the room temperature versus to the plate-like features in 200°C sample, in Figure 46 and Figure 50, respectively. The distinctive features motivate the desire to determine the phase distribution developed throughout the image. The next series of images are the fractured surfaces of each temperature with their corresponding chemical mapping distribution. In the room temperature specimen below, dimpled ridges appear to occur with the content of In and Sn. When dimples are apparent, this corresponds to a ductile fracture. This analysis is telling about the phase mapping as some compound with In and Sn is ductile explaining the response of the break to the characteristics. Ductile ridge formation occurs predominantly in the In and Sn regions. Analyzing the other regions leads to the conclusion that they are smooth or unfused particles that are bunched. The top right region of just Cu can be correlated to the unfused bunch of particles, potentially leaving a gap, which would pull out with no strength.

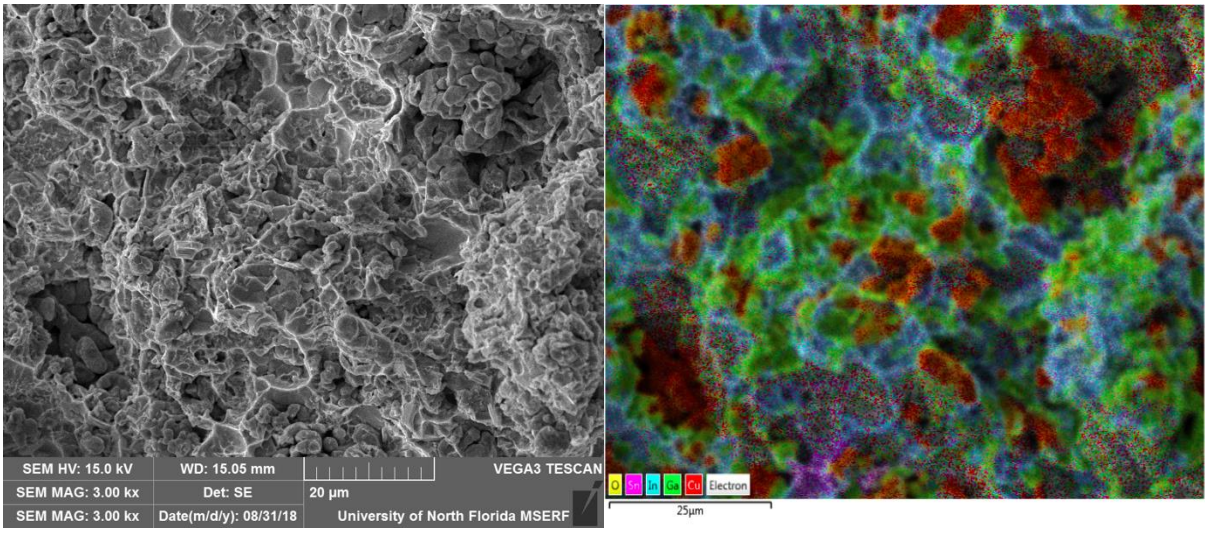

Figure 46: SEM image and EDS of fractured surface at 1:1 cured at room temperature.

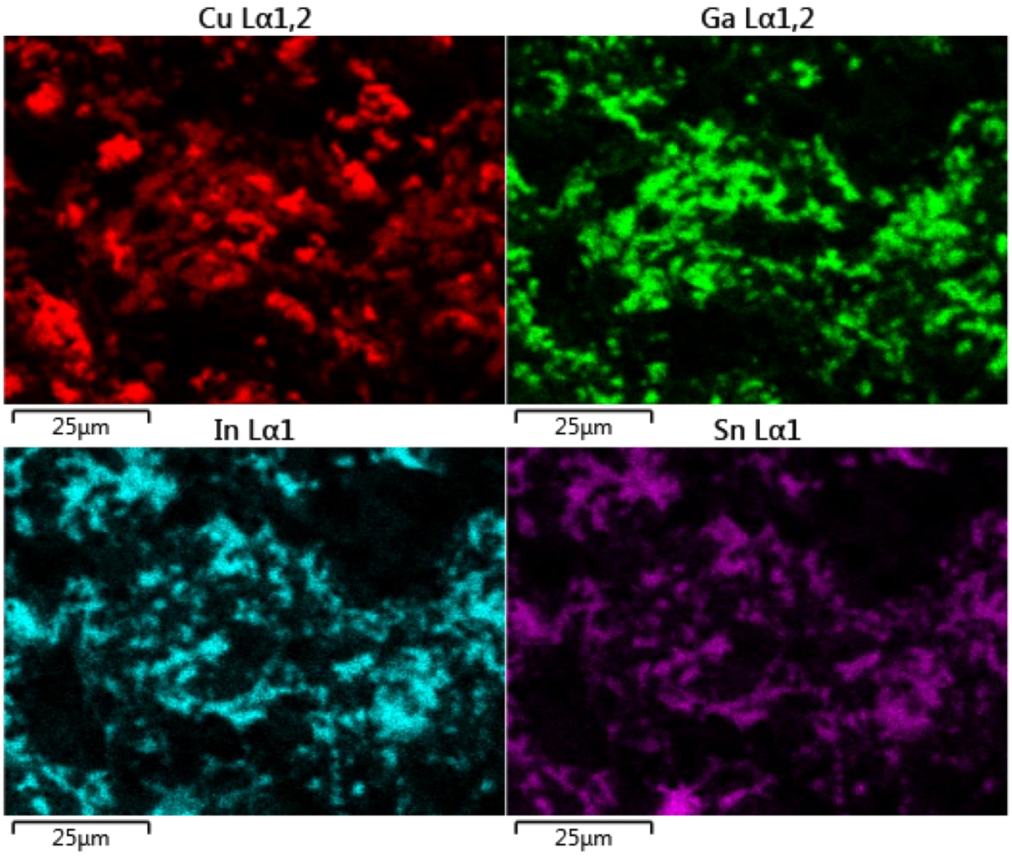

Figure 47: Individual chemical mapping images of elements displayed throughout the fractured cross-section of 1:1 cured at room temperature.

As the sample is heated to the middle cure temperature 100°C more flat features develop compared to the room temperature. It is clear that the flat-like regions are composed of Cu and Ga, forming an IMC of some composition. These mixed plate-like features, with Cu and Ga, form an incoherent or weakly bonded interface with the surrounding matrix, resulting in a decrease of tensile strength of the bulk sample. The dimples still appear throughout the microstructure the regions that consist of In and Sn. The areas of In and Sn surround the flat-like regions, Cu and Ga. There are less areas existing with pure Cu. Ga can diffuse into the Cu particles with the addition of thermal energy. As the diffusion progresses, different phases are formed. The diffusion and formation of intermediate phases between pure Cu and pure Ga are due to the cure temperature.

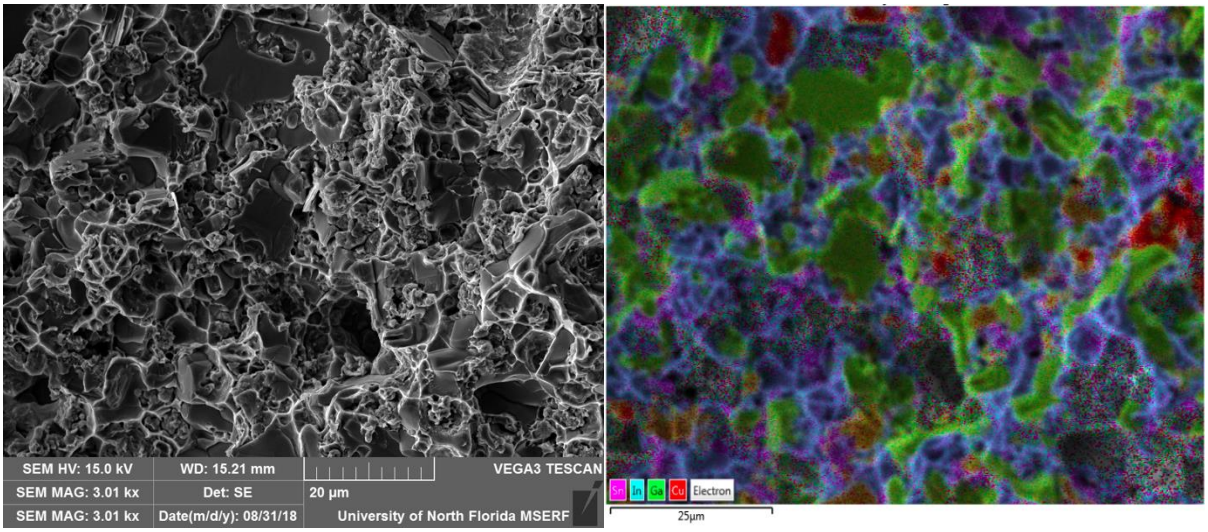

Figure 48: SEM image and EDS of fractured surface at 2:1 cured at 100°C.

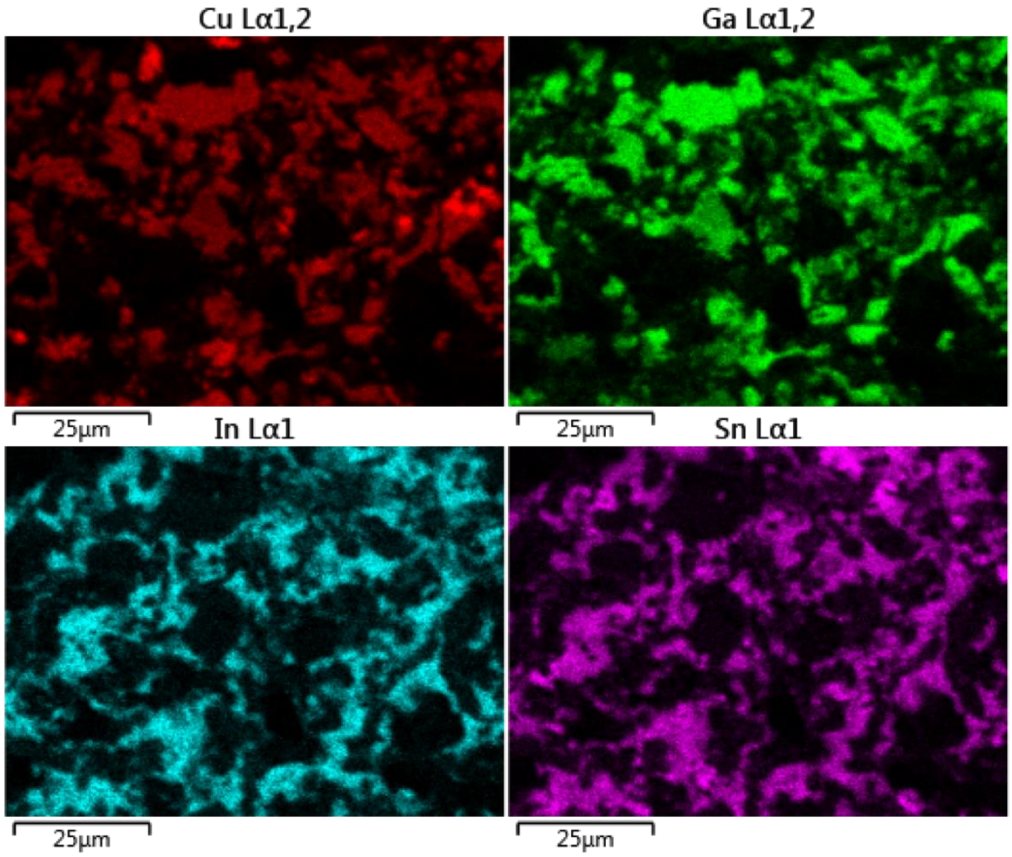

Figure 49: Individual chemical mapping images of elements displayed throughout the fractured cross-section of 2:1 cured at 100°C.

In the 200°C sample below, the plate-like regions correspond to a heavy Cu and Ga content and the absence of In and Sn. These flat regions appear to be a weakly bonded interface that delaminates under tensile stress, indicated by a lack of apparent plasticity on the surfaces. Intuitively, as the relative proportion of these regions that occupy the cross-sectional area increase, the tensile strength of the entire bulk composite will decrease. This weakly bonded interface may correspond to a new phase that can be identified using XRD. As specimens are further annealed the flat features result in a larger surface area throughout the microstructure. The regions of pure Cu have also decreased in size from room temperature to 200°C. There does not appear to have the same unbonded particle bundles as in the room temperature case.

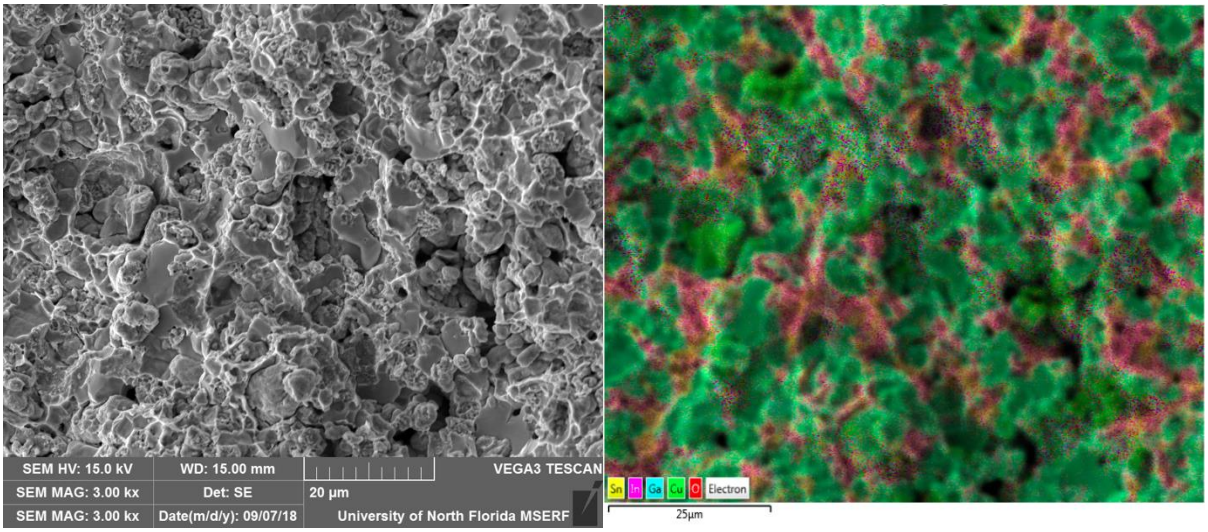

Figure 50: SEM image and EDS of fractured surface at 1:1 cured at 200°C.

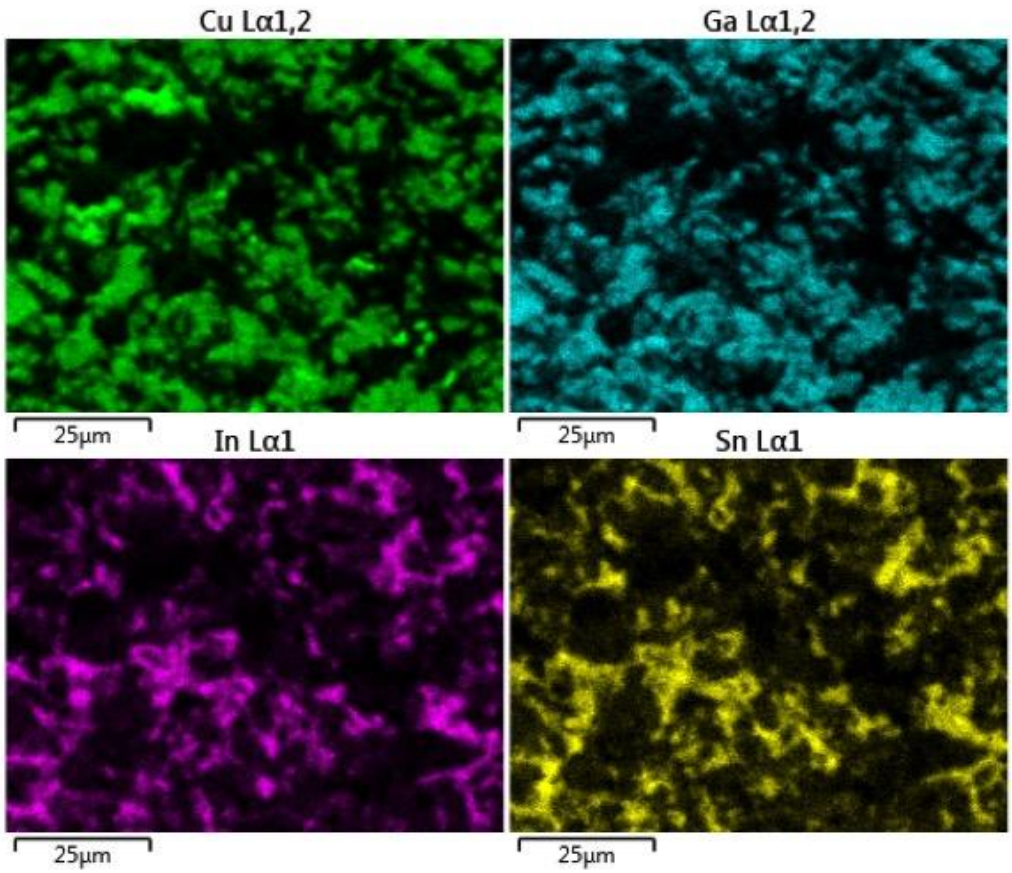

Figure 51: Individual chemical mapping images of elements displayed throughout the fractured cross-section of 1:1 cured at 200°C.

Quantitatively determining weight percentage of the element that a feature contains is beneficial data in making conclusions about specific regions. Exclusively choosing a region on the fractured surface and calculating the composition of the element it includes in the spectrum is done with a process in EDS called spot identification. The figures and tables below show the quantity of the elements in the specific features. The fractured surface of the 2:1 cured at 100°C is specifically analyzed in different spectrums on the surface. The content shows approximately double the composition of Ga compared with Cu in the plate-like surface. Based on the relative ratio, evidence supports that these regions are $CuGa_2$.

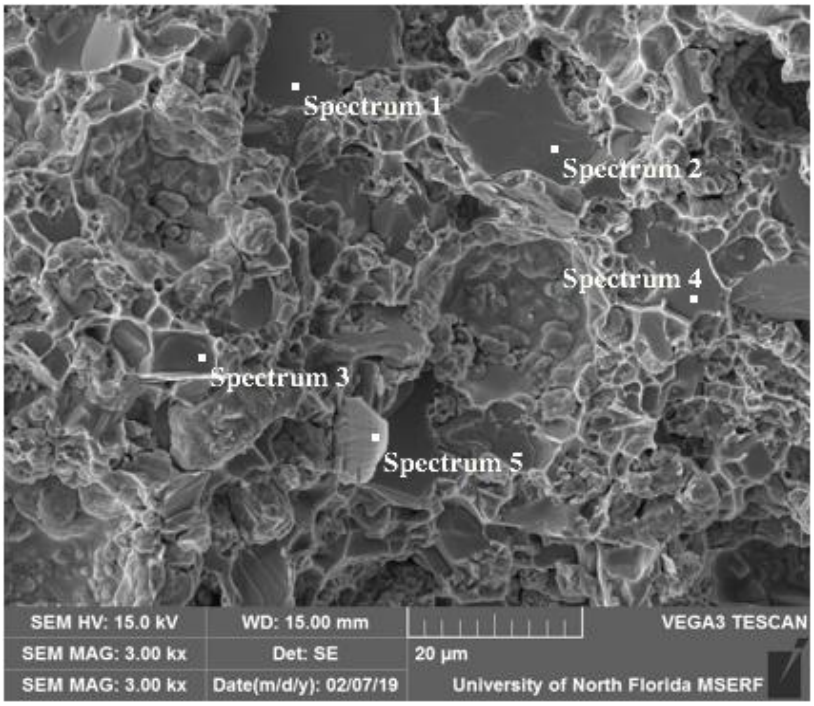

Figure 52: Fractured surface of 2:1 at 100°C.

Table 3: Composition in weight percent of each element in the given spectrum in Figure 51.

Spectrum	1	2	3	4	5
Cu	31.72	31.90	33.99	35.09	35.19
Ga	66.65	66.66	65.33	58.19	58.87
In	0.93	0.78	0.62	2.44	1.93
Sn	0.70	0.66	0.06	1.67	1.42

The highest cure temperature, at 200°C, for the 2:1 ratio is now analyzed using spot identification pictured in the SEM image and table below. With the spectrums placed on the flat surfaces, the composition of Cu increases over Ga as opposed to the sample previously mentioned cured at 100°C, causing the 200°C sample to become more brittle than at 100°C. This indicates that a new phase of Cu-Ga has emerged due to an increase in annealing temperature. Two possibilities exist based on the data collected using spot identification for this sample. First, a new phase, approximately Cu_4Ga_3 may have formed. Alternatively, there may now also be the presence of $CuGa_2$ and Cu_2Ga phases, which are both present in the phase diagrams and are stable phases. XRD will determine which phases exist in these samples.

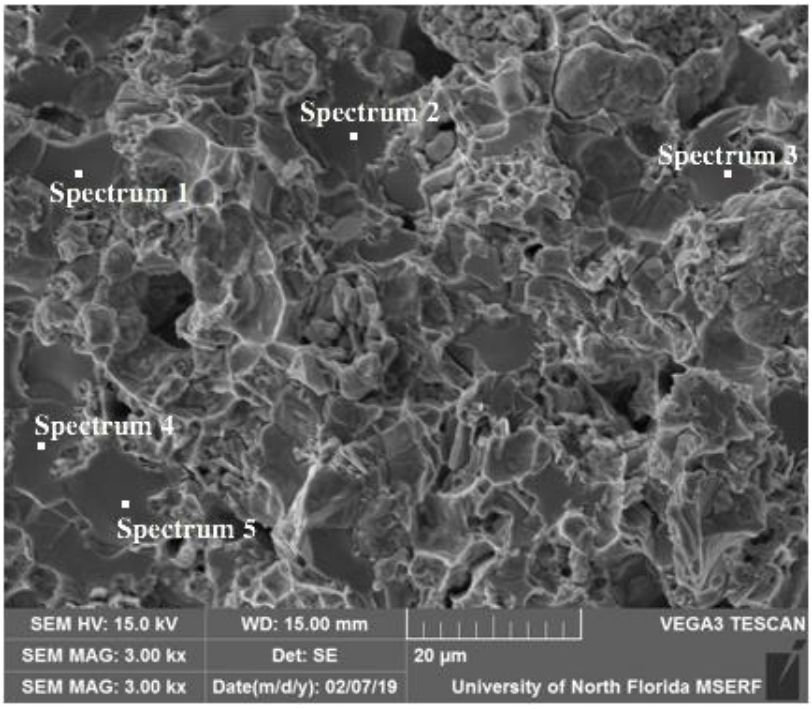

Figure 53: Fractured surface of 2:1 at 200°C.

Table 4: Composition in weight percent of each element in the given spectrum in Figure 52.

Spectrum	1	2	3	4	5
Cu	50.19	53.61	53.01	53.29	56.27
Ga	37.03	41.49	43.53	43.26	39.1
In	6.04	2.66	1.78	2.01	2.56
Sn	4.04	2.24	1.67	1.44	2.07

Quantitative analysis is helpful is determining potential elements in the area being determined. For exact phase correlation, XRD was performed on the 2:1 specimen cured at room temperature and the 2:1 specimen cured at 200°C. At room temperature, there is a $CuGa_2$ IMC, In_3Sn compound, and just Cu being detected. As the sample is annealed, XRD is performed and $CuGa_2$ still identified in the structure but with the formation of the hypothesized new brittle phase Cu_2Ga, also. The In-Sn phase and pure crystalline Cu are still existent, but the intensity of pure Cu x-rays detected is significantly less, which may be due to either the presence of less material or differences in x-ray cross-section as the new phases emerge. This validates the elements that compose the flat features on the micrographs in the locations on the fractured surface and the decrease and pure Cu as the cure temperature is raised. The anticipation of calculating the weight percent using EDS has guided the promising results in XRD analysis shown in Figure 54 and Figure 55 on the next two pages.

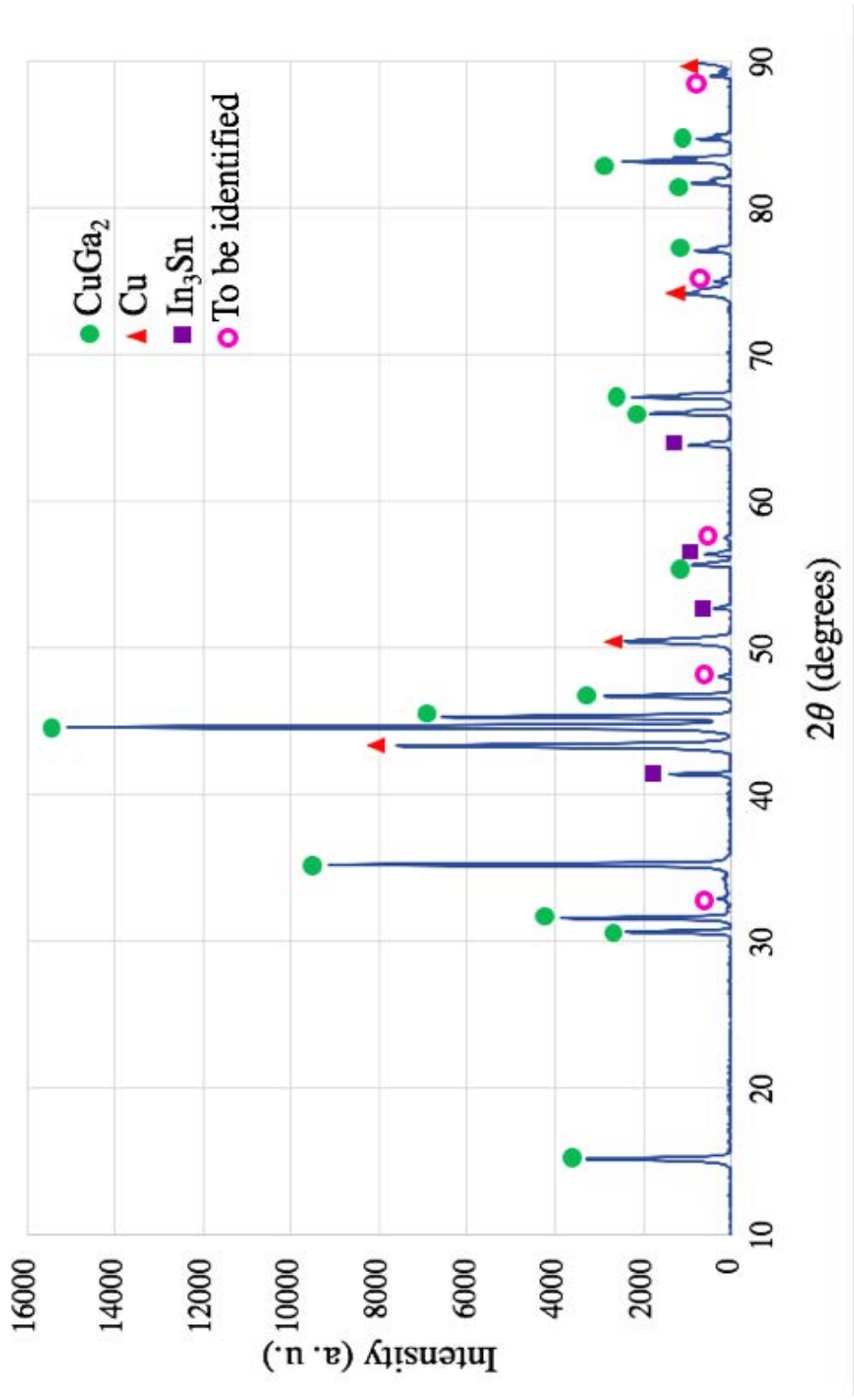

Figure 54: XRD spectrum of 2:1 at room temperature.

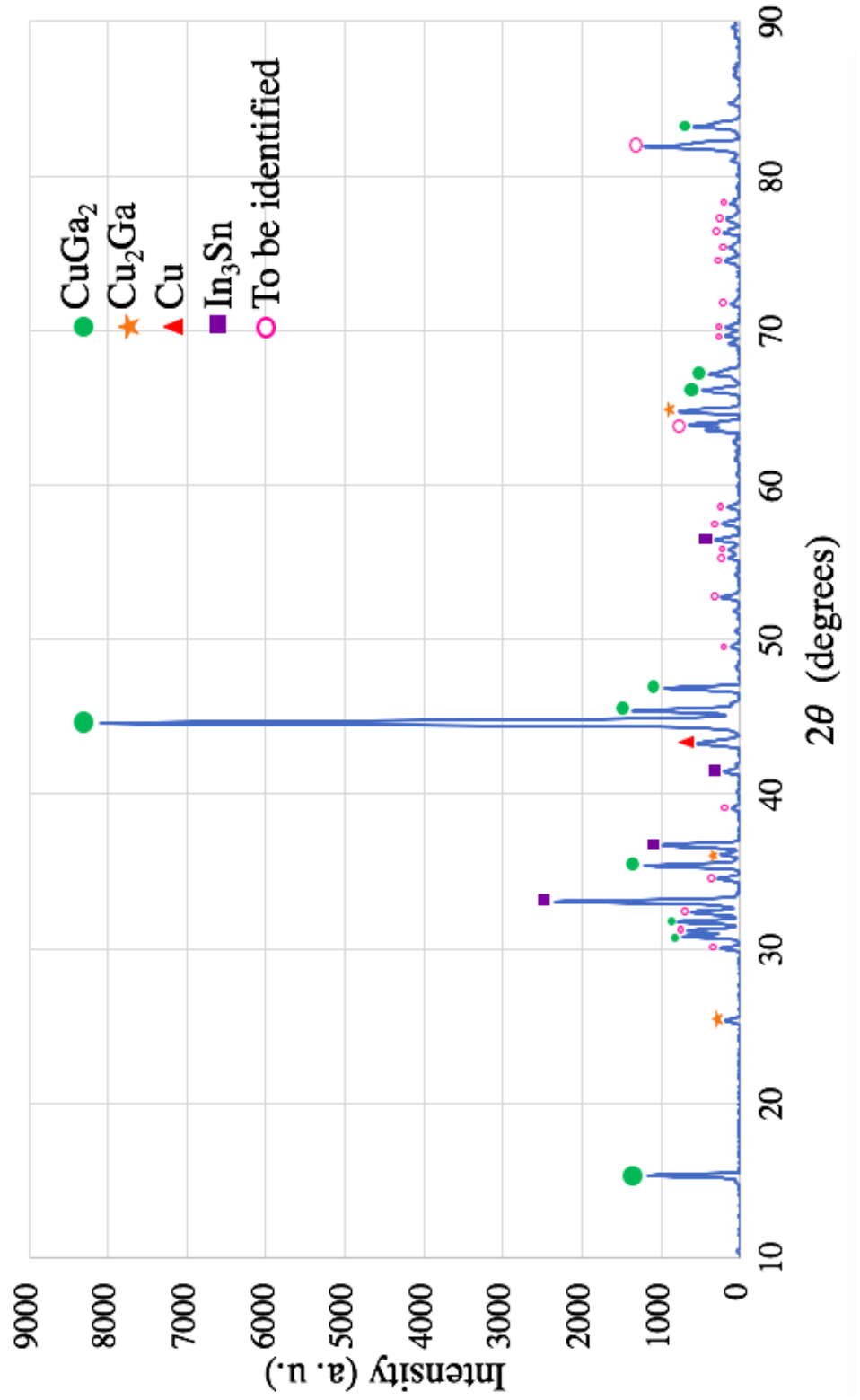

Figure 55: XRD spectrum of 2:1 at 200°C.

CONCLUSION

This work reports on three areas of study: 1) development of microstructure, 2) mechanical properties, and 3) characterization of the phases developed in a novel Ga-Cu amalgamation. This amalgamation was characterized for mechanical properties and microstructure.

The hypothesis for the development of the microstructure proposed in this thesis was guided by different compositional amalgamations from previous literature. With the addition of the Cu component into Galinstan, it is believed that the Cu and Ga interact to form an IMC. In and Sn form a metal bond surrounding the Cu and Gu phase. This specific formation is later validated in the EDS mapping.

The mechanical properties were evaluated using tensile testing, with ultimate tensile strength being the focus. The 2:1 specimen cured at 100°C had the greatest average value in strength of ~32MPa, followed by all of the room temperature samples which obtained similar averages ~22MPa. As the samples were annealed, they became much weaker with the average of 200°C samples ultimate tensile strengths being ~12MPa. The brittle nature of the samples as temperature increased created a problem in mechanically testing these specimen as they broke in the shoulder of the tensile bar making the results invalid.

The SEM micrographs showed unchanging surface area for samples at 2:1, 1:1, and 4:3 at room temperature that were polished. Another micrograph of the same ratio cured at all three different cure temperatures revealed that pores are highly dependent on temperature which may also affect the tensile strength, as there are a greater number of pores in the 200°C cross-section area than the 100°C or room temperature, respectively. The phases developed in the EDS mapping are validated in the XRD results. $CuGa_2$, pure Cu, and In_3Sn are found in both, room temperature and 200°C. In the 200°C sample, it is likely that more Cu has reacted with Ga, and there is the

addition of a new Cu_2Ga phase. As the IMC of Cu and Ga is heated and Cu increases in composition in the IMC, the structure becomes more brittle. As annealing temperature is increased from room temperature to 200°C, the relative portion of the sample volume composed of IMC increases. As the fractography show no sign of plasticity in these regions, it is likely that they are weakly bonded to the surrounding matrix of In and Sn. As the cross section becomes composed of more IMC, the tensile strength decreases.

For the optimal result of this joining method, a decrease in IMC would be ideal due to the properties and weaker mechanical performance. The increase in temperature developed a greater amount of Cu_2Ga and $CuGa_2$ IMCs which is undesirable. A room temperature cured material has the formation of pure copper in the phases with less development of the IMC which is significant in having the optimal tensile strength and thermal conductivity.

This work will have impacts on the application of Ga-alloy TIMs in real IC devices. The contributions on microstructural evolution from this work motivate further work into the measurement of thermal conductivity changes as the microstructure changes are critical to the use of these materials in devices as TIMs.

REFERENCES

[1] J. Gwinn and R. Webb, "Performance and testing of thermal interface materials," *Microelectronics,* no. 34, pp. 215-222, 2003.

[2] S. Liu, K. Sweatman, M. Stuart and K. Nogita, Ga-Based Alloys in Microelectronic Interconnects: A Review.

[3] K. M. Razeeb, E. Dalton, G. L. W. Cross and A. J. Robinson, "Present and future thermal interface materials for electronic devices," *International Materials Reviews,* pp. 1-17, 2017.

[4] J. Hansson, T. M. Nilsson, L. Ye and J. Liu, "Novel nanostructured thermal interface materials: a review," *International Materials Reviews,* pp. 1-18, 2017.

[5] C. P. Feng, L. Bai, R.-Y. Bao, S.-W. Wang, Z. Liu, M.-B. Yang, J. Chen and W. Yang, "Superior thermal interface materials for thermal management," *Elsevier,* no. 12, pp. 80-85, 2019.

[6] F. Streb, D. Schweitzer, M. Mengel and T. Lampke, "Evaluation of Characterization Methods for Solid Thermal Interface Materials," *SEMI-THERM Symposium,* pp. 269-278.

[7] F. a. F. IonGwin - Fundamental, "Welcome to MyHeatSinks," MyHeatSinks (MHS), 2019. [Online]. Available: https://myheatsinks.com/learn/tim/. [Accessed 2019].

[8] S. Chinkanjanarot, "Multiscale Modeling: Thermal Conductivity of Graphene/Cycloaliphatic Epoxy Composites," *Reserach Gate,* p. 113, January 2018.

[9] T. L. Bergman, A. S. Lavine, F. P. Incropera and D. P. Dewitt, Fundamentals of Heat and Mass Transfer, Jefferson City: John Wiley and Sons, 2011.

[10] D. R. Askeland and W. J. Wendelin, The Science and Engineering of Materials, Boston: Cengage Learning, 2016.

[11] R. W. Messler Jr., "Soldering: A Subset of Brazing," *Joining of Materials and Structures,* vol. 2004, pp. 389-446, 2007.

[12] Y. Gao and J. Liu, "Gallium-based thermal interface material with high compliance and wettability," *Applied Physics A Materials Science and Processing,* no. 107, pp. 701-708, 30 March 2012.

[13] C. A. MacKay, "Amalgams for Improved Electronics Interconnection," in *IEEE Micro*, Microelectronics and Computer Technology Corooration, 1993, pp. 46-58.

[14] H. H. J. Jamal Al-Deen and S. A. Shahee, "Replacement Of Mercury With Gallium Alloy In Dental Fills," *International Journal of Scientific and Engineering Research,* vol. 6, no. 12, pp. 619-631, December 2015.

[15] M. M. Fathi and V. Mortazavi, "A Review on Dental Amalgam Corrosion and Its Consequences," *Journal of Research in Medical Sciences,* pp. 42-51, 2004.

[16] F. Shaini, A. Shortall, A. Ellakwa and P. Marquis, "Handling characteristics of a palladium-free gallium-based alloy compared with a high copper dental amalgam in a simulated clinical trial," *Journal of Oral Rehabilitation,* no. 28, pp. 1029-1036, 2001.

[17] A. A. Stanfield and S. H. Mannan, "Gallium Based Interconnects for Flip-chip Assembly," *IEMT/IMC Proceedings,* pp. 347-352, 1998.

[18] M. Heim, J. Holowczak, L. Tessarotto and V. Greenhut, "Copper/Gallium Amalgam-A Material for Joining Ceramics and Metals," *The American Ceramic Society,* pp. 513-521, 1999.

[19] S.-J. Hong and C. Suryanarayana, "Mechanism of Low Temperature Theta-CuGa2 Phase Formation in Cu-Ga Alloys by Mechanically Alloying," *Journal of Applied Physics,* vol. 96, no. 11, pp. 6120-6125, 2004.

[20] Y. Shu, T. Ando, Q. Yin, G. Zhou and Z. Gu, "Phase Diagram and Structural Evolution of Tin/Indium (Sn/In) Nanosolder Particles: From Non-Equilibrium State to Equilibrium State," *The Royal Society of Chemistry,* vol. 00, pp. 1-11, 2013.

[21] C. P. Muzzillo, C. E. Campell and T. J. Anderson, "Cu-Ga-In thermodynamics: experimental study, modeling, and implications for photovoltaics," *Springer Science and Business Media New York,* 2015.

[22] J. R. Davis, Tensile Testing, Materials Park: ASM International-The Materials Information Society, 2004.

[23] D. Brandon and W. D. Kaplan, Microstructural Characterization of Materials, West Sussex: Wiley, 2008.

[24] M. Dumont, A. Borbely, A. Kostka, A. K. Pyalla and P. M. Sander, "Characterization of Sauropod Bone Structure," *Researchgate,* pp. 150-170, 2016.

[25] T. O. University, "Phys 7.1: The Atomic Basis of Matter," University of Reading, 1996. [Online]. Available: http://www.met.reading.ac.uk/pplato2/h-flap/phys7_1.html. [Accessed 21 March 2018].

[26] stratasys, "GrabCAD: Design Community, CAD Library, 3D Printing Software," Stratsys, 2019. [Online]. Available: https://grabcad.com/. [Accessed 2019].

[27] S. Stagon, A. Knapp, P. Elliot and H. Huang, "Metallic Glue for Ambient Enviroments Making Stridee," *Advanced Materials and Processes,* pp. 22-25, January 2016.

[28] A. I. Ancharov, T. F. Grigoryeva, A. P. Barinova and V. V. Boldyrev, "Interaction between Copper and Gallium," *Russion Metallurgy,* vol. 2008, no. 6, pp. 475-479, 2008.

[29] J. Tang, X. Zhao, J. Li, R. Guo, Y. Zhou and J. Liu, "Gallium-Based Liquid Metal Amalgams: Transitional-State Metallic Mixtures (TransM2ixes) with Enhanced and Tunable Electrical, Thermal, and Mechanical Properties," *Applied Materials and Interface,* no. 9, pp. 35977-35987, 2017.

[30] D. L. Smith, H. J. Caul and W. T. Sweeny, "Some physical properties of gallium-copper-tin alloys," *The Journal Of The American Dental Association,* vol. 53, no. 315, pp. 677-685, 1956.

APPENDIX A: MATLAB CODE FOR THE GENERATION OF THE STRESS VERSUS STRAIN CURVE FOR EACH SAMPLE

```
clear all

% [a1,b1,c1]=xlsread('C:\Users\HP\Desktop\CNT Research\Aug 24 Testing\1 part
Excel\sample21.xlsx');  %load data (a=time, b=force, c=disp)
filename='F:\THESIS\Mechanical Properties EXCEL DATA\.xlsx';
% Reads and stores Columns from Excel sheet Column by Column
[a1]=xlsread(filename,'A:A');  %load data (a=time)
%Locates Last time row entered
ColSize=numel(a1);
%make the range to import the bl and cl array from. %eliminates faulty
%enteries
B_Rng=['B1:B',num2str(ColSize)];
C_Rng=['C1:C',num2str(ColSize)];

[b1]=xlsread(filename,B_Rng);  %load data (b=force)
[c1]=xlsread(filename,C_Rng);  %load data (c=disp)
csa=(3.5*3.5);   % cross-sectional area
length=31;          %length

%strain1=a1(:,3)/length;  % normalize strain; neg since written for comp \\changed//
strain1=c1/length;  % normalize strain; neg since written for comp

eps=strain1-strain1(1);      %zero strain

% sig=a1(:,2)/csa;   % divide load from teststar file by cross-sectional area\\changed//
sig=b1/csa;   % divide load from teststar file by cross-sectional area
sig=sig-sig(1);                %zero stress
len=size(eps,1);
plot(eps,sig,'r-')
hold on
count=0;i=1;
while (eps(i,1)<0.002)
   count=count+1;
   strain(i,1)=eps(i,1);
   stress(i,1)=sig(i,1);
   i=i+1;
end
% S is for use with polyval to determine error estimates and predictions
%Create New variables that only go to 0.2% and fit curve using those
P=polyfit(strain,stress,1);
% calculate slope of quadratic fit at inital point using derivative for range 0-.2%
qdslope=P(1);
```

```
% calculate failure parameters
ystrain=0;
ystress=0;
ultstrain=0;
ultstress=0;
len_strain=size(eps,1);
count=2;
while (ystrain==0) && (count<len)
   if (abs(eps(count))-.002)*qdslope>abs(sig(count))
      ystress=sig(count-1);
      ystrain=eps(count-1);
   end
   count=count+1;
end
if count==len_strain
   disp('yield not reached for this specimen')
else
   [i,k]=max(sig);
   ultstress=i;
   ultstrain=eps(k);
end
%Create integration scheme using sig and eps to calculate toughness
%Intr_P=polyint(P);
%A_u_Curve=(polyval(Intr_P,x2)-polyval(Intr_P,0));
Toughness=trapz(eps,sig);
%%%%%%%%

plot(ystrain,ystress)
hold on
title('2:1 °C (Sample #)')
xlabel('Strain (mm/mm)')
ylabel('Stress (MPa)')
set(gca,'Fontname','Times New Roman','FontSize',12)
grid on

ystress
ystrain
ultstress
ultstrain
```

APPENDIX B: STRESS-STRAIN CURVES FOR ALL OF THE SPECIMEN

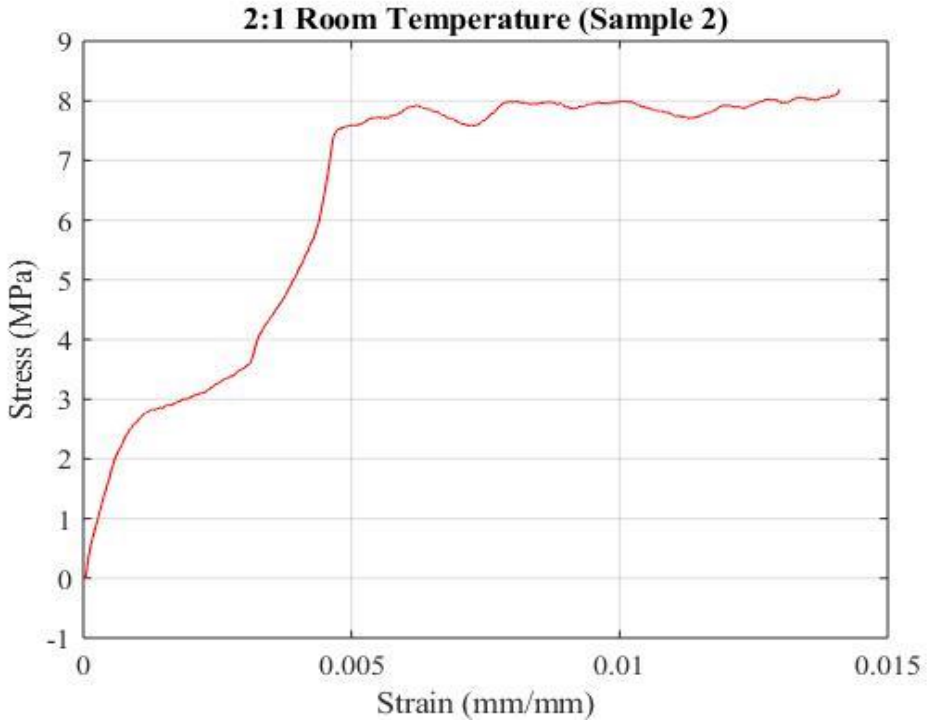

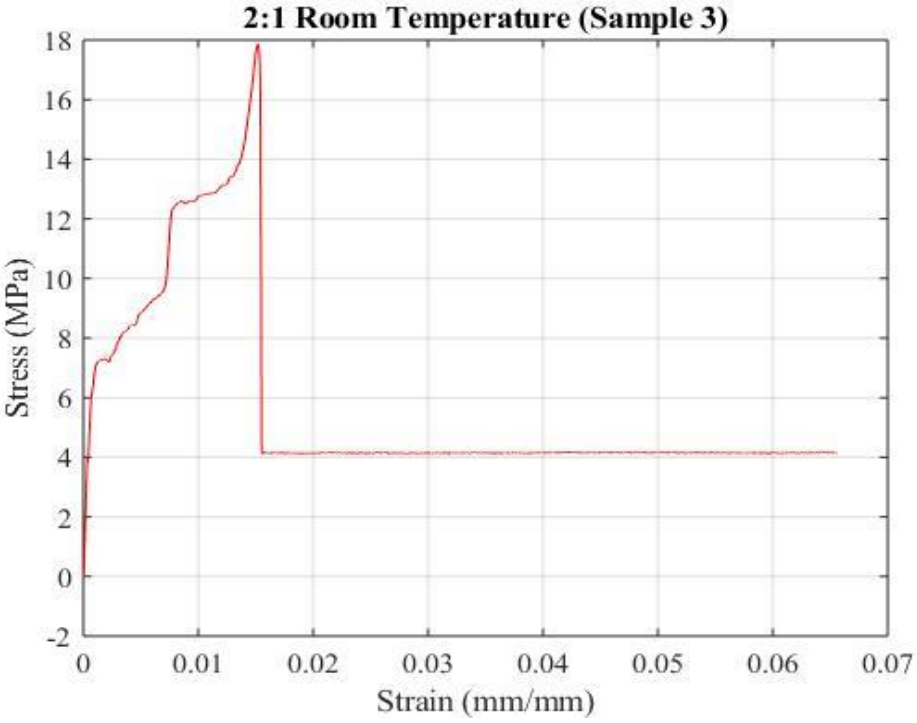

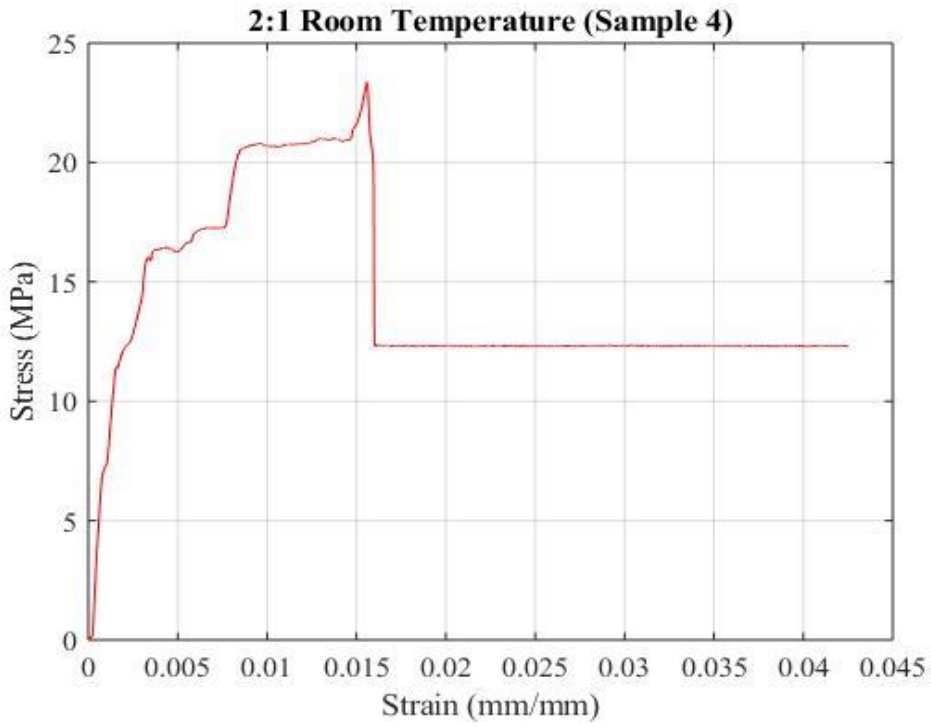
2:1 Room Temperature (Sample 4)
Stress (MPa)
Strain (mm/mm)
0
5
10
15
20
25
0
0.005
0.01
0.015
0.02
0.025
0.03
0.035
0.04
0.045

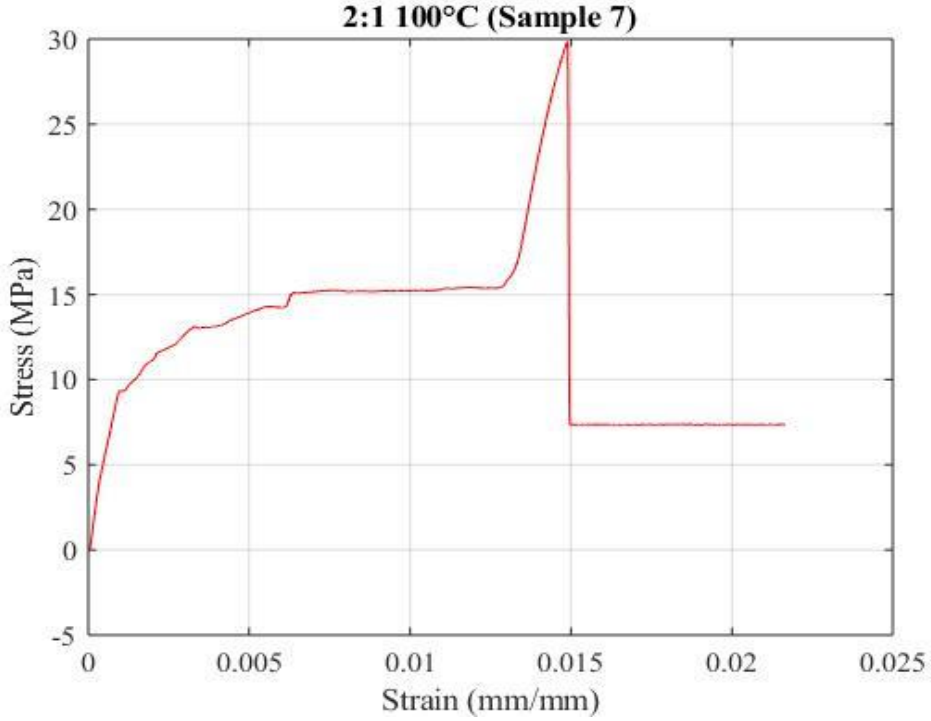
2:1 100°C (Sample 7)
Stress (MPa)
Strain (mm/mm)
-5
0
5
10
15
20
25
30
0
0.005
0.01
0.015
0.02
0.025

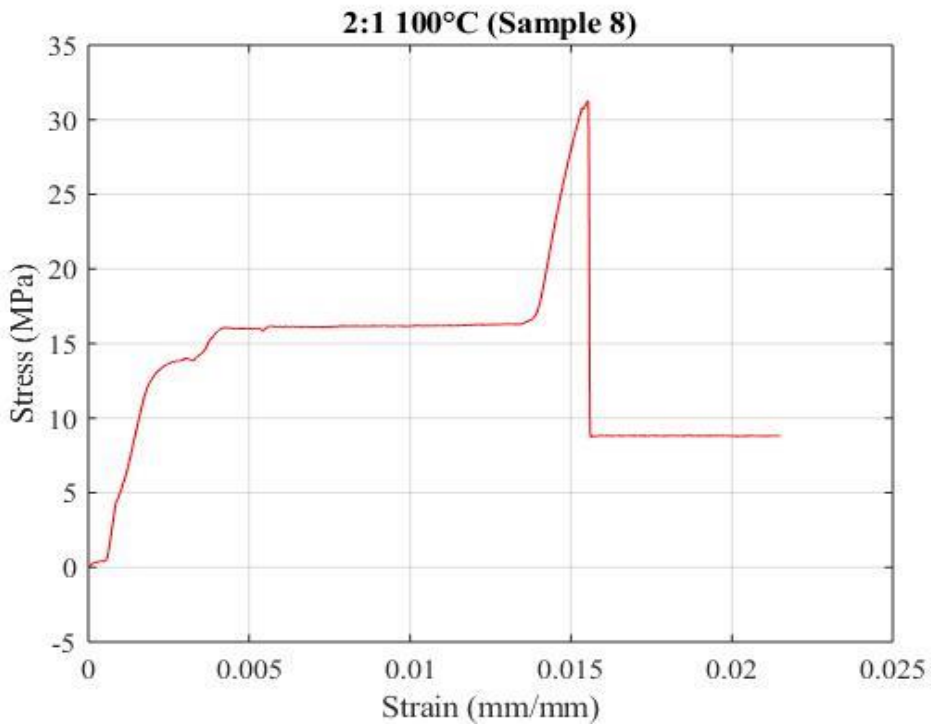
2:1 100°C (Sample 8)
Stress (MPa)
Strain (mm/mm)
35
30
25
20
15
10
5
0
-5
0
0.005
0.01
0.015
0.02
0.025

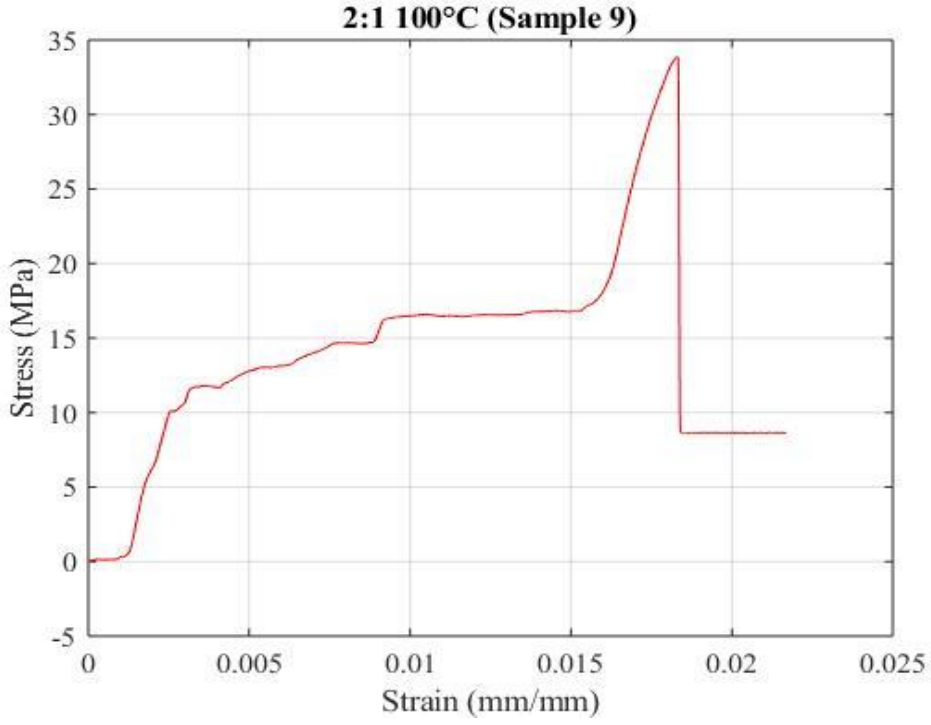
2:1 100°C (Sample 9)
Stress (MPa)
Strain (mm/mm)
35
30
25
20
15
10
5
0
-5
0
0.005
0.01
0.015
0.02
0.025

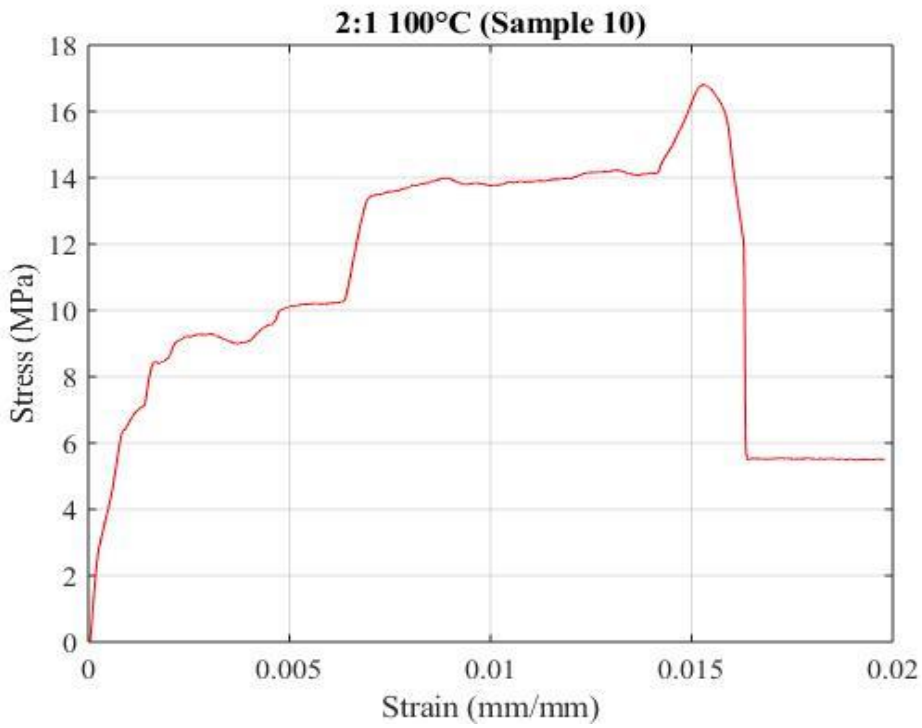
2:1 100°C (Sample 10)
Stress (MPa)
Strain (mm/mm)
0
2
4
6
8
10
12
14
16
18
0
0.005
0.01
0.015
0.02

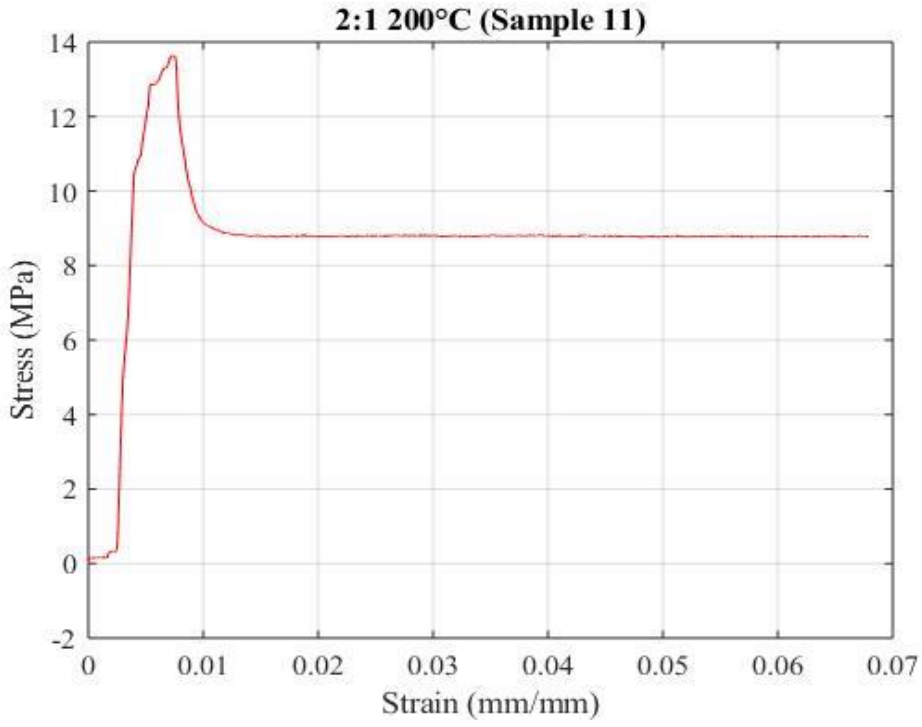
2:1 200°C (Sample 11)
Stress (MPa)
Strain (mm/mm)
-2
0
2
4
6
8
10
12
14
0
0.01
0.02
0.03
0.04
0.05
0.06
0.07

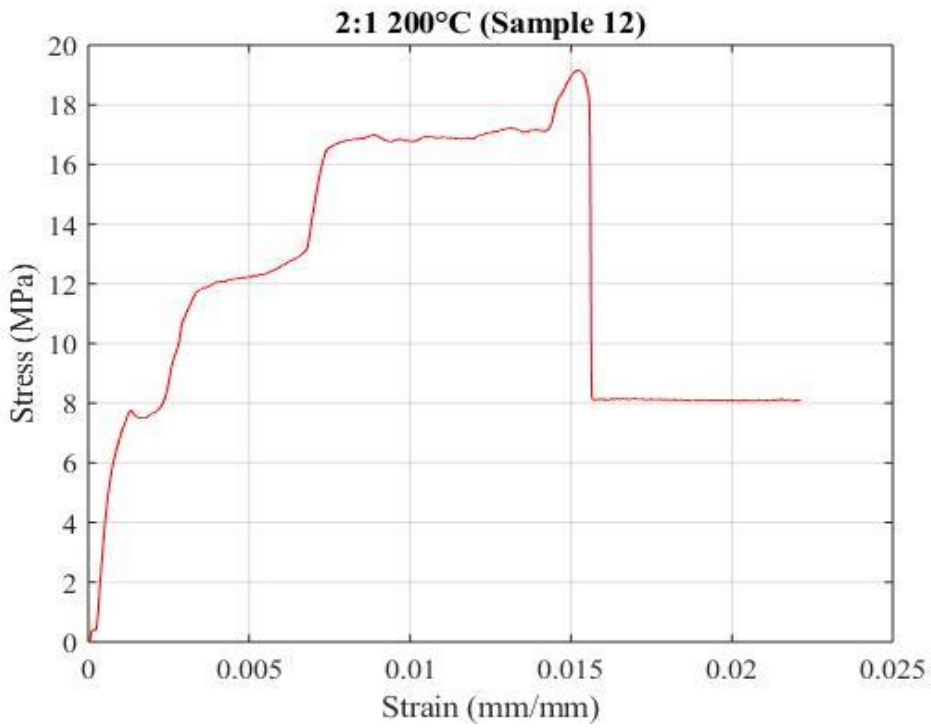
2:1 200°C (Sample 12)
Stress (MPa)
Strain (mm/mm)
0
2
4
6
8
10
12
14
16
18
20
0
0.005
0.01
0.015
0.02
0.025

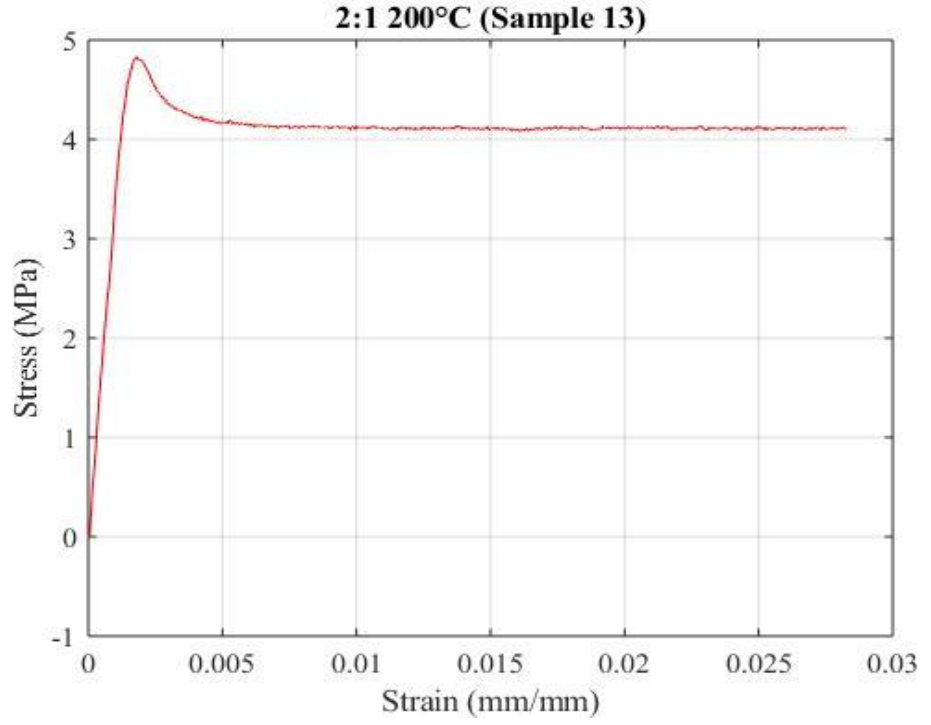
2:1 200°C (Sample 13)
Stress (MPa)
Strain (mm/mm)
-1
0
1
2
3
4
5
0
0.005
0.01
0.015
0.02
0.025
0.03

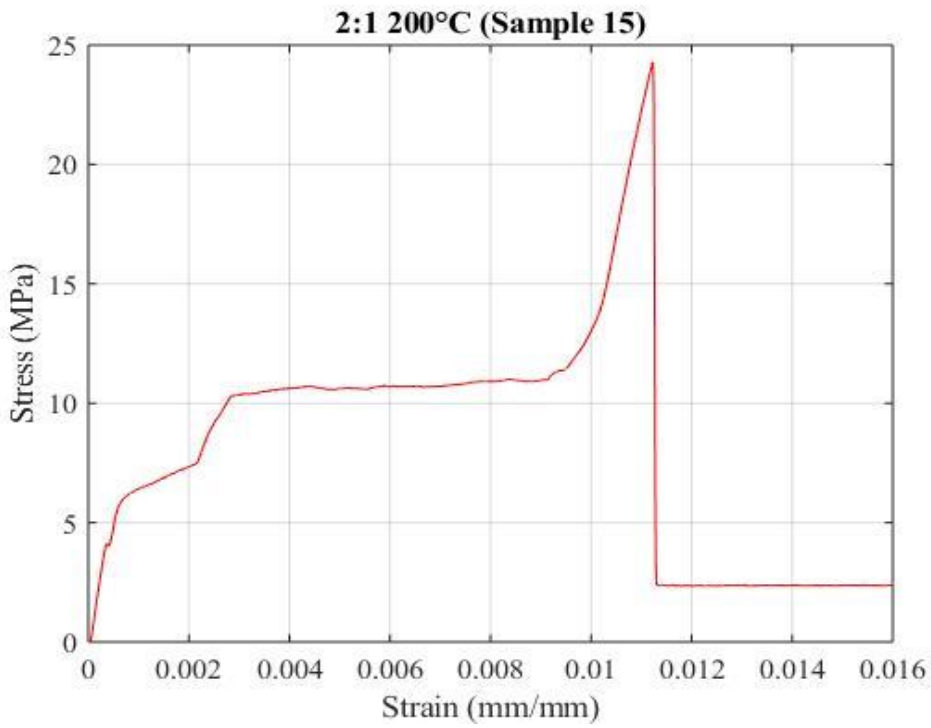
2:1 200°C (Sample 15)
Stress (MPa)
Strain (mm/mm)
0
5
10
15
20
25
0
0.002
0.004
0.006
0.008
0.01
0.012
0.014
0.016

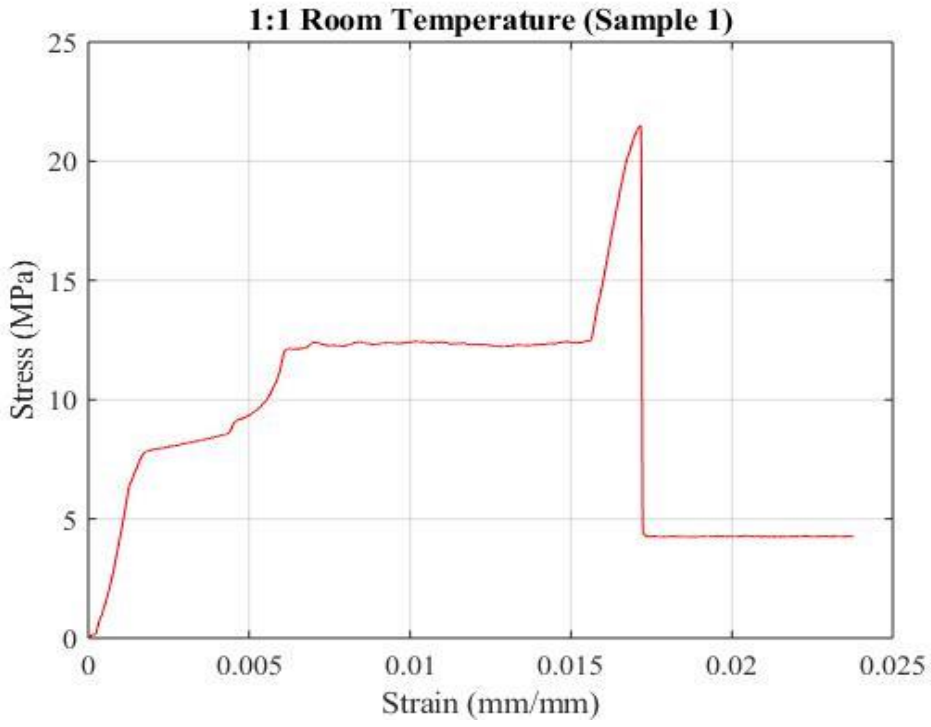
1:1 Room Temperature (Sample 1)
Stress (MPa)
Strain (mm/mm)
0
5
10
15
20
25
0
0.005
0.01
0.015
0.02
0.025

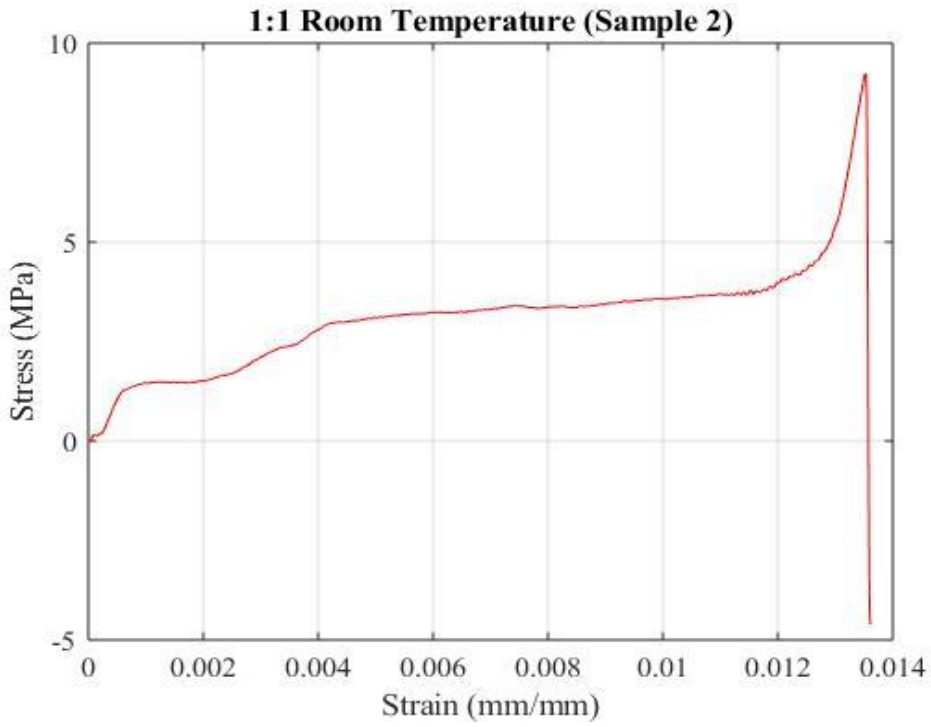
1:1 Room Temperature (Sample 2)
Stress (MPa)
Strain (mm/mm)
10
5
0
-5
0
0.002
0.004
0.006
0.008
0.01
0.012
0.014

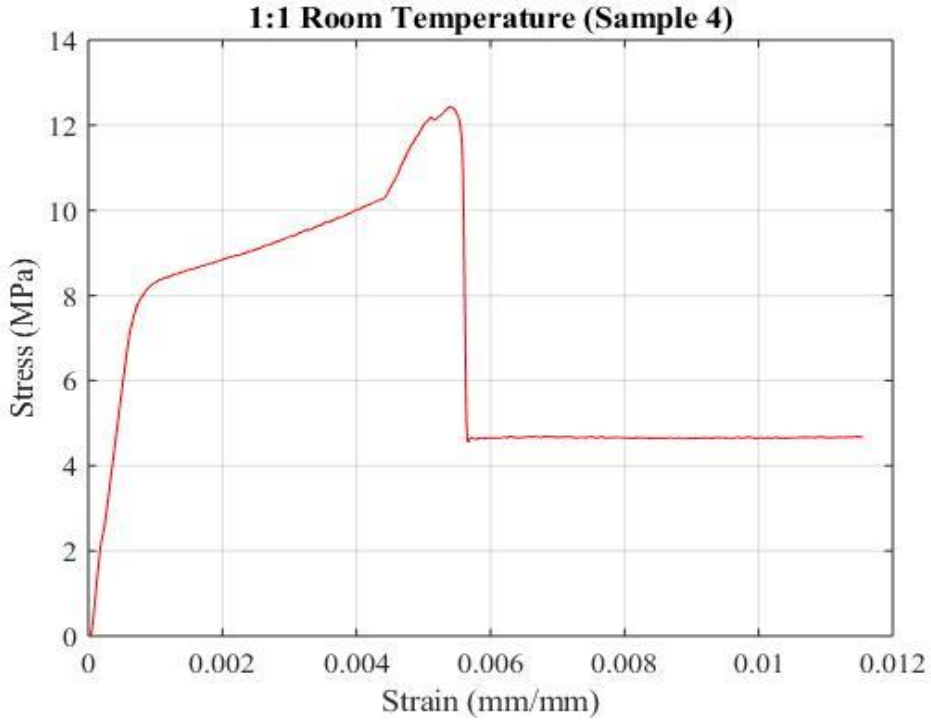
1:1 Room Temperature (Sample 4)
Stress (MPa)
Strain (mm/mm)
14
12
10
8
6
4
2
0
0
0.002
0.004
0.006
0.008
0.01
0.012

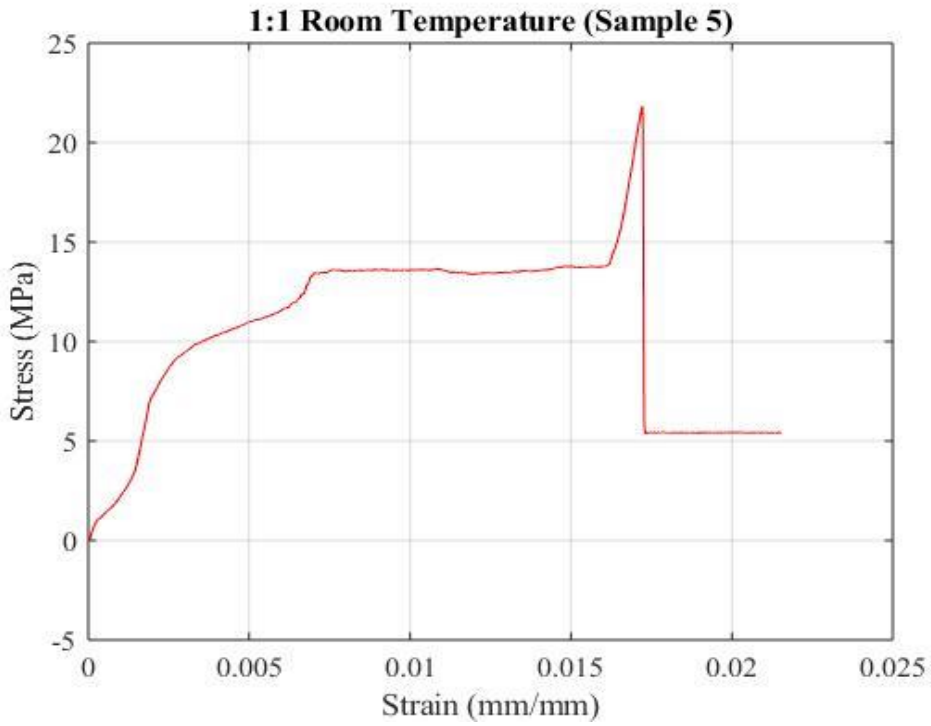
1:1 Room Temperature (Sample 5)
Stress (MPa)
Strain (mm/mm)
25
20
15
10
5
0
-5
0
0.005
0.01
0.015
0.02
0.025

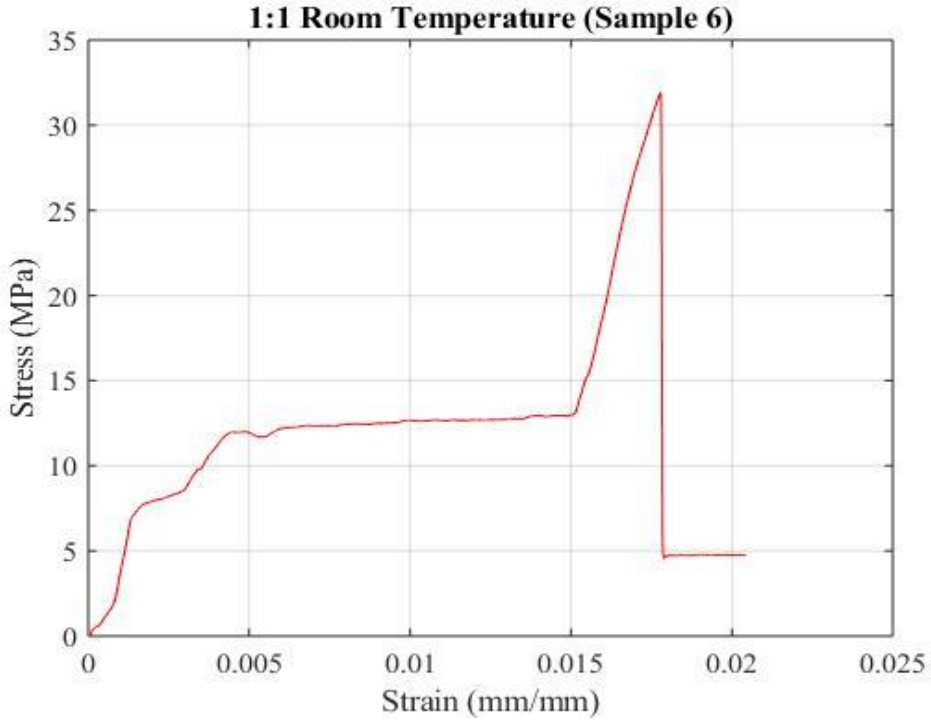
1:1 Room Temperature (Sample 6)
Stress (MPa)
Strain (mm/mm)
35
30
25
20
15
10
5
0
0
0.005
0.01
0.015
0.02
0.025

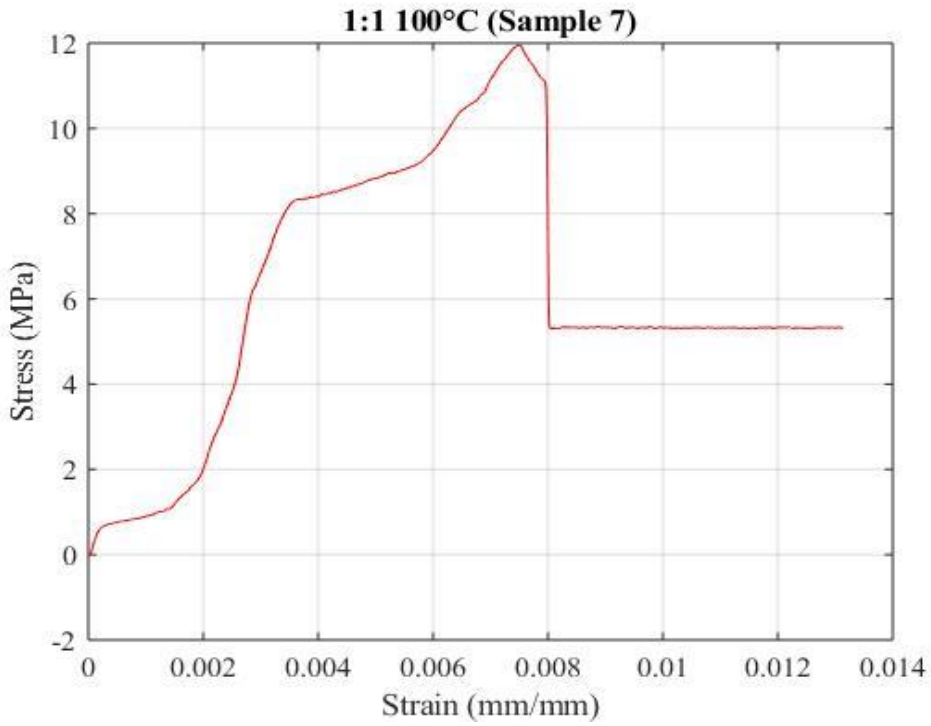
1:1 100°C (Sample 7)
Stress (MPa)
Strain (mm/mm)
12
10
8
6
4
2
0
-2
0
0.002
0.004
0.006
0.008
0.01
0.012
0.014

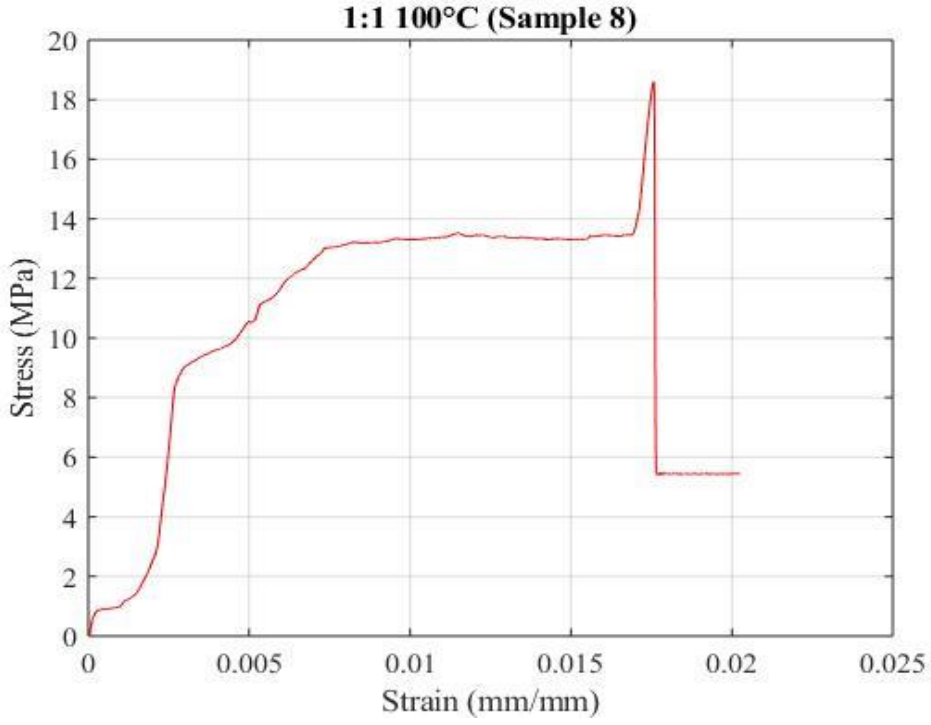
1:1 100°C (Sample 8)
Stress (MPa)
Strain (mm/mm)
20
18
16
14
12
10
8
6
4
2
0
0
0.005
0.01
0.015
0.02
0.025

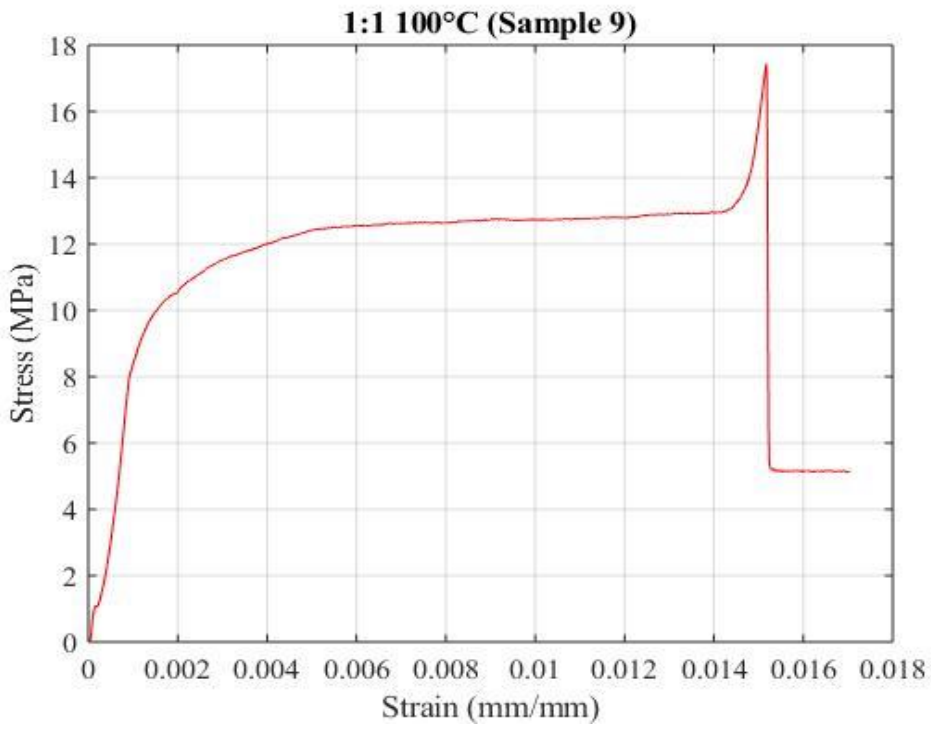
1:1 100°C (Sample 9)
Stress (MPa)
Strain (mm/mm)
0
2
4
6
8
10
12
14
16
18
0
0.002
0.004
0.006
0.008
0.01
0.012
0.014
0.016
0.018

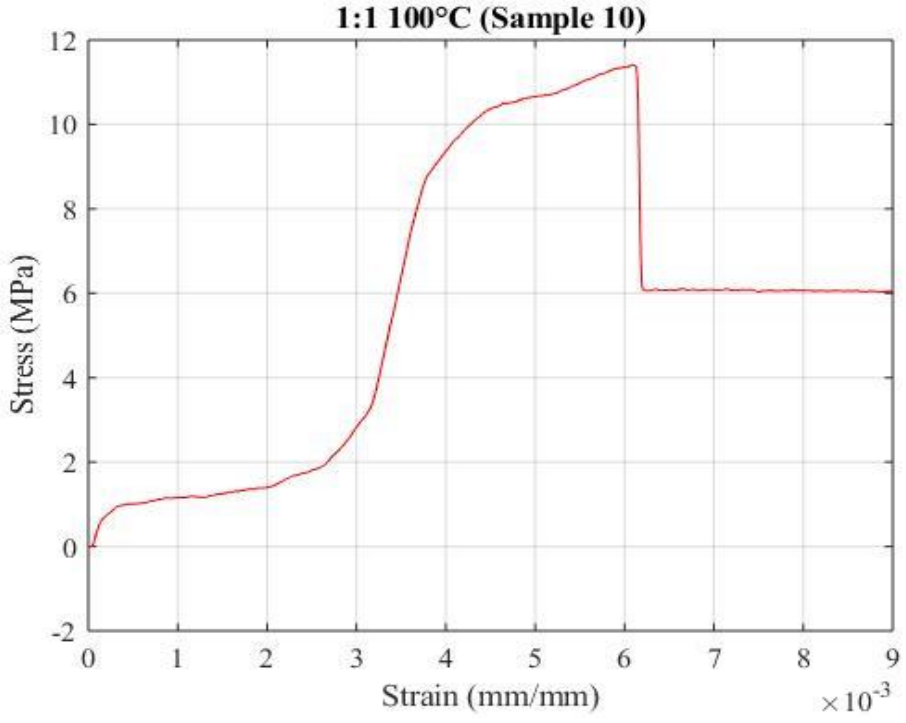
1:1 100°C (Sample 10)
Stress (MPa)
Strain (mm/mm)
×10-3
-2
0
2
4
6
8
10
12
0
1
2
3
4
5
6
7
8
9

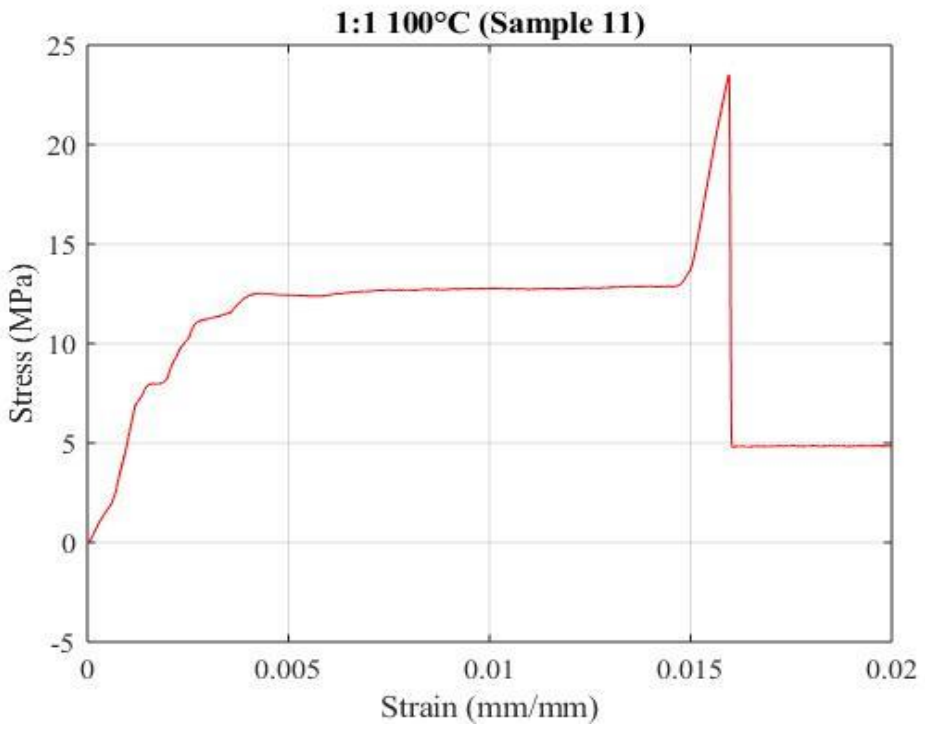
1:1 100°C (Sample 11)
Stress (MPa)
Strain (mm/mm)
25
20
15
10
5
0
-5
0
0.005
0.01
0.015
0.02

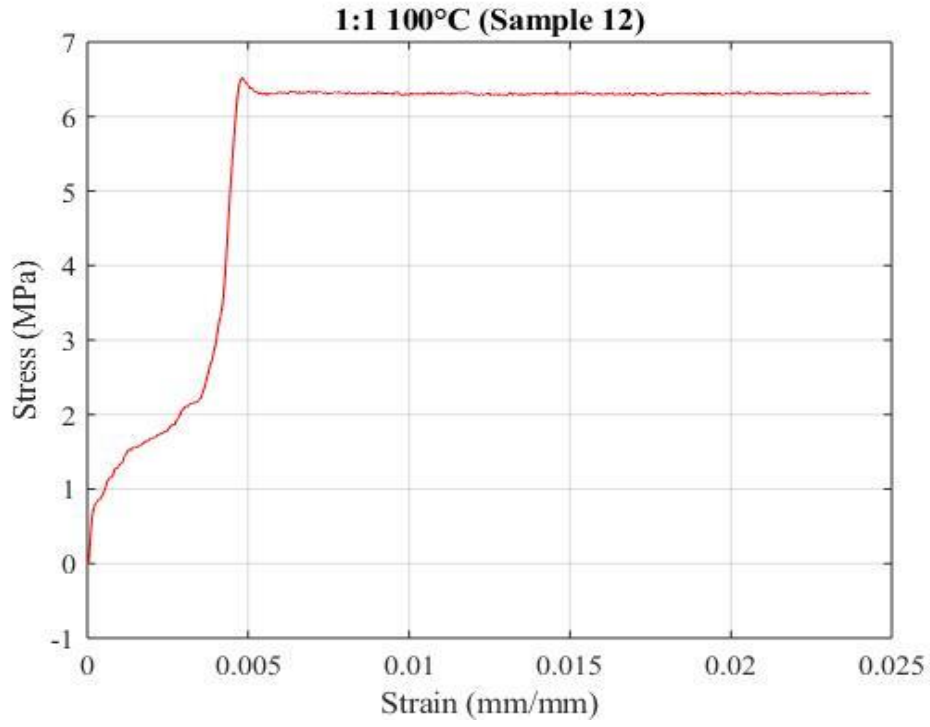
1:1 100°C (Sample 12)
Stress (MPa)
Strain (mm/mm)
7
6
5
4
3
2
1
0
-1
0
0.005
0.01
0.015
0.02
0.025

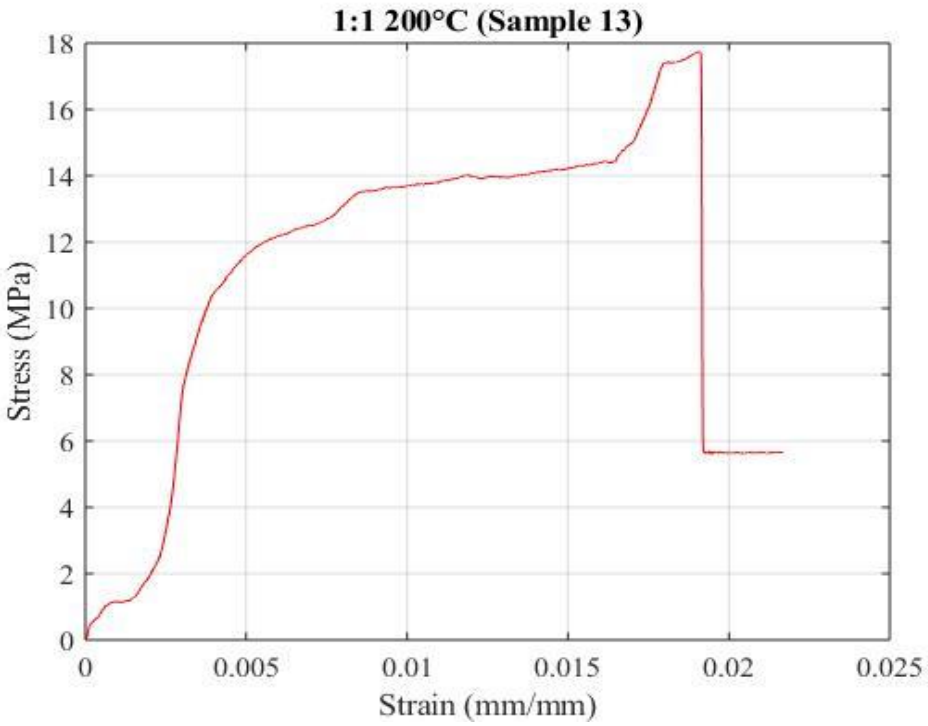
1:1 200°C (Sample 13)
Stress (MPa)
Strain (mm/mm)
0
2
4
6
8
10
12
14
16
18
0
0.005
0.01
0.015
0.02
0.025

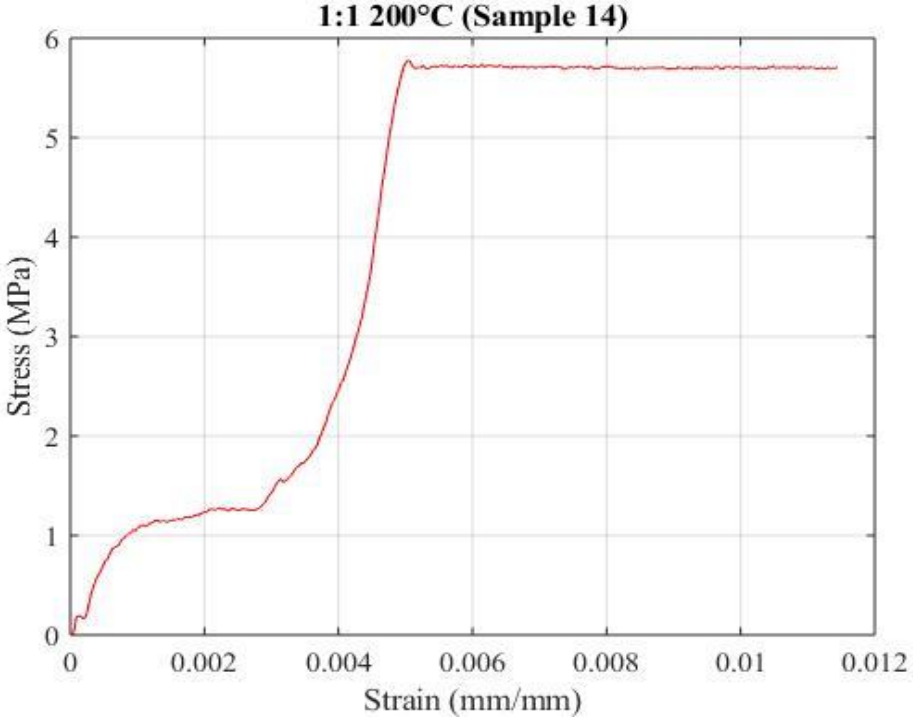
1:1 200°C (Sample 14)
Stress (MPa)
Strain (mm/mm)
0
1
2
3
4
5
6
0
0.002
0.004
0.006
0.008
0.01
0.012

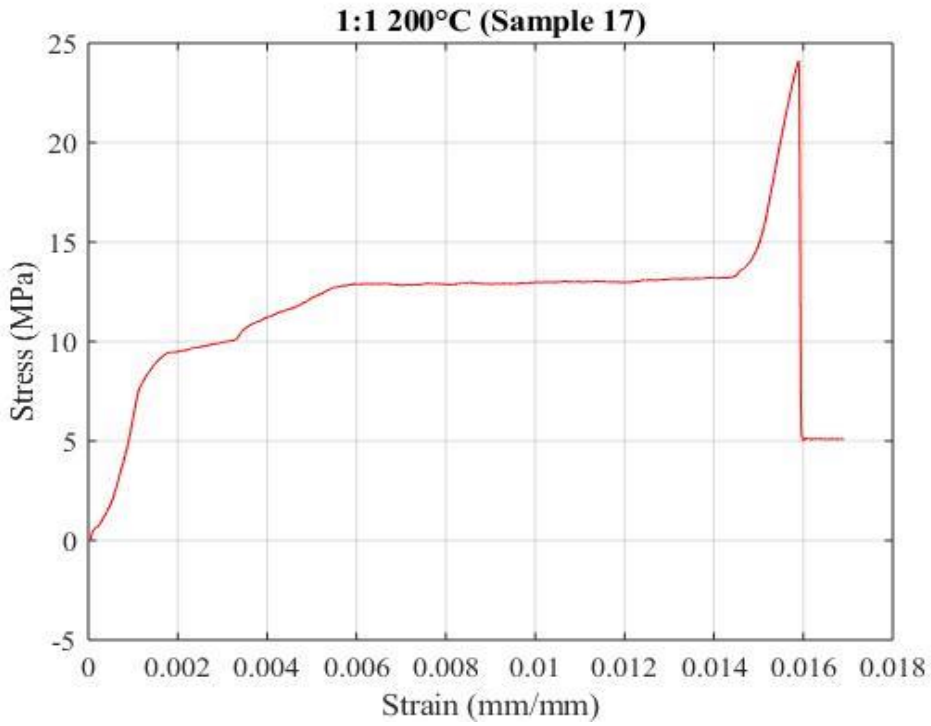
1:1 200°C (Sample 17)
Stress (MPa)
Strain (mm/mm)
25
20
15
10
5
0
-5
0
0.002
0.004
0.006
0.008
0.01
0.012
0.014
0.016
0.018

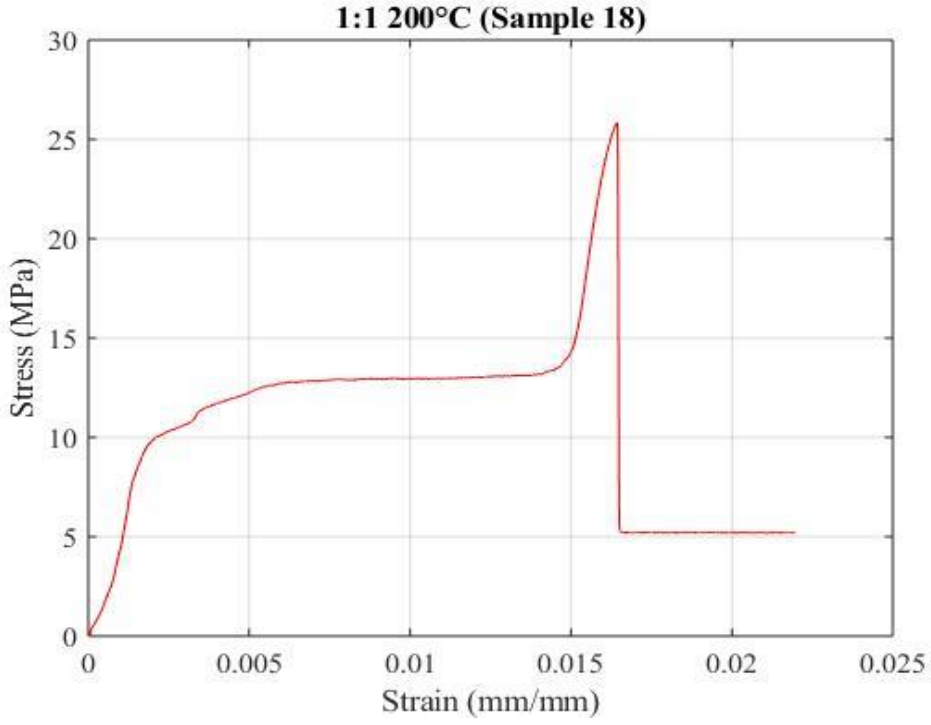
1:1 200°C (Sample 18)
Stress (MPa)
Strain (mm/mm)
30
25
20
15
10
5
0
0
0.005
0.01
0.015
0.02
0.025

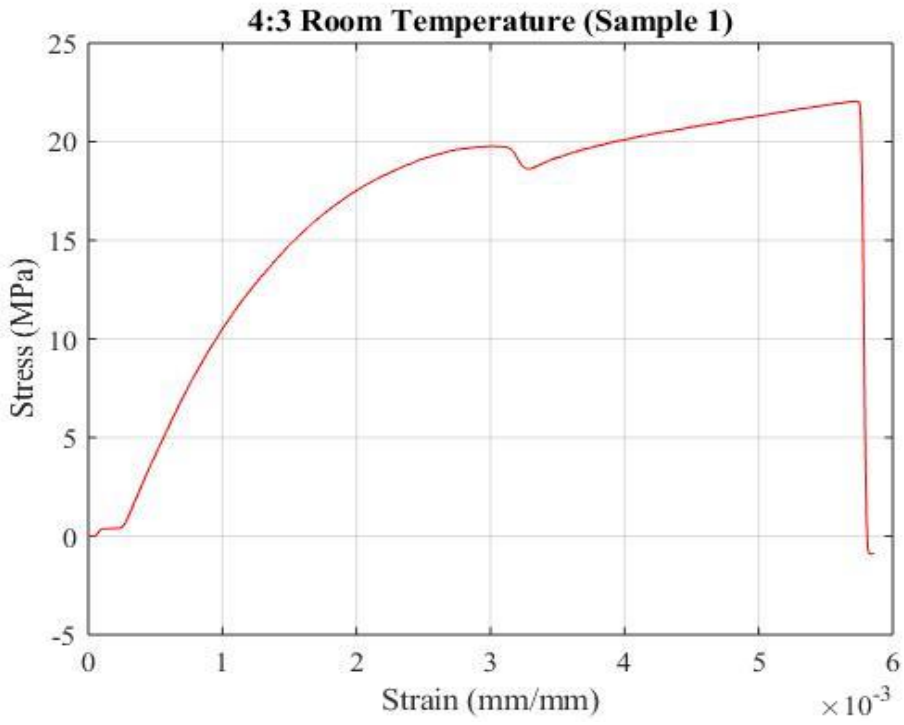
4:3 Room Temperature (Sample 1)
Stress (MPa)
Strain (mm/mm)
×10^-3
25
20
15
10
5
0
-5
0
1
2
3
4
5
6

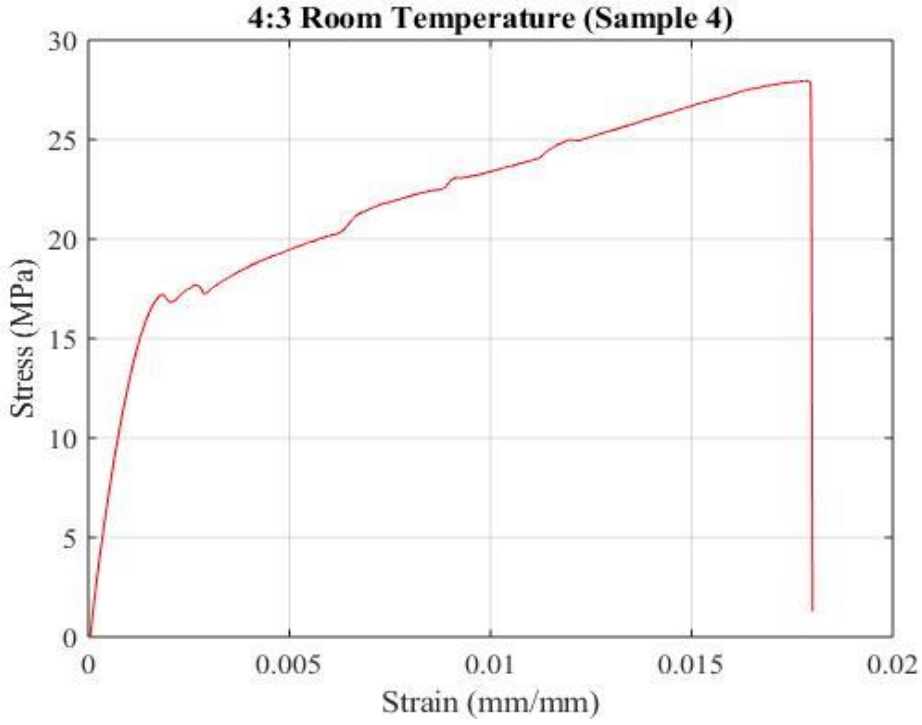
4:3 Room Temperature (Sample 4)
Stress (MPa)
Strain (mm/mm)
30
25
20
15
10
5
0
0
0.005
0.01
0.015
0.02

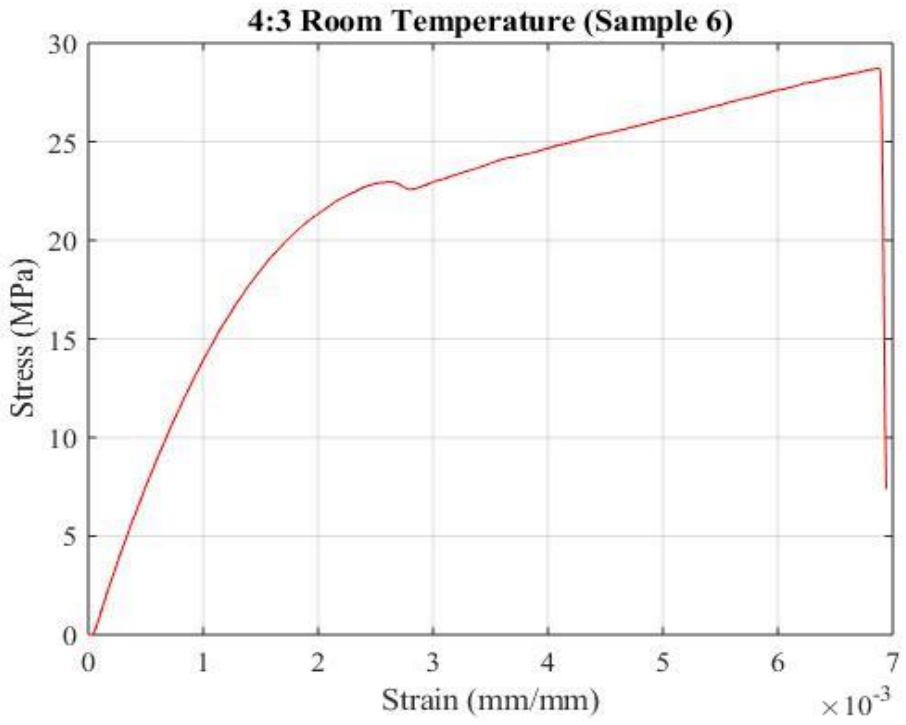
4:3 Room Temperature (Sample 6)
Stress (MPa)
Strain (mm/mm)
×10^-3
0
5
10
15
20
25
30
0
1
2
3
4
5
6
7

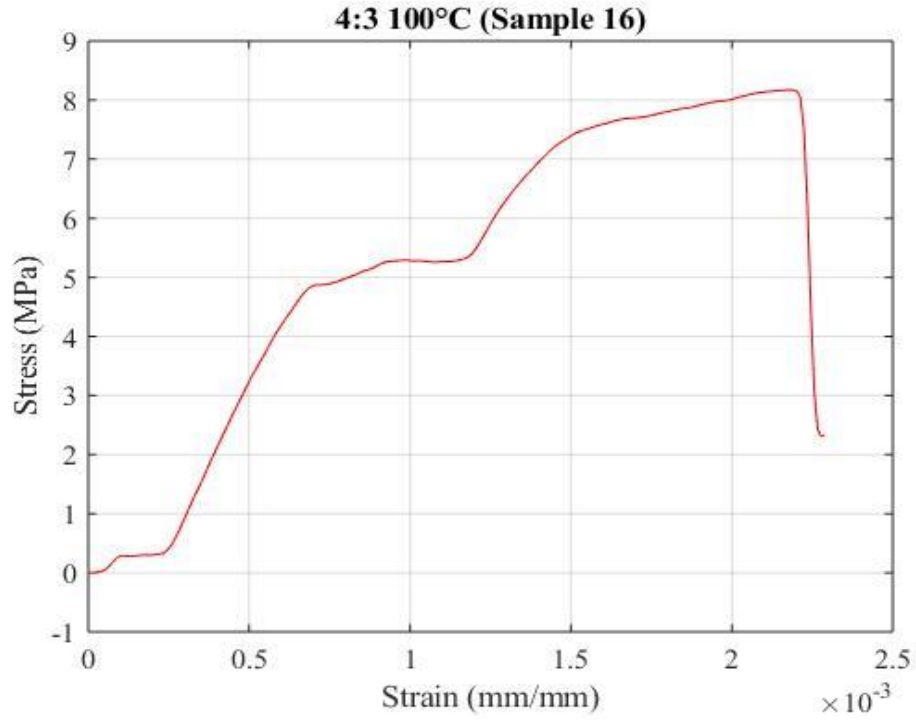
4:3 100°C (Sample 16)
Stress (MPa)
Strain (mm/mm)
×10^-3
-1
0
1
2
3
4
5
6
7
8
9
0
0.5
1
1.5
2
2.5

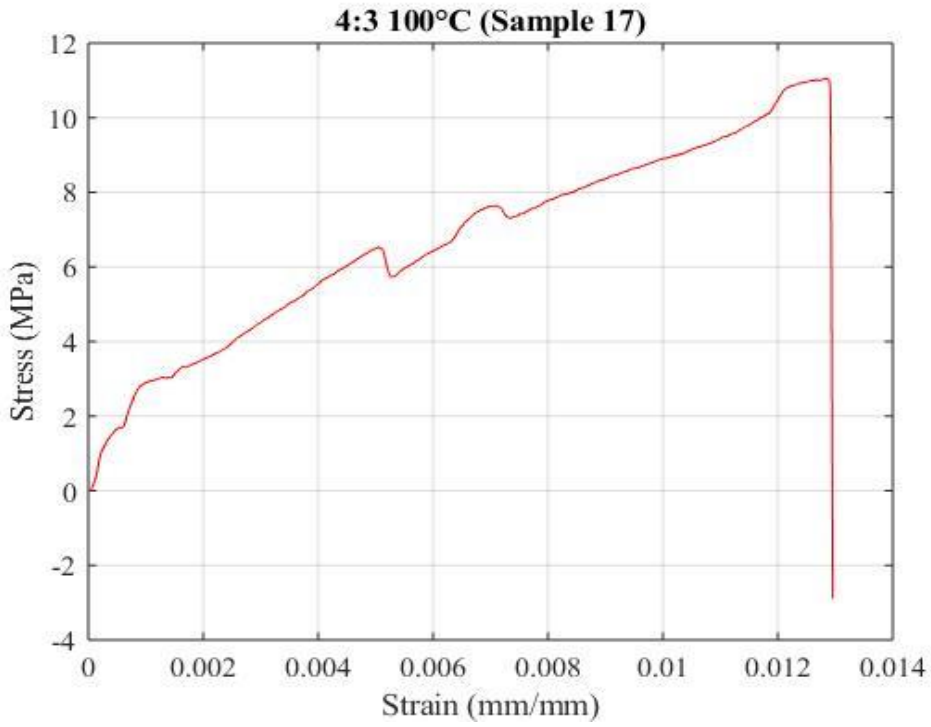
4:3 100°C (Sample 17)
Stress (MPa)
Strain (mm/mm)
12
10
8
6
4
2
0
-2
-4
0
0.002
0.004
0.006
0.008
0.01
0.012
0.014

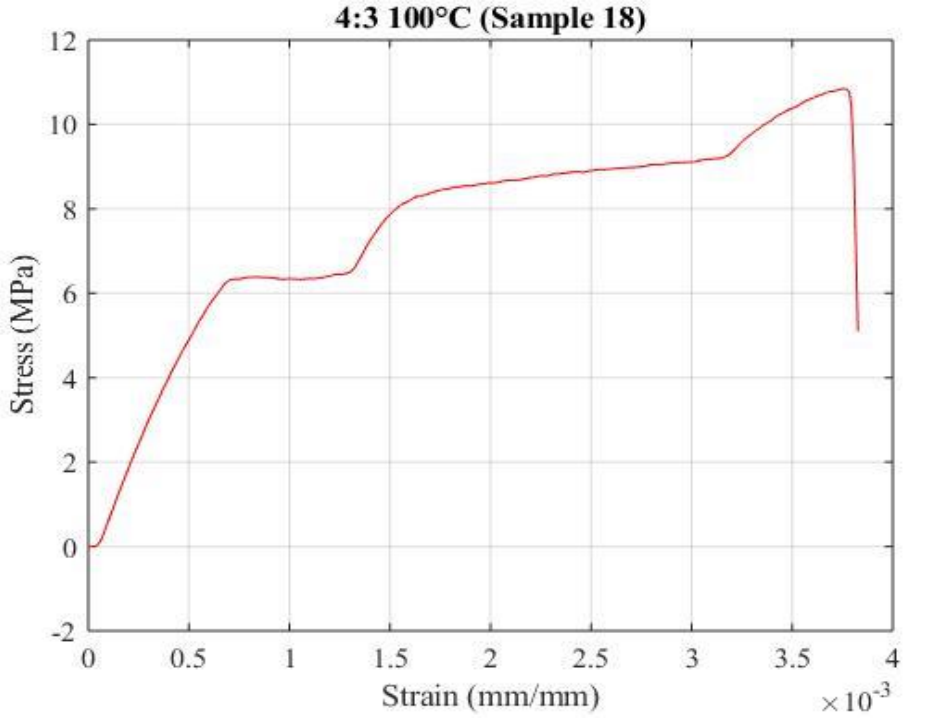
4:3 100°C (Sample 18)
Stress (MPa)
Strain (mm/mm)
×10-3
12
10
8
6
4
2
0
-2
0
0.5
1
1.5
2
2.5
3
3.5
4

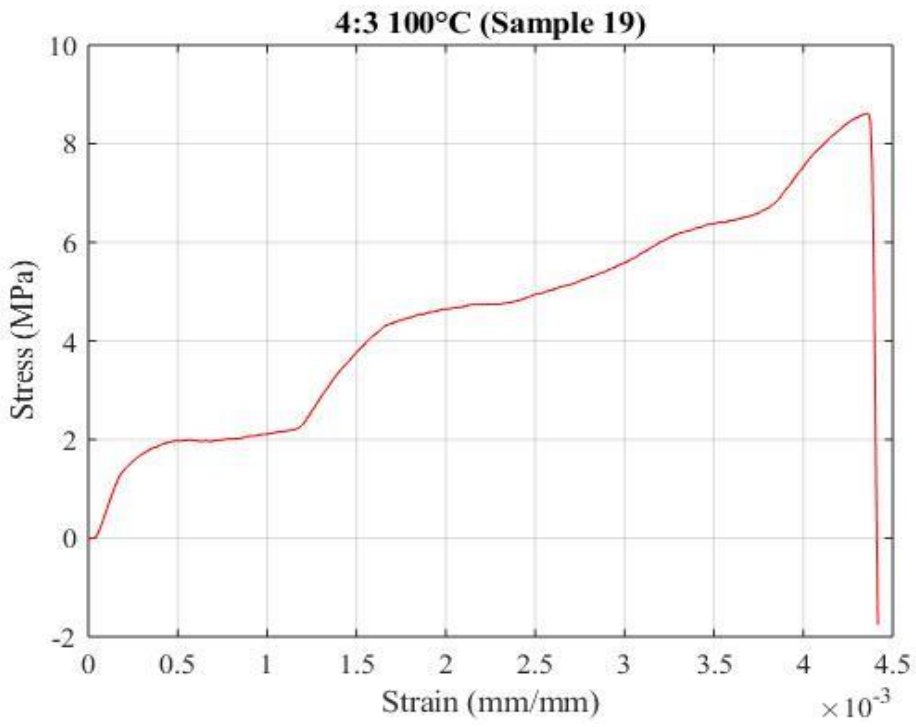
4:3 100°C (Sample 19)
Stress (MPa)
Strain (mm/mm)
×10^-3
10
8
6
4
2
0
-2
0
0.5
1
1.5
2
2.5
3
3.5
4
4.5

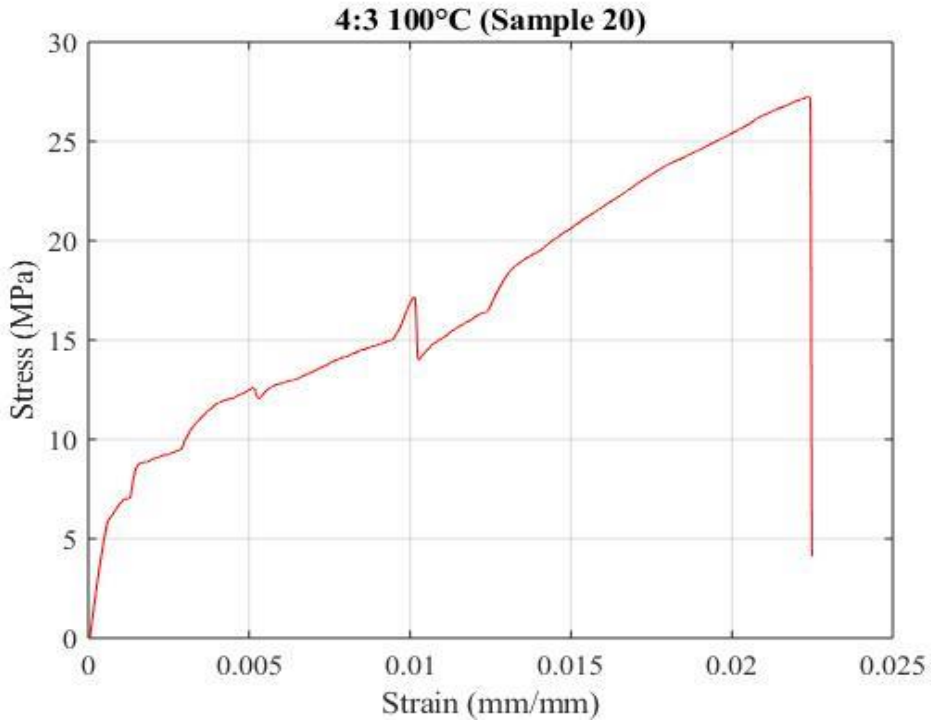
4:3 100°C (Sample 20)
Stress (MPa)
Strain (mm/mm)
30
25
20
15
10
5
0
0
0.005
0.01
0.015
0.02
0.025

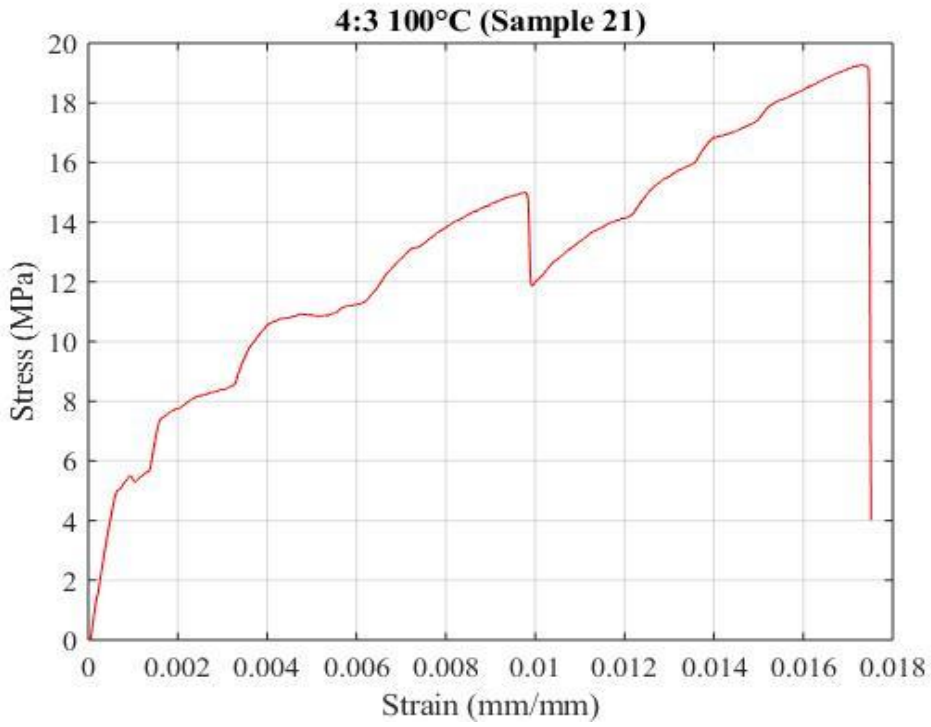
4:3 100°C (Sample 21)
Stress (MPa)
Strain (mm/mm)
0
2
4
6
8
10
12
14
16
18
20
0
0.002
0.004
0.006
0.008
0.01
0.012
0.014
0.016
0.018

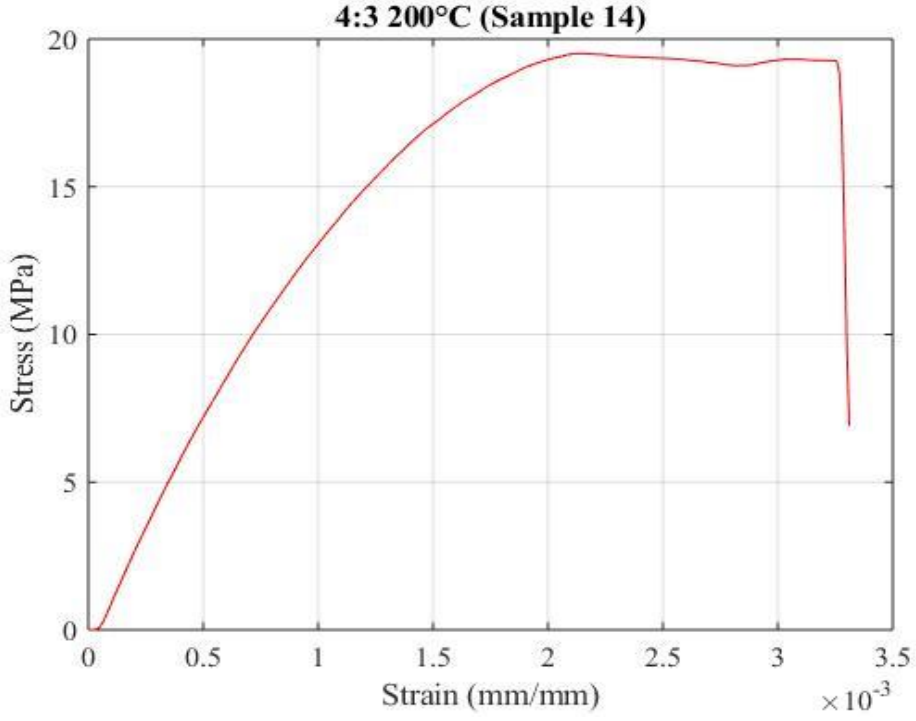
4:3 200°C (Sample 14)
Stress (MPa)
Strain (mm/mm)
×10-3
0
5
10
15
20
0
0.5
1
1.5
2
2.5
3
3.5

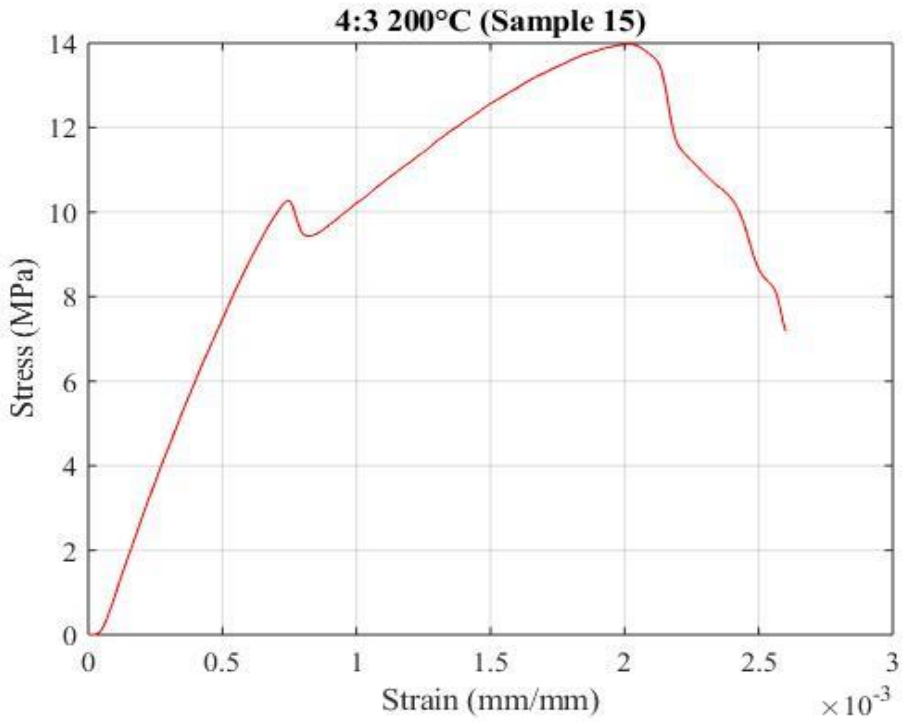
4:3 200°C (Sample 15)
Stress (MPa)
Strain (mm/mm)
×10^-3
0
2
4
6
8
10
12
14
0
0.5
1
1.5
2
2.5
3